uOttawa

L'Université canadienne
Canada's university

FACULTÉ DES ÉTUDES SUPÉRIEURES ET POSTOCTORALES

uOttawa

L'Université canadienne
Canada's university

FACULTY OF GRADUATE AND POSDOCTORAL STUDIES

Stéphanie Trottier
AUTEUR DE LA THÈSE / AUTHOR OF THESIS

M.A.Sc. (Mechanical Engineering)
GRADE / DEGREE

Department of Mechanical Engineering
FACULTÉ, ÉCOLE, DÉPARTEMENT / FACULTY, SCHOOL, DEPARTMENT

Experimental and Numerical Analysis of the Sooting Propensity of Binary Fuel Mixtures

TITRE DE LA THÈSE / TITLE OF THESIS

Matthew Johnson
DIRECTEUR (DIRECTRICE) DE LA THÈSE / THESIS SUPERVISOR

CO-DIRECTEUR (CO-DIRECTRICE) DE LA THÈSE / THESIS CO-SUPERVISOR

EXAMINATEURS (EXAMINATRICES) DE LA THÈSE / THESIS EXAMINERS

Donald Gauthier

William Hallett

Gary W. Slater
LE DOYEN DE LA FACULTÉ DES ÉTUDES SUPÉRIEURES ET POSTDOCTORALES /
DEAN OF THE FACULTY OF GRADUATE AND POSTDOCORAL STUDIES

Experimental and Numerical Analysis of the Sooting Propensity of Binary Fuel Mixtures

Stéphanie Trottier

A thesis submitted to the Faculty of Graduate and Postdoctoral Studies
in partial fulfillment of the requirements for the degree of

MASTER OF APPLIED SCIENCE

in Mechanical Engineering

Ottawa-Carleton Institute for Mechanical and Aerospace Engineering

University of Ottawa

Ottawa, Canada

Your file Votre référence
ISBN: 0-494-14963-9
Our file Notre référence
ISBN: 0-494-14963-9

ABSTRACT

The sooting behaviour of binary fuel mixtures was evaluated both experimentally and through computer simulations. The soot volume fraction of laminar diffusion flames of mixtures of ethylene/propane, methane/ethylene, methane/propane, methane/ethane, methane/butane, ethane/propane and ethane/ethylene fuels was measured using two-dimensional line of sight attenuation. It was found that a synergistic effect could be demonstrated for the ethylene/propane, methane/ethylene, methane/ethane and ethane/ethylene mixtures. The synergistic effect translated into a higher soot concentration for a mixture fraction than for either of the pure fuels. The methane/propane, methane/butane and ethane/propane mixtures were not seen to have such an effect. Through experiments where the flame temperature was kept constant, it was determined that the synergistic effect in the methane/ethylene mixture was very temperature-dependent whereas the synergistic effect in the ethylene/propane mixture was not. This phenomenon was further studied through the modeling of the ethylene/propane mixture. The modeling included the gas phase chemistry as well as a two-equation soot model. The simulation results again demonstrated and confirmed the presence of a synergistic effect. Through analysis, it was found that this effect could be directly correlated to a synergistic effect in the concentration of n-C_4H_5 and n-C_4H_3 species that could be traced back to an interaction between ethylene and methyl radical species. This then led to a synergistic effect in the concentrations of benzene and phenyl. These results yield further insight in the pathways to soot formation and highlight the importance of further analyzing binary fuel mixtures as a means of understanding soot formation in practical devices.

Acknowledgement

I would like to thank my supervisor, Dr. Matthew Johnson, for his unwavering support, patience and encouragement. Thank you for the great enthusiasm you demonstrated throughout this project.

I would also like to thank Greg Smallwood and Dave Snelling for their interest and encouragements.

I am grateful for financial support from the University of Ottawa and the Graduate Student Scholarship Supplement Program of the National Research Council of Canada. I am also very grateful to the Combustion Group for their generous help though financial support and the use of their research facilities.

I would also like to thank Hongsheng Guo for is invaluable help with the modeling aspect of this research. Your advice and patience was greatly appreciated. I am grateful to Dan Gareau, Bob Sawchuk and all of the Combustion Group for their invaluable help and their sense of humour; you have made this thesis very enjoyable. I would also like to thank Kevin Thomson for his support, advice, encouragement and books on tape!

I am grateful to Timothy Setterfield for his help in experimental setup and measurements.

Merci à mes parents pour leurs nombreux conseils judicieux! Merci aussi à mes amis, je pouvais toujours compter sur vous pour un sourire.

Finally, I am most grateful to Cagri Ayranci. Thank you for the laughs and encouragements every single day of this project. I could never ask for a better partner. Thank you.

Contents

List of Figures

List of Tables

Nomenclature

a	Acceleration of Flow through Flame	m/s^2
d	Diameter	m
E (m)	Refractive Index Function of Soot	
$f_v(r,z)$	Soot Volume Fraction	Parts per million [PPM]
$F_v(Z)$	Radially Integrated Soot Volume Fraction	m^2
I_λ	Attenuated Intensity	W/ster m^3
$I_{\lambda 0}$	Non-Attenuated Intensity	W/ster m^3
K	Thermal Conductivity	W/mK
K_0	Slope of Thermal Conductivity ($K=K_0*T$)	W/m
$K_{e\lambda}$	Optical Extinction Coefficient	1/m
m	Complex Refractive Index of Soot	
$\dot{m}$	Mass Flow Rate	g/s
Nu	Nusselt Number	
Pe	Peclet Number	
r	Radial Position	m
T	Temperature	K
V_z	Velocity of Flow in Flame	m/s
Ys	Soot Yield	
z	Flame Height	m

Greek Symbols

α	Fraction of Reactive Surface Sites Available	
ε	Emissivity	
λ	Wavelength	m
ρ_s	Density	g/cm^3
ρ_{sa}	Scattering to Absorption Ratio	
σ	Stefan Boltzman Radiation Constant	W K^4/m^2
τ	Transmittance	

Subscript

c_fuel	Carbon in the fuel
g	Gas
j	Junction
s	Soot

Acronyms

CARS	Coherent Antistokes Raman Spectroscopy
CCD	Charge-Coupled Device
Hg	Mercury
FL	Focal Length
HACA	Hydrogen Abstraction, Carbon Addition
LOSA	Line Of Sight Attenuation
PAH	Polycyclic Aromatic Hydrocarbon
PM	Particle Matter

1 PROBLEM DEFINITION

1.1 Introduction

With increasing sensitivity to environmental concerns, pollutant emissions have become an essential aspect of the study of combustion. The formation of soot, a primary contributor to airborne particulate matter (PM), has been increasingly scrutinized due to the known environmental and health effects of the airborne particulates. The emission of fine particulate matter (PM) is a primary environmental concern and has been linked to serious health effects in humans and animals, adverse effects in plants, and environmental damage [1]. Furthermore, soot is known to be composed of carcinogenic species and has been identified as having a variety of impacts on the climate change phenomena. It is therefore crucial to gain better understanding of the complex phenomena leading to soot formation and gain insight on how to reduce these emissions.

An extensive amount of research is continually being done both experimentally and numerically in an effort to try to understand the chemical paths that lead to soot formation. The knowledge of the pathways to soot formation is therefore always evolving. However, the complexity of the process is such that many uncertainties still remain. Most of the research has been concentrated on analyzing the sooting behaviour of elemental fuels. This in itself is warranted but studying fuel mixtures also could yield complementary information. The usefulness of looking at this process through a fuel mixture perspective is two-fold. First, in a theoretical aspect, it is generally agreed that studying the behaviour of mixtures of structurally different fuels can lead to better understanding of the actual formation process. Secondly, since a complete understanding of the soot formation process seems unlikely at this point, the study of fuel mixtures therefore allows for the observation of the behaviour of more relevant and realistic representations of fuels actually in use (for example commercial fuels), and to assess their actual behaviours.

The purpose of this study is to observe the sooting behaviour of an array of binary fuel mixtures. From previous research, it is thought that in certain mixtures, the sooting propensity over the mixture range could not be simply explained by the relative sooting propensity of the fuels, but could demonstrate that there exists a synergistic effect in the sooting propensity of these mixtures. What is meant by synergistic effect is the fact that for a certain mixture, the sooting propensity is higher than for any of the two fuels. Understanding the origin of this phenomenon can help understand the relative importance and interaction of different species in the pathways to soot formation. The mixtures studied will be composed of combinations of methane, ethylene, ethane, propane and butane. These fuels were chosen because they are simple in their composition, they are industrially relevant and it is thought that the analysis of their sooting behaviour can help understand the relative importance of different pathways to soot formation. The sooting behaviour of these fuels will be observed experimentally as well as numerically. It is hoped that the combination of these two analysis tools can help identify the cause of the experimentally measured behaviour through the analysis of the numerical simulations that allows an in-depth look at the species and formation rates involved.

1.2 Soot Formation in Diffusion Flames

To understand where this research would contribute to the present knowledge of the soot formation process, the different pathways presently identified in the literature will be presented. A great deal of uncertainty remain as to the validity of many of these pathways as well as their relative importance which leads to disagreement between researchers and makes further research in this area very important. It should be noted that this research will focus on diffusion flames since they represent a more relevant and comparable system for many industrial applications.

The preliminary step to soot formation is through fuel pyrolysis. Pyrolysis refers to the chemical decomposition of the fuel in high temperature conditions in the absence of oxygen. It has been established for diffusion flames that the pyrolysis of the fuel was the rate-controlling step in the formation of soot [2] which makes the sooting behaviour mainly dependent on the fuel structure as well as the flame temperature [3, 4].

The soot formation process itself can be subdivided into four sub processes: the inception of the first ring structured molecule, the formation and growth of polycyclic aromatic hydrocarbons (PAHs), soot inception and growth, and soot oxidation. The first ring inception refers to the first aromatic ring formation during aliphatic fuel combustion. An aliphatic hydrocarbon is composed of linear chains of carbon atoms, whereas, aromatic hydrocarbons are composed of rings of carbon atoms. It was first determined that one of the most probable path to the formation of the benzene aromatic ring involved acetylene (C_2H_2) with n-C_4H_3 and n-C_4H_5 [5, 6, 7]. Recent evidence gathered by Miller and Melius [8] has however introduced some restrictions to this path stating the tendency of the isomers n-C_4H_5 and n-C_4H_3 involved in the reaction to transform into the more stable species i-C_4H_5 and i-C_4H_3. They have found evidence that these isomers would not be present in large enough quantities to account for the rate of aromatic formation. However, there is still some disagreement about the relative stability of both isomers and therefore, these reactions are still thought to be important [9, 10]. Another pathway has recently been identified for the

first ring formation through the propargyl (C_3H_3) recombination into either phenyl (C_6H_5) or benzene (C_6H_6). Comparison of experimental and modeling concentration of species has further confirmed the importance of this pathway [11, 12, 13, 14, 15, 16, 17]. Another possible pathway brought forward would consist of the formation of fulvene (C_6H_6) from reactions involving allyl (C_3H_5) and propargyl to form fulvene which is then converted to benzene [15, 18, 19]. Fulvene is composed of a 5-carbon ring and is converted to benzene, a species having a 6-carbon ring, through H atom catalysis.

Following the formation of the first ring, there are a number of different hypothesis as to the path followed for the growth of the aromatic to a polycyclic aromatic hydrocarbon (PAH). The most popular model at this point is the Hydrogen Abstraction Carbon Addition (HACA) model [20]. This model expresses the sequential growth through a hydrogen abstraction acetylene addition reaction pathway. Good agreement has been found between this model and experimental results in premixed and diffusion flames [6, 21]. Another possible process for the growth of PAH has recently been proposed where growth could also proceed through reactions of aromatics with odd-carbon numbered radicals (e.g. C_3H_3) [12,14].

An additional reaction path has recently been suggested which diverges from the traditional process by which the first aromatic is formed and then grows into PAH species. Melius and co-workers [22] recently proposed that there could exist a pathway through which larger PAHs, naphthalene ($C_{10}H_8$) and phenantrene ($C_{14}H_{10}$), could be formed directly from the combination of cyclopentadienyl species (C_5H_5). Other researchers have found indications of the possible relevance of this pathway [12, 14, 18, 19]. However, some doubt as to this process has been introduced through the analysis of the sooting tendencies of benzene doped methane flames under different levels of premixing [21]. As would be expected, benzene doping resulted in higher concentration of cyclopentadienyl, but surprisingly, the naphthalene concentration monotonically decreased. This pathway to PAH production is therefore still highly controversial and uncertain.

It is generally agreed that the soot inception proceeds through reactions with heavy PAH species [12, 23]. Therefore, the coagulation of PAH species is the main path to soot inception, and surface reaction of acetylenic species would contribute to soot growth [19, 24].

Finally, in diffusion flames, if the flame temperature is sufficiently high, all the soot produced in the flame will be oxidized in the top portion of the flame. It has been found that OH is the main soot oxidant [25] while O_2 and O contribute to a lesser degree.

As explained previously, there is still some disagreement about the different pathways involved in the first ring formation and PAH growth steps and their relative importance in different fuels. Whereas the traditional viewpoint considered even carbon numbered species to be main culprits in soot production, explaining the high sooting propensity of fuels such as acetylene and ethylene, the possible involvement of odd-numbered carbon species raises the possibility that the role of other fuels, such as methane and propane, in soot formation could be much more important than anticipated.

Indications that the role of methane was indeed significant have been provided by different researchers. It has been demonstrated that, at equal temperatures, premixed methane flames produced higher benzene and PAH concentration than ethane flames [16]. As well, it was found that by substituting some of the carbon content of an n-heptane premixed flame with carbon provided by methane addition, significant increases in benzene, PAH and soot concentrations were obtained [26]. Intuitively, the addition of methane would reduce the acetylene content of the flame as well as increase the hydrogen content. These two factors would lead to lower benzene and PAH concentration by impeding the acetylenic reactions for first ring formation and the HACA path to growth. For n-heptane flames doped with CH_4, the increase in the C_6H_6, PAH and soot concentrations hints at the involvement of a different process. This was also shown in a flow reactor where again, the addition to methane to n-heptane led to an increase of PAH concentrations [27]. These results indicate that, through the odd-carbon numbered pathways, methane would contribute to the sooting propensity through the first ring inception. It was also found that the increase was more

pronounced in the larger PAHs, further emphasizing the role of odd-carbon numbered species in the PAH growth [27].

As well, propane as a fuel could also play an important role in soot formation if its dehydrogenation path to propargyl is considered [19]. The relevance of this pathway was demonstrated through a study of methane flames doped with propane (C_3H_8), propene (C_3H_6) and allene (C_3H_4). In the propane doped flame a noticeable increase in the propene, allene and more importantly in the soot concentration were measured. As well, by comparing the chemical species resulting from a pure acetylene/argon diluted diffusion flame and an acetylene/allene (C_3H_4) flame, a significant increase in the benzene concentration resulted from the allene addition [28]. This was interpreted as having resulted from the more direct path to propargyl formation from the allene pyrolysis through dehydrogenation, and therefore, an increase in the propargyl combination reactions.

2 FUEL MIXTURES

The fact that the different pathways seem to vary in importance in different fuels led to the possibility that their interactions in fuel mixtures might lead to synergistic or competing effects in the sooting propensity of these mixtures. In this context, a synergistic effect is observed when the rate of soot formation for a given mixture of fuels is greater than for any of the individual fuel components.

The presence of a synergistic effect was indeed established for mixtures of allene (C_3H_4) / acetylene (C_2H_2) and vinyl-acetylene (C_4H_4) /acetylene (C_2H_2) as well as mixtures of acetylene (C_2H_2)/, allene (C_3H_4)/, vinyl-acetylene (C_4H_4) /, and 1,3-butadiene (C_4H_6) / benzene (C_6H_6) both experimentally and numerically [29]. It was found in experiments done behind reflected shock waves that the soot amount produced by any of these mixtures was noticeably larger than the soot amount produced by any of their individual components. It was interpreted, through numerical simulations that in the mixtures containing acetylene, vinyl-acetylene or 1-3 butadiene, the synergistic effect would be attributable to an acceleration of the acetylene addition step in the first ring formation or the HACA growth process. As well, although no numerical verification was done, it was proposed that the synergistic effect seen in mixtures of allene/benzene or allene/acetylene was again due to the acceleration of the acetylene based pathways. It was proposed that the first ring formation path in the allene/acetylene mixture was not through the tradition path leading to phenyl and benzene but through the addition of acetylene to propargyl to form benzyl (C_7H_7). As well, the soot yield was seen to show the synergistic behaviour for all mixtures except in the acetylene/benzene mixture. This was confirmed through qualitative trends of numerical results and was explained through the complex involvement of acetylene which is noticeably different in aliphatic and aromatic fuels. In aliphatic fuels, acetylene would directly contribute to the formation of aromatic rings and to their growth, whereas, in aromatic fuels, the more efficient ring formation process through phenyl/benzene reactions would be hindered by the acetylene reaction with phenyl.

To further explain this phenomena, recent experiments done by Hwang and co-workers [30] have analyzed ethylene/propane ((C_2H_4/C_3H_8) mixtures. The basic starting point for these experiments was an assessment of whether odd-carbon numbered species could contribute to the synergistic effect as well. For both co-flow and counter-flow ethylene/propane flames, a synergistic effect was measured through the range of mixtures in constant carbon flow conditions. The soot volume fraction and PAH concentrations were seen to be enhanced for certain mixture conditions. These results indicate that, contrary to the traditional viewpoint, acetylene may not be solely responsible for the first ring formation and growth. Evidently, adding propane to an ethylene mixture would tend to decrease the acetylene concentration, reducing the rate of first ring formation through this species. However, the fact that a maximum soot and PAH concentration is reached for an intermediate mixture of ethylene and propane tends to confirm the importance of the propargyl combination reaction. As mentioned previously, propargyl is readily formed during the propane pyrolysis through the dehydrogenation process. Numerical simulation results have confirmed that the C_2H_2 concentration monotonically decreases as the mixture fraction of propane is increased. However, the C_3H_3 concentration profile was seen to have a synergistic behaviour. This indicates the possibly of a complementary behaviour in the soot formation pathways between the acetylene and propargyl reactions.

Hwang and co-workers [31] have further explored the role of the propargyl combination reaction on this synergistic effect by measuring the effect of oxygen addition on the sooting propensity of ethylene. The addition of a small amount of oxygen to the ethylene flame was seen to induce an increase in the soot concentration. This was numerically correlated to an increase in C_3 species concentration, while C_2 species concentration continuously decreased with increasing O_2 concentration. In contrast, measurements showed that addition of oxygen to a propane diffusion flame actually reduced the sooting propensity. It was then proposed that in ethylene flames, the addition of oxygen would enhance the following reactions:

$$C_2H_2 + O_2 \Leftrightarrow CH_2 + CO_2$$

$$C_2H_2 + CH_2 \Leftrightarrow C_3H_3 + H$$

This would explain the different behaviours in ethylene and propane flames as well as solidify the importance of the propargyl combination pathway to benzene formation.

However a similar, but less pronounced synergistic effect was seen in an ethylene/ethane flame [30]. Ethane does not have a direct path to propargyl formation during its pyrolysis. This led Yoon and co-workers [32] to look at an array of mixtures created from mixing methane (CH_4), ethane (C_2H_6), propane (C_3H_8) and propene (C_3H_6) with ethylene in a counter-flow diffusion flame. As from previous experiments, their results indicated a synergistic effect in the PAH and soot concentrations for the ethane/ and propane/ethylene mixtures. No synergistic effect was seen in the propene/ethylene mixtures, which leads to some doubts about the possible role of the propargyl in this phenomenon since propene is a product of the propane dehydrogenation in the string of reactions leading to propargyl. As well, a synergistic effect was seen at the PAH level for the methane/ethylene mixture, but was not visible at the soot level. The numerical modeling of the flames revealed that the methyl radical (CH_3) concentrations in the methane peaked much higher in the flame than for the other fuels. The fact that the methyl radical is formed lower in the flame for the other fuels may explain the synergistic effect by the fact that this radical could then lead to propargyl in a region in the flame where the propargyl combination would lead to benzene more efficiently.

However, it is very important to notice here that the temperature of the different flames was not accounted for. The previous authors dismissed the possible effect of temperature on this phenomenon by considering that the adiabatic flame temperature decreased monotonically and more importantly, that the propargyl based reactions and the PAH agglomeration process, considered to be predominant, were less sensitive to temperature [30]. Recent information obtained from work by Roesler and co-workers [33] has indicated that this may not be the case. These authors studied methane/ethylene mixtures in which the adiabatic flame temperature was kept constant through nitrogen dilution and contrary to previous findings noticed a synergistic effect in the soot concentration over the range of mixtures. A synergistic behaviour was observed as well in a methane doped n-heptane flame [26]. This

yields further evidence that the methyl radicals can indeed play an important role. A synergistic effect was measured in the benzene concentration, implying the possible importance of the methyl radical reactions leading to propargyl which would then lead to benzene. However, the synergistic effect is also seen at the larger PAH level in different proportions. There seem to be two separate trends in the PAH concentration behaviour, some larger PAH follow the benzene behaviour and increase in similar proportions, whereas others are seen to have a smaller increases. This seems to indicate that indeed, PAH growth could be due to both odd-carbon and even-carbon number species. This was investigated by Lee and co-workers [34] who reported that the synergistic effect in the PAH concentrations becomes more pronounced with measurements done at higher wavelength, corresponding to concentration measurements of larger PAHs. This was done by minimizing the possible effect on the first ring formation by doping the ethylene/propane mixture with benzene. It was confirmed that since the synergistic effect was still measurable although less pronounced, it could be due to a combination of the first ring formation and PAH growth pathways.

These findings confirm the possible role of the odd-carbon numbered species and its interaction with other traditional soot formation species, mainly acetylene. It was also proposed that the growth of PAHs through odd-carbon numbered species reactions could also contribute to the synergistic effect, through its interaction with the HACA process.

2.1 Outline of Research

The purpose of this thesis is to help clarify the different pathways to soot formation and their relation with the synergistic effect in fuel mixtures. It is hoped that this work will provide a basis of knowledge of the sooting propensity of industrially relevant fuels. The behaviours of binary fuel mixtures composed of methane, ethylene, ethane, propane and butane are investigated to assess the interaction between even and odd-numbered carbon species in the pathways to soot formation as well as gain insight into the roles of propargyl and the methyl radical in the formation process.

An annular co-flow diffusion flame was used. The sooting propensity was measured using the 2-dimensional line of sight attenuation optical diagnostic which provided good accuracy and ease of use and analysis. As well, because temperature is known to be a key factor in the sooting behaviour of diffusion flames, the flame temperatures were monitored using a fine gauge thermocouple. Constant adiabatic flame temperature experiments were also conducted by preheating the fuel and air.

Finally, to further understand the origin of the synergistic effect in the mixtures, numerical simulations were done for the ethylene/propane mixtures. The chemical kinetics model used in this case was optimized for C_3 species combustion [35]. Unlike previous attempts [30], these simulations included a soot model which permitted direct correlation of the behaviour and identification of the reactions and species responsible. The simulations were done using a simplified soot model. The model is a two-equation model where soot inception is based on the benzene and phenyl concentration [36]. From the combination of experimental and numerical results, it is thought that a deeper understanding could be gained of the different species involved in soot formation and their role in the synergistic effect found in certain fuels mixtures.

3 SETUP

3.1 Experimental Setup

3.1.1 Burner Configuration

The sooting propensity of the different mixtures was studied using a laminar diffusion flame burner shown in Figure 3-1. This burner is composed of an inner brass fuel tube which has a diameter of 10.9 mm, surrounded by an outer tube of a 100 mm diameter through which the co-flow air is delivered. The air flow passes through two thicknesses of sintered metal foam as well as glass beads to ensure a uniform velocity profile.

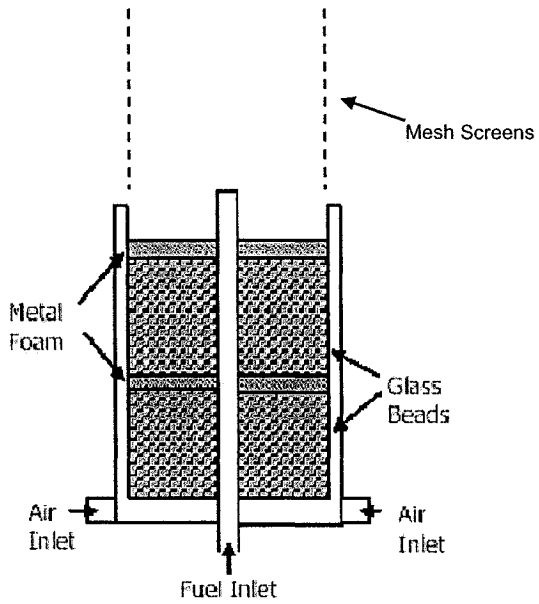

Figure 3-1 Burner Configuration

To ensure the stability of the flame studied, the burner was surrounded by a mesh screen in which holes allowed optical access. This screen helped prevent disturbances to the shielding air flow and to the flame. Sufficient length of the fuel tube (L/D=100) was left preceding the burner to ensure fully developed laminar flow.

3.1.2 Fuel and Air Flow Configuration

To obtain a proper basis for comparison, all of the mixture flow rates were defined to have constant carbon content. This allows a direct comparison of the soot yield of the different flames based on the same carbon input. The flow rates used were based on the conditions established by Gülder and co-workers and corresponded to a carbon flow rate of 3.2 mg/s [37, 38]. The following table presents the corresponding flow rates, velocities and Reynolds numbers for each of the pure fuels.

Table 3-1 Summary of Fuel Flow Conditions

Fuel	Volume Flow Rate (cc/min)	Mass Flow Rate (g/min)	Velocity (cm/s)	Reynolds Number
Methane (CH_4)	390	0.26	6.7	45
Ethylene (C_2H_4)	194	0.23	3.5	44
Ethane (C_2H_6)	194	0.24	3.5	52
Propane (C_3H_8)	128	0.24	2.3	58
Butane (C_4H_{10})	97	0.24	1.7	64

The fuels were combined in binary fuel mixtures: ethylene/propane, methane/ethylene, methane/propane, methane/butane, methane/ethane, ethylene/ethane and ethane/propane. The carbon content was kept constant for all these mixtures by adjusting the flow rates of each of the two fuels found in a mixture so that the contribution of each fuel to the carbon flow rate varied from 0 to 100%. The surrounding air flow was again based on the conditions established previously [37, 38]. This flow rate was kept constant for all mixtures at 284 L/min, corresponding to a velocity at the inlet of 63 cm/s.

The fuel flow rates were controlled by Aalborg GFC mass flow controllers. For the fuel control, three different mass flow controllers were used with ranges of 0-100 cc/min, 0-200 cc/min and 0-500 cc/min for nitrogen. These were linked to switch valves which allowed using the desired flow controller for each fuel to be used according to the needed flow rate. These flow controllers were originally calibrated for nitrogen by the supplier and a new calibration was therefore done over the full range of the three flow controllers for all the fuels of interest using a bubble flow meter. The conversion factor found was used to determine the flow setting for each fuel. It should be noted that the conversion factor measured was similar but had small discrepancies from the value given by the supplier, enhancing the necessity of performing this calibration.

The air flow meter was again an Aalborg GFC mass flow controller with a range of 0-1000 L/min. Pressure gauges placed immediately upstream of the flow controllers were monitored to ensure that all flow meters were operated at their optimal range (i.e.. 20 PSI for fuel and 50 PSI for air). Downstream of the flow controllers, all fuel lines were joined together in a single line which allowed fuels to be combined. A long length of tube was allowed before the burner to ensure proper mixing of the fuels.

3.1.3 2D LOSA Optical Diagnostics

3.1.3.1 Setup Description

The sooting propensity of the different mixtures was assessed using a technique called Two-Dimensional Line of Sight Attenuation (2D LOSA). This technique being an optical diagnostic, it has the advantage of causing essentially no disturbance to the flame itself. The details of this technique were presented by Snelling et al. [39]. The fact that this method is 2 dimensional is a noticeable advantage, making an efficient technique for obtaining the full flame soot profile. As well, this technique was developed to have great sensitivity, which is essential for the study of low sooting flames like methane. Finally, the optical setup shown in Figure 3-2 and Figure 3-3 was precisely designed to minimize the beam steering that might occur. This is done by optically conjugating the center of the flame and the collection plane. This means that for light passing through a point, whether it is still collimated or diffuse due to beam steering, it will be imaged at the same spatial location on the collection optics, minimizing spatial distortions.

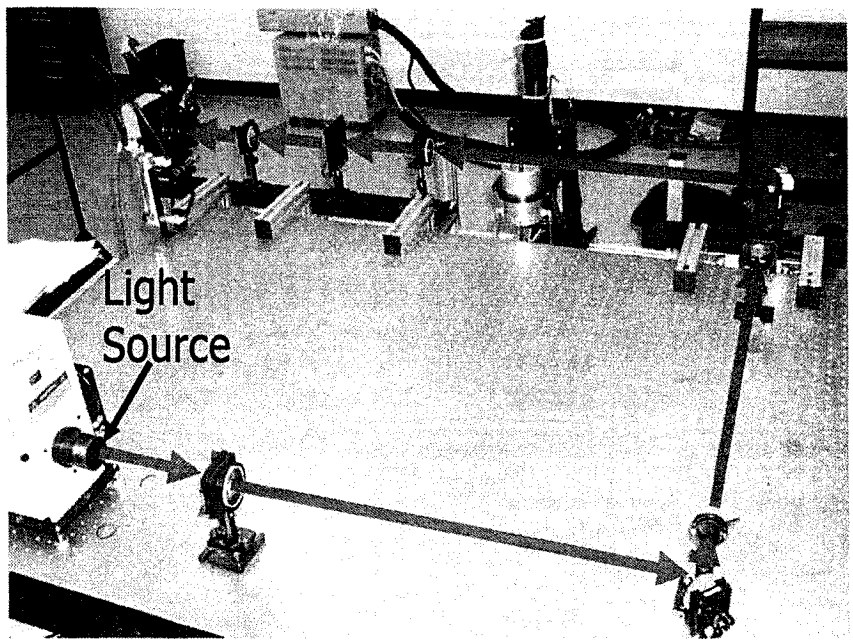

Figure 3-2 Photograph of Optical Table

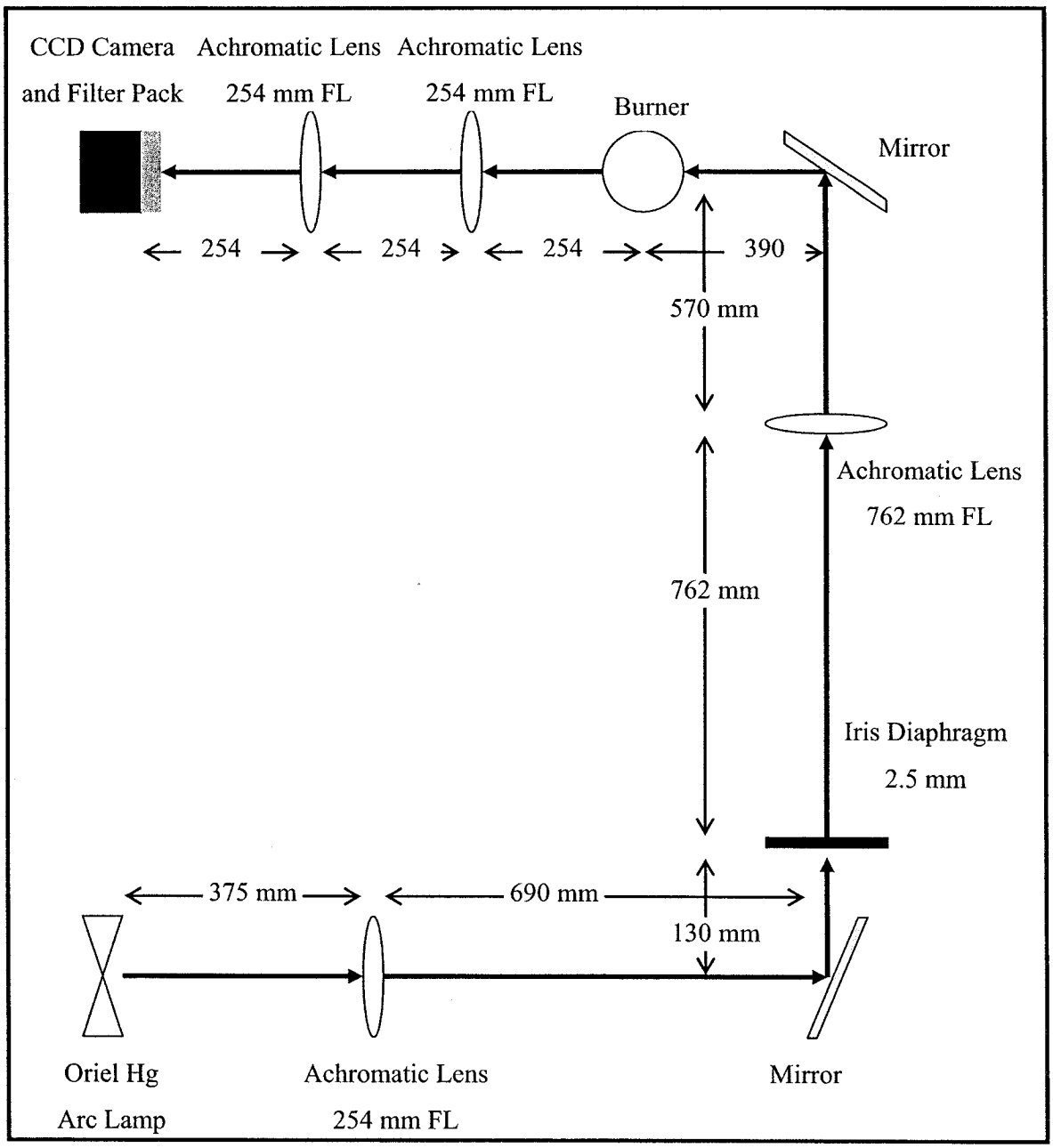

Figure 3-3 Optical Table Layout for 2D LOSA Experiment

The optical arrangement illustrated in Figure 3-3 was chosen to have one-to-one imaging. The detector used was a water-cooled 16 bit CCD array of 1152 x 1242 pixels where each pixel corresponds to a 22.6 μm x 22.6 μm area of the flame. The detector was controlled using Roper Scientific Winview/32 software. The exposure time was adjusted to ensure maximum intensity without saturating the camera, this saturation occurred at an intensity of 65 500 counts. To ensure that measurements were done at the desired wavelength, in this case 577 nm, a filter pack was placed in front the of CCD camera. The signal was treated with a filter centered at 577 nm with a 20 nm bandwidth. This wavelength was chosen because it is optimal for the lamp emission.

The lamp source used was a 100 W Oriel mercury arc lamp. The advantage of using an arc lamp over a laser is simply that using an arc lamp allows the use of a wider range of wavelengths and eliminates the spectral coherence encountered with lasers resulting in speckle. This system permits measurements at very low soot concentrations with very low noise levels [39].

3.1.3.2 Analysis Description

Because of the one-to-one imaging of the flame and the size of the detector, four sets of pictures were taken throughout the height of the flame to capture the full flame. The translation stage allowed moving the burner vertically to achieve this. Each picture was taken at 18 mm height intervals. At each vertical position in the flame, a total of four images were taken.

Two of these four pictures were taken while the flame was not in the optical path. The first one measured the contribution of the environment to the intensity when the lamp signal was not present while the second measured the total intensity with the lamp. The difference between these two yielded I_0, or the non-attenuated intensity. The same technique was repeated with the flame present in the optical path. One picture was taken with the lamp intensity attenuated by the flame. A second was taken of the flame intensity only. The difference between these two I. The ratio between I and I_0 yielded the transmittance as illustrated in Figure 3-4.

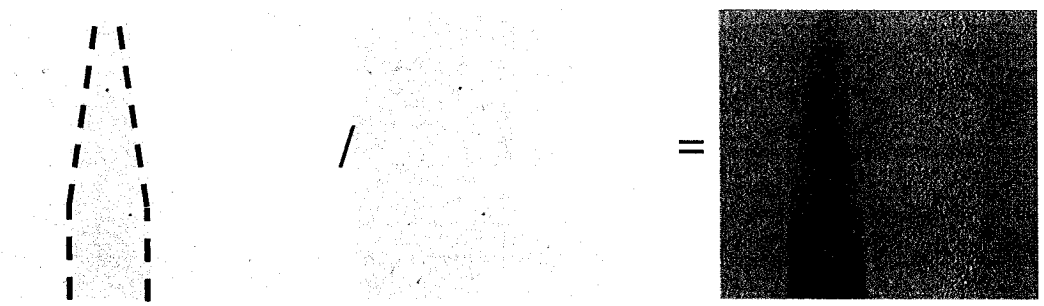

Attenuated Intensity, I Non-attenuated Intensity, I_0 Transmittance, τ

Figure 3-4 Transmittance Calculation

To reduce shot noise, or the random noise that would occur in any one picture, five frames of every picture were taken and averaged. The transmittance (τ) was calculated individually for each of these five frames. Before averaging these frames, the transmittance for each was normalized and centered.

It was expected that, in the region outside the flame, the transmittance resulting from the ratio of I/I_0 would be one. This did not always occur due to the varying intensity of the lamp, as illustrated in Figure 3-5, where the outside region of the flame on the right hand side has a transmittance of 0.98 instead of 1. The transmittance in the flame was therefore normalized to ensure that outside of the region of the flame the transmittance was 1 as shown in

Figure **3-6.**

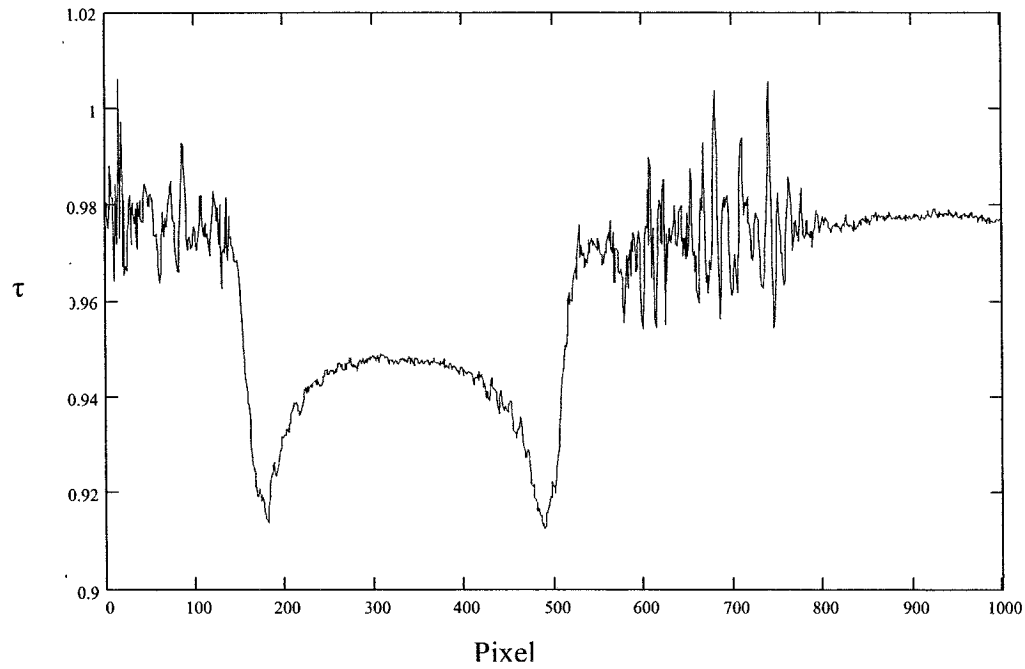

Figure 3-5 Transmittance before Normalizing

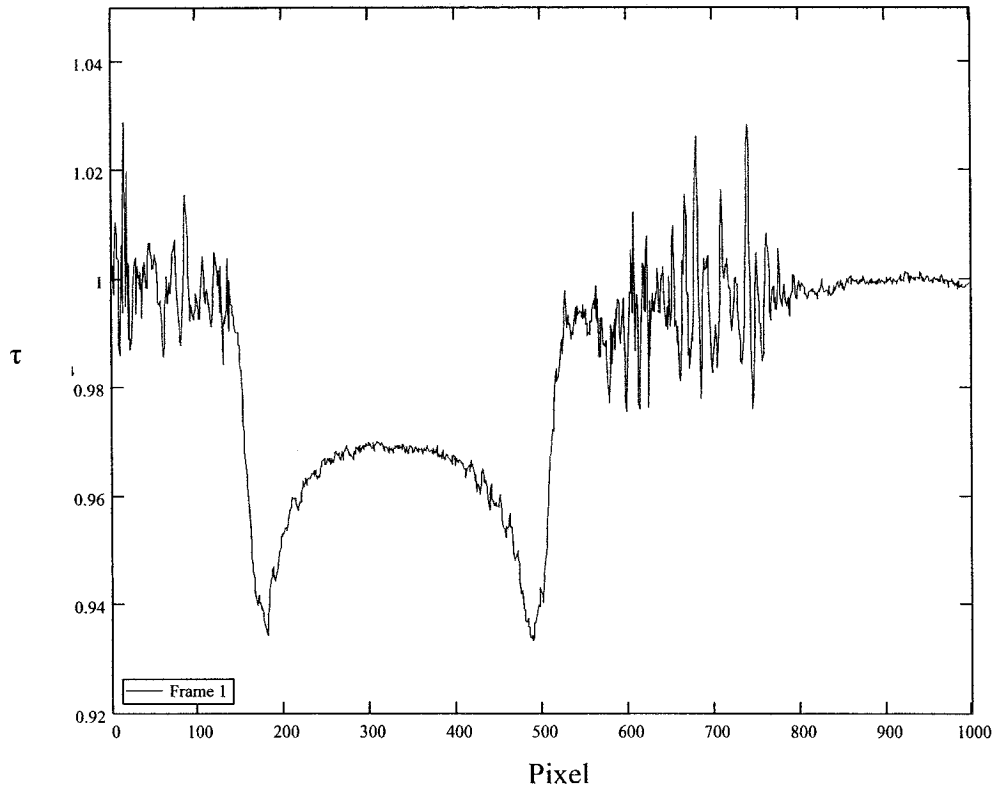

Figure 3-6 Transmittance after Normalizing

Although the flames were generally stable, there was slight movement between the different frames, especially higher in the flame as illustrated in Figure 3-7. The mesh screen around the burner helped in reducing these variations but it was found that when processing the images each frame had to be re-centered.

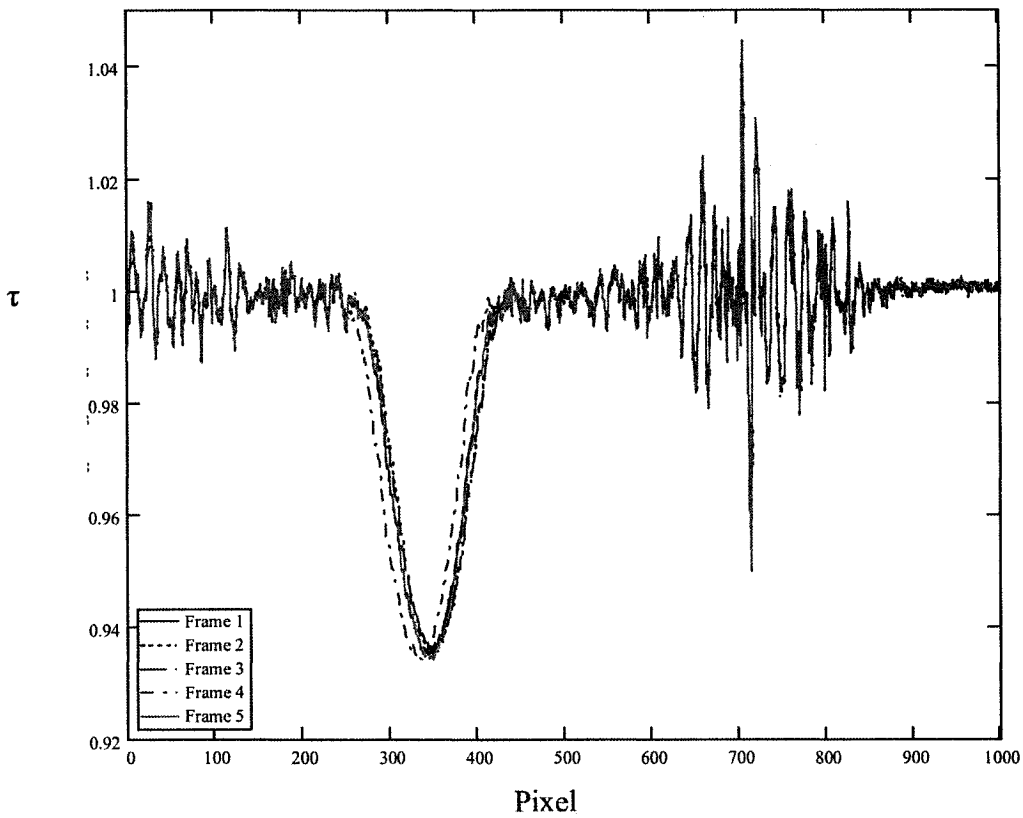

Figure 3-7 Non-centered Transmittance of 5 Different Frames

To center each frame, the transmittance curves were first smoothed individually. Following this, all five frames were aligned as shown in

Figure 3-8. The centering was done using a spline fit and, for each height, two points on each side of the flame were found where the transmittance had dropped 1/3 of the difference between the maximum and minimum value. The center for each height is then defined as the middle points between these two points.

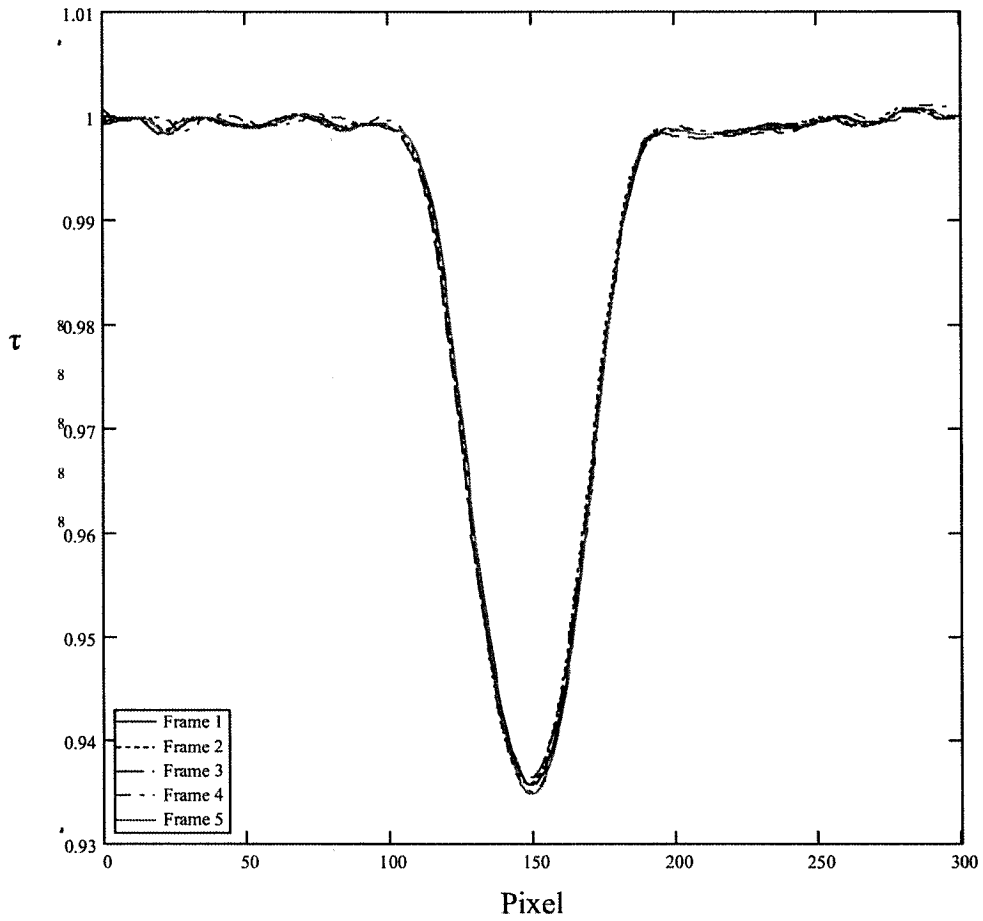

Figure 3-8 Centered and Smoothed Transmittance of 5 Different Frames

The smoothing was done using the Loess algorithm found in MathCAD. This algorithm uses a second order polynomial fit on a defined span. The span was dictated by the amount of smoothing needed for the inversion algorithm in low sooting flames with large noise-to-signal ratios. Accordingly, a constant span of 0.08 mm was used for all flames. It was found that the span affected the smoothing and the resulting peak soot volume fraction as shown in Figure 3-9; however, the radial integral of the signal was unaffected as illustrated in Figure 3-10. This indicates that the smoothing span will have no effect on the soot yield, the comparison basis of the different flames we will use. The method for calculating the soot yield will be explained shortly.

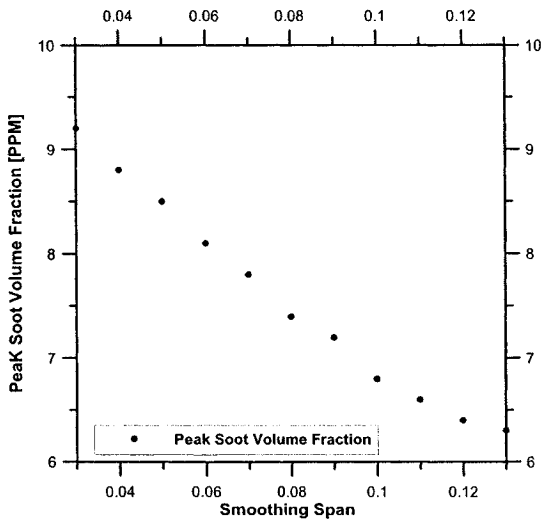

Figure 3-9 Effect of Smoothing Parameters on Peak Soot Volume Fraction of Ethylene Flame

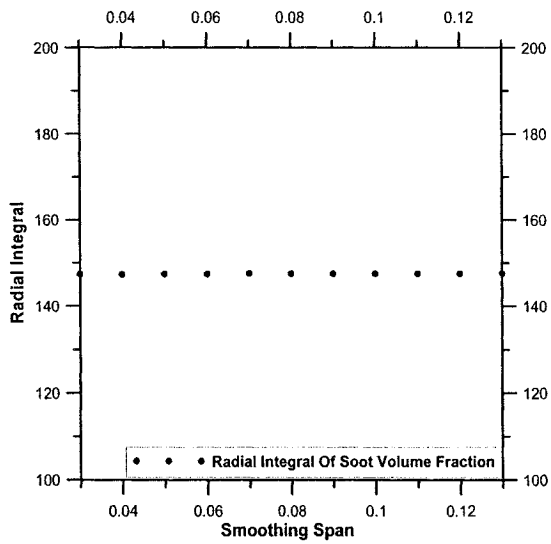

Figure 3-10 Effect of Smoothing Parameter on Radial Integral of Soot Volume Fraction of Ethylene Flame

Following the normalization and the centering of the five different frames, these five transmittances are averaged. The resulting transmittances can be related to yield the soot volume fraction contained in the flame. From the Bouguer-Lambert-Beer law [40] integrated along a path in a flame, the following relation is obtained:

$$\ln(I_\lambda / I_{\lambda 0}) = \int_{-\infty}^{\infty} k_{e\lambda} ds \qquad \text{(Eq. 3-1)}$$

where: I_λ is the lamp intensity attenuated by the flame

$I_{\lambda 0}$ is the non-attenuated lamp intensity

$K_{e\lambda}$ is the optical extinction coefficient

If we assume that the primary particles are in the Rayleigh range and that the fractal aggregates are small, we can apply the first order theory of scattering by aggregates [40] which allows stating that:

$$f_v = \frac{\lambda k_{e\lambda}}{6\pi E(\tilde{m})(1+\rho_{sa})} \qquad \text{(Eq. 3-2)}$$

where: λ is the wavelength

$E(m)$ is the refractive index of soot

f_v is the soot volume fraction

ρ_{sa} Scattering to absorption ratio

This approximation is based on the knowledge that soot has a branch like aggregate structure and does not aggregate in large spheres [41]. As well, it was proven that, for extinction based measurements, whether the primary particles were considered individually or in an aggregate structure, the soot volume fraction was found to be the same [42].

It is assumed here that ρ_{sa} =0 which was found to be true for small aggregates [41]. The refractive index function for the absorption of soot, E(m), at a wavelength (λ) of 577 nm was taken as 0.258 [39]. This value is still widely disputed and, from values tabulated by Krishnan et al. [43] from different researchers, it is estimated that the uncertainty of this value is ±0.05. The implications of these assumptions will be discussed in section 4.1.

From (Eq. 3-1), we see that the optical extinction coefficient (ke_λ) can be obtained from a tomographic inversion of the data assuming radial symmetry, reconstructing the 2D data from a line of sight measurement. Many techniques exist to do this; however, a study has shown that the three-point Abel inversion technique is optimal in this context [44]. The algorithm presented by Dash [44] was used. Through this process, the soot volume fraction $f_v(r)$ was calculated radially across the flame at 2 mm vertical increments and at every 2 pixel radially using (Eq. 3-2).

This analysis was done using MathCAD to obtain a map of the soot volume fraction in the flame. This map in itself is useful in understanding the different sooting profiles of the mixtures. However, because the different fuels are known to have noticeably different sooting profiles, comparing them solely based on the soot volume fraction or its peak value can be misleading. For example, if the peak soot volume fraction is used, a peak soot volume fraction situated on the annulus region of the flame, as shown in Figure 3-11, actually represents more soot than a peak measured on the centerline of the flame, as shown in Figure 3-12, due to the different areas of the flame associated with these positions.

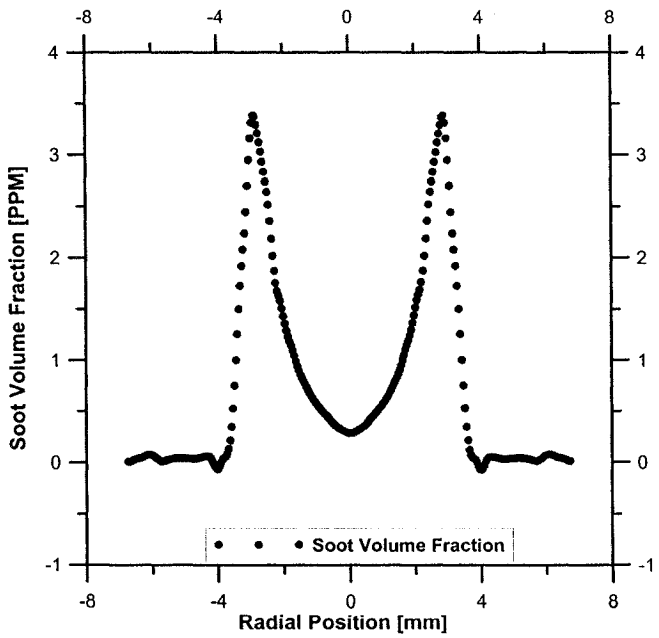

Figure 3-11 Radial Profile of Soot Volume Fraction at Height = 32 mm in Propane Flame

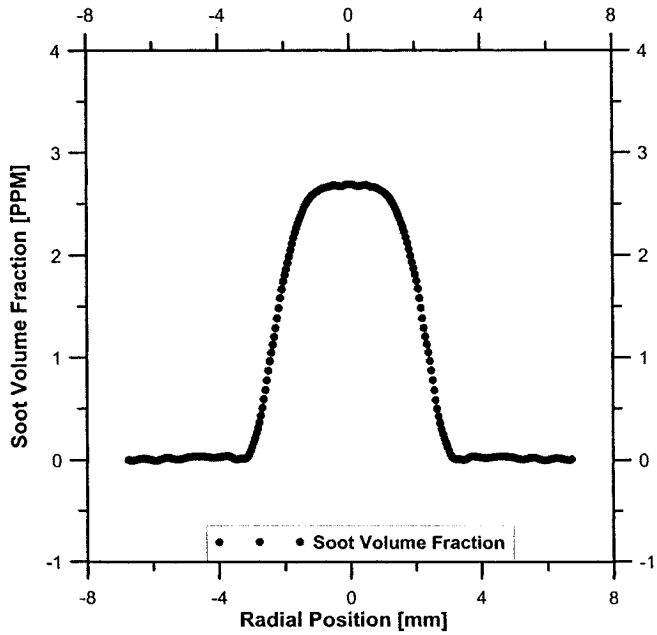

Figure 3-12 Radial Profile of Soot Volume Fraction at Height = 48 mm in Propane Flame

To properly compare the sooting propensity of the different mixtures, it is important to account for the radial variation of soot volume fraction. This effect can be clarified by integrating the soot volume fraction (fv) radially throughout the flame at various positions along the flow direction as follows:

$$F_v(z) = \int_0^R 2\pi r f_v(r,z)dr \qquad \text{(Eq. 3-3)}$$

where $F_v(z)$ is the radially integrated soot volume fraction for a given height
r is the radial position

This value was multiplied by the velocity and the density as to obtain a mass flux of soot.

$$\dot{m}_{Soot} = \rho_s V_z F_v(z) \qquad \text{(Eq. 3-4)}$$

where m_{soot} is the mass flux of soot

ρ_s is the density of soot

V_z is the flow velocity for a given height

The density of soot was taken as 1.9 g/cm^3 which corresponds to the value used in the numerical simulations and is within the range determined by Nishida and co-workers [45]. The velocity was evaluated as follows:

$$V_z = \sqrt{2az} \qquad \text{(Eq. 3-5)}$$

Where a is the flow acceleration, $a = 25m/s^2$ [46].

z is the axial position in the flame

This velocity assumes that the flame is buoyancy driven. This has been demonstrated to apply to both ethylene and methane flames [47, 48] and is assumed in this case to also be applicable to propane flames. Although this buoyancy model is approximate in the lower part of the cooler methane flame, any discrepancy is minor since our focus is on the maximum mass flux of soot corresponding to a higher position in the flame. As well, a comparison of the velocity obtained with this model and the velocity obtained through numerical modeling demonstrated that there is relatively good agreement. The agreement is best on the side of the flame, and larger differences are found on the centreline as shown in Figure 3-13. At the heights of interest, the difference is less than 20%. As well, it is expected that all fuels would have very similar velocity profiles due to similar co-flow air velocities. Therefore, the slight departure of the model from actual velocities is negligible in this relative study.

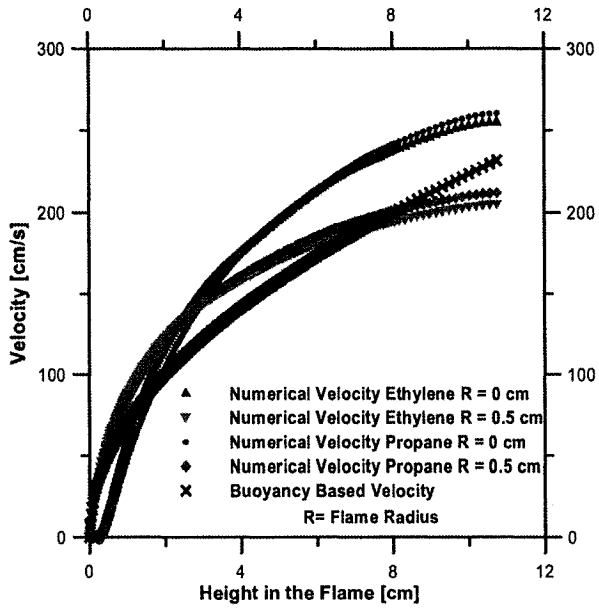

Figure 3-13 Comparison of Numerical and Buoyancy Driven Flow Velocities in Ethylene and Propane Flames

A uniform basis for comparison, the percent carbon conversion or local soot yield (Y_s), can be determined by taking the ratio of the local mass flux of soot at an axial position in the flame to the mass flux of carbon in the fuel as follows:

$$Y_s = \frac{\dot{m}_{soot}}{\dot{m}_{c\_fuel}} \qquad \text{(Eq. 3-6)}$$

where m_{c_fuel} is the mass flux of carbon at the inlet

Y_s is the soot yield

The maximum local soot yield in each flame is a convenient measure by which to compare the maximum production of soot for different fuel mixtures.

3.1.4 Temperature Measurement

3.1.4.1 Thermocouple Setup

Flame temperature measurement is an area that to this day still challenges researchers. The measurement can be very complex considering all variables involved and has led to the development of an impressive number of techniques, mostly optical. However, in this series of experiments, considering the scope of the research, it was found that a thermocouple-based measurement would be the most appropriate method. Thermocouple measurements are known to present significant challenges. However, techniques have been developed that allow an accuracy that was deemed sufficient in the present study without having to resort to the much more involved optical techniques. The technique used here is based on that presented by McEnally et al. [49]. The authors claim that the absolute accuracy of the technique is within 50 K and the relative accuracy is within 5 K [21].

The thermocouple used was an uncoated R-type (Platinum / 13% Rhodium-Platinum) thermocouple supplied by Omega with a junction of about 240 μm. It should be noted that since this is a diffusion flame, catalytic effects are expected to be negligible. The diameter of the thermocouple leads was 75 μm which minimized conduction errors while allowing easy manipulation of the thermocouple compared to smaller diameter wires. The thermocouple was mounted on a variation of the bracket initially proposed by Cundy et al. [50]. The present thermocouple was inserted in the flame by a pneumatic rapid insertion system, shown in Figure 3-14, having a travel distance of 1" functioning with nitrogen pressure. This was done to minimize the deposition of soot during insertion.

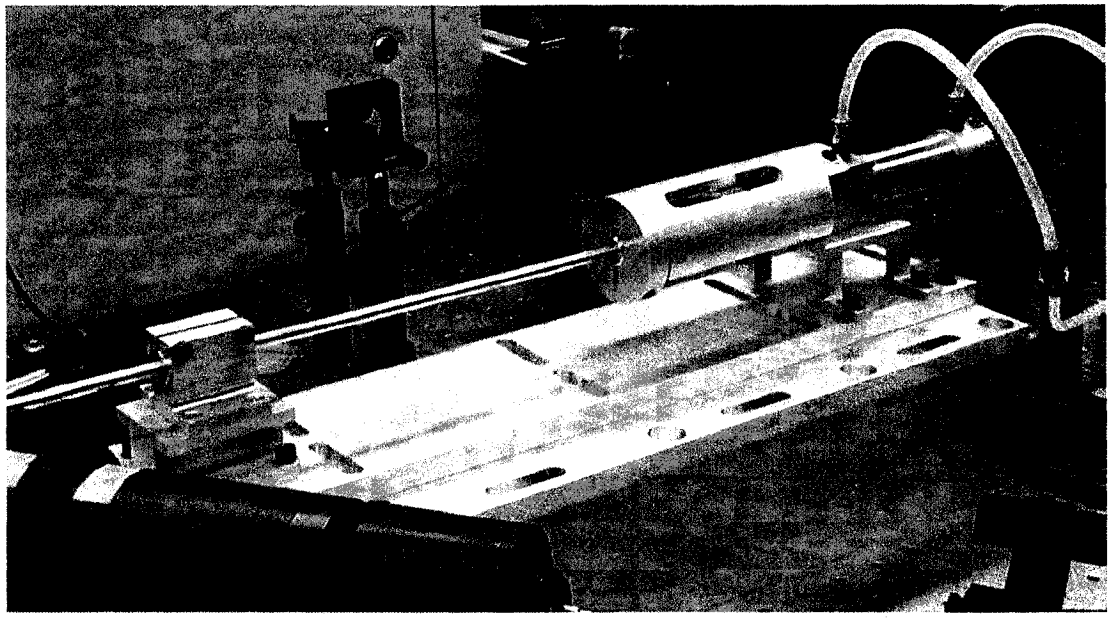

Figure 3-14 Pneumatic Rapid Insertion System

The travel distance was sufficient so that the thermocouple did not disturb the flame when retracted. When inserted in the flame, the stretched length of thermocouple was long enough to ensure that the ceramic tubes did not disturb the flame itself, although the surrounding air flow was disturbed. It was found that the ceramic tubing size had a noticeable influence on the strength of this disturbance; accordingly, the smallest ceramic tubes that could endure the shock of rapid insertion were used. Because of the force of the system as it is activated and of the fragility of the thermocouple, it was found that the insertion system had to be slowed down with a valve limiting the nitrogen flow. The resulting insertion time, measured with a video camera, was 0.6 s. The transient response time for the thermocouple was estimated to be 0.2 s [49].

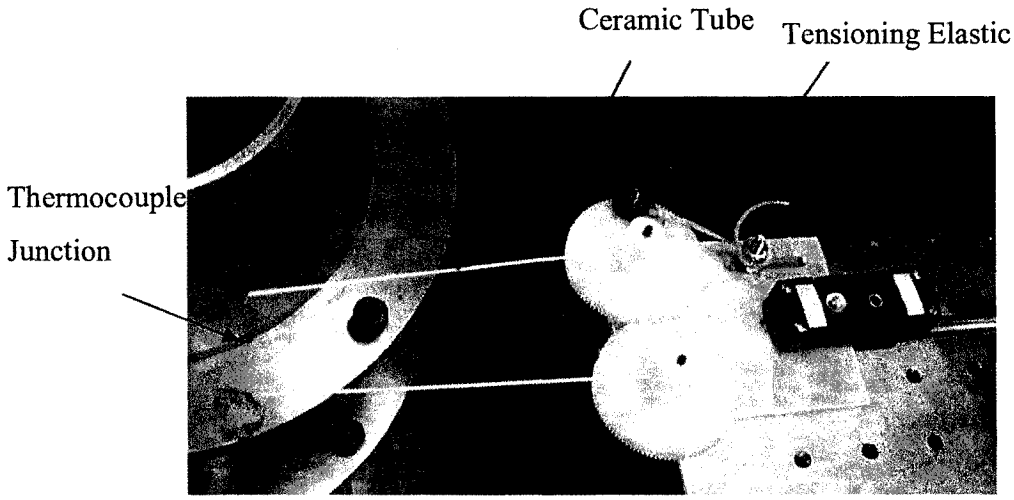

Figure 3-15 Thermocouple Setup

To maintain accurate vertical position and ensure that no sagging occurred when the thermocouple was inserted in the flame, the thermocouple was kept in tension using one elastic connected to a gear system as shown in Figure 3-15. The gear system ensured that both thermocouple leads were pulled by equal amounts, maintaining the centering of the thermocouple. The leads were connected to a thermocouple extension and measured by a data acquisition card connected to LabVIEW. The DAQ card had an onboard cold junction. The LabVIEW program controlled the rapid insertion system through a pulse and correlated the data acquisition to the insertion and retraction sequence. Soot deposition was an issue throughout the measurements. To remove the soot from the thermocouple leads and bead, the thermocouple was inserted, following each measurement, in an oxidation region of the flame, near the tip of the flame for an extended period of time (10 s). It was verified, through repeatability measurements, that the thermocouple was properly cleaned in this fashion.

3.1.4.2 Temperature Correction

The junction temperatures measured had to be corrected for the time response and soot deposition. To account for this, the behaviour of the measurement over the time of insertion was observed. The first step was to correct for the soot deposition which is known to have a very big impact on the measurement. Soot deposition tends to reduce the measured temperature in a linear fashion over time [49]. As well, it was essential to account for the radial profile of the temperature in the flame. In the lower portion of the flame, a high temperature region exists in the outside annulus of the flame. Higher in the flame the temperature peaked in the centerline illustrated in Figure 3-16. This was significant since the thermocouple had to traverse this annular region to reach the centre of the flame.

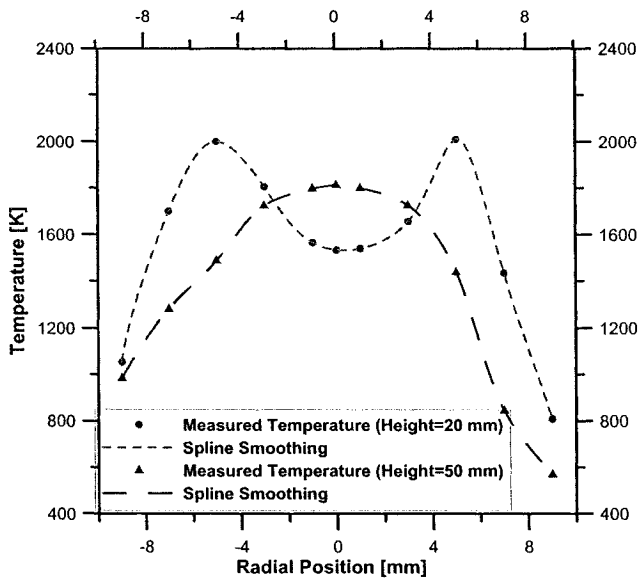

Figure 3-16 Radial Temperature Profile in Ethylene Flame

The temperature-time profile was analyzed to account for these phenomena. A sample temperature-time profile of a flame centreline temperature measurement at a height of 20mm in shown in Figure 3-17. The first peak in the flame temperature is interpreted as being the temperature measured through the high temperature annular region of the flame. Following this peak, the temperature is seen to have a linear descending slope, which would be the steady soot deposition stage once the thermocouple is in place. There is another temperature peak seen at the end of the insertion time when the thermocouple junction is retracted through the annular region.

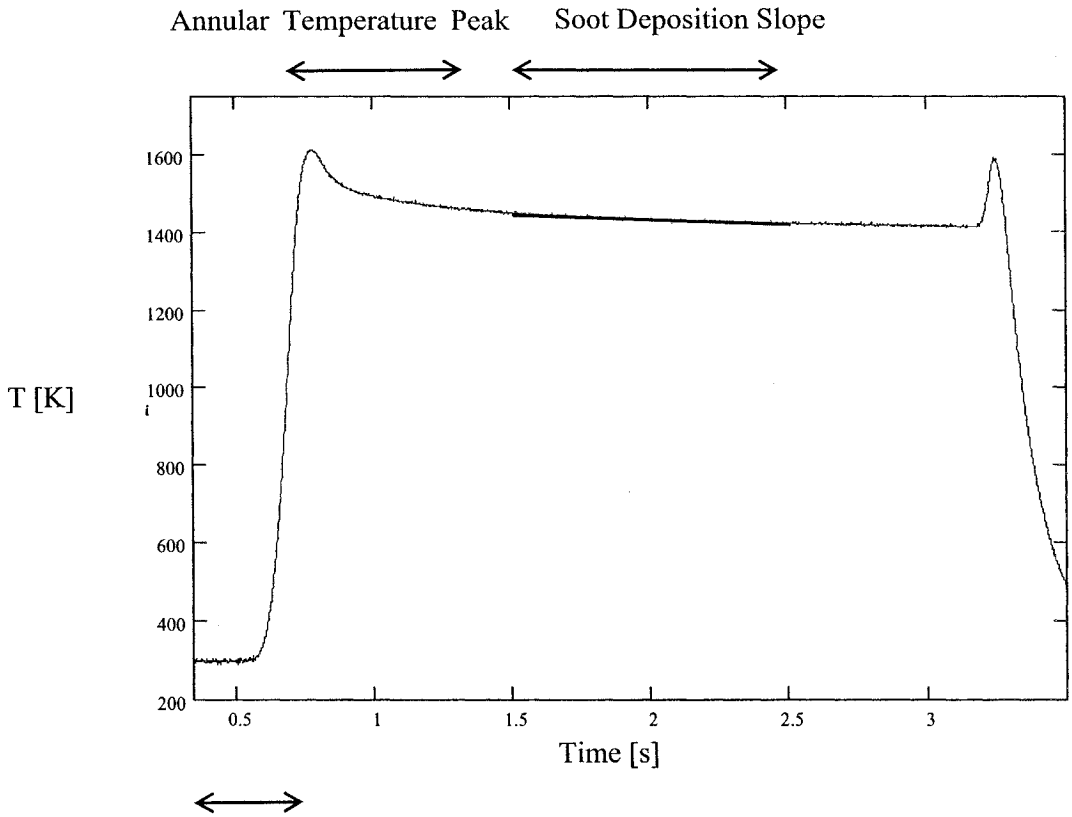

Figure 3-17 Centreline Temperature Measurement over Time (Height=20mm)

Higher in the flame, the temperature peaks in the centreline as previously demonstrated. Therefore, no peak temperature is found as the thermocouple is inserted or retracted as shown in Figure 3-18. As well, it is apparent from the soot deposition slope that temperature is less affected by soot deposition higher in the flame.

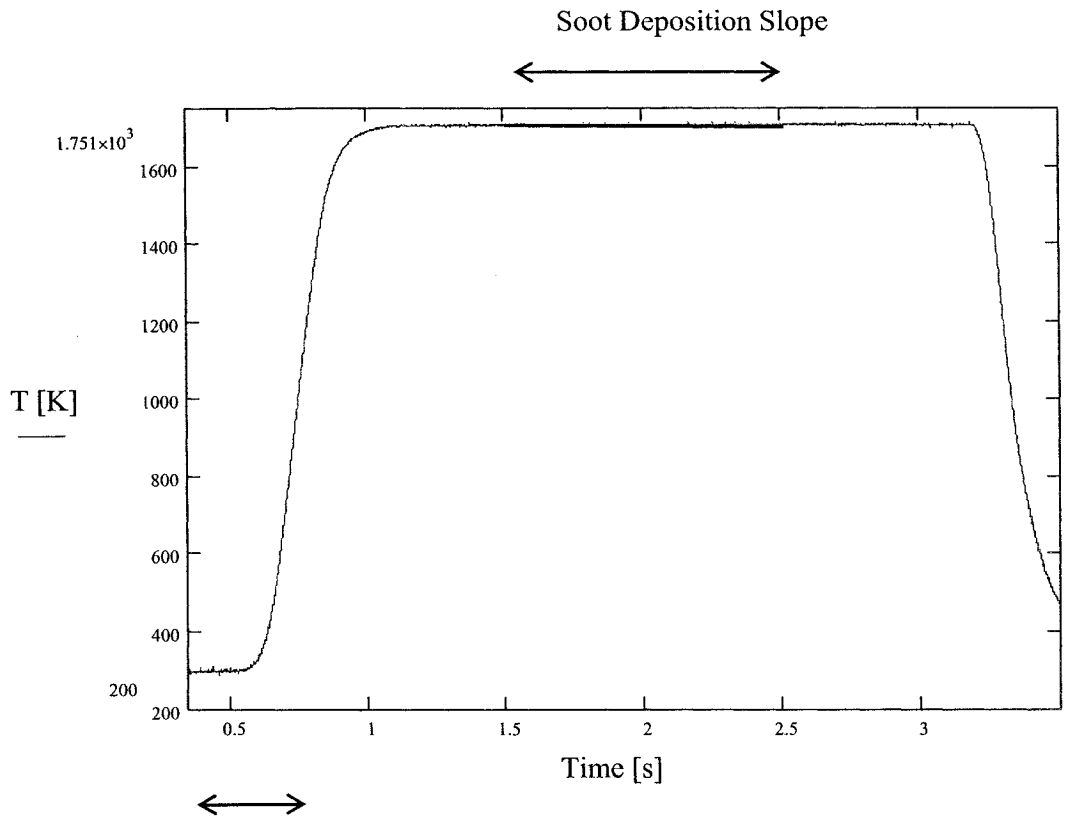

Figure 3-18 Centreline Temperature Measurement over Time (Height=50mm)

To correct for these effects, the data were smoothed and the slope was calculated over a time period of a second, from 1.5 to 2.5 seconds. Using this slope, the temperature at the initial point of insertion can be found by estimating the time of initial measurement in the desired position. This time is found by adding the time it takes to insert the thermocouple in the desired position as well as its transient response time. The "initial temperature" traced back in this fashion is the junction temperature which can then be correlated to the gas temperature. This is done according to the analysis presented by McEnally et al [49] which assumes that the conduction in the thermocouple wires, radiation to the junction and heat generation resulting from surface reactions is negligible. The energy balance at the junction is [49]:

$$\varepsilon_j \sigma T_j^4 = \frac{K_{g_0} Nu_j}{2d_j}(T_g^2 - T_j^2) \qquad \text{(Eq. 3-7)}$$

where ε_j is the temperature dependent junction emissivity

σ is the Boltzmann radiation constant

T_g is the gas temperature

T_j is the junction temperature

K_{g0} is the slope of the temperature dependent gas thermal conductivity

Nu_j is the junction Nusselt number

d_j is the junction diameter

Where the left hand side represents the radiation heat loss per unit area of the junction, and the right hand side is the convection heat gain per unit area. Typically, the velocity in the flame is 1 m/s, yielding a Peclet number at the junction of about 0.6. From the low Peclet number expansion for spheres from Acrivos and Taylor [51] the corresponding Nusselt number was found to be 2.26 [49]. The emissivity was based on measurements over a temperature range of 600 to 1450K done on S type thermocouples [52] which have a composition similar to the thermocouples used here. These values were interpolated to yield the temperature dependent values used in this analysis.

It should be noted that:

$$K_{g_0} = \frac{K_g}{T_m} \qquad \text{(Eq. 3-8)}$$

where K_g is the gas thermal conductivity

T_m is the mean temperature

The slope of the temperature dependent thermal conductivity was based on a linear fit the thermal conductivity of air and was found to be $6.54^* 10^{-5}$ W/mK^2 [49]. The values used in this analysis for emissivity, diameter and Nusselt number do not account for soot deposition; extrapolating back to the 'initial temperature' minimizes this error.

3.2 *Numerical Simulation Setup*

3.2.1 Two Equation Soot model

The purpose of this study was to understand the underlying interactions in the sooting propensity of binary fuel mixtures. Experimental results have yielded interesting insight in the behaviour, but to fully understand the phenomena it is important to know the underlying species behaviour. An experimental assessment of all the species of interest is impossible; however, numerical simulations allow an in-depth analysis of the species behaviour and the different reactions involved. To understand the synergistic effect that was experimentally measured in certain mixtures, the ethylene/propane mixtures were modeled since these represented the strongest synergistic effect.

The numerical code used to model the diffusion flame was developed by Guo et al. [53]. This model solved a 2D problem representing the centreline of half of the burner used in the experiments. The meshing density was 87x186 nodes distributed as shown Figure 3-19 as to optimize the positioning of the nodes in the regions of interest. It was found that, due to RAM limitations, this mesh density corresponded to the maximum that could be solved with our computational capabilities. It should be noted that for this mesh density, the convergence time was about 3 weeks on a 2.8 GHz Pentium 4 computer.

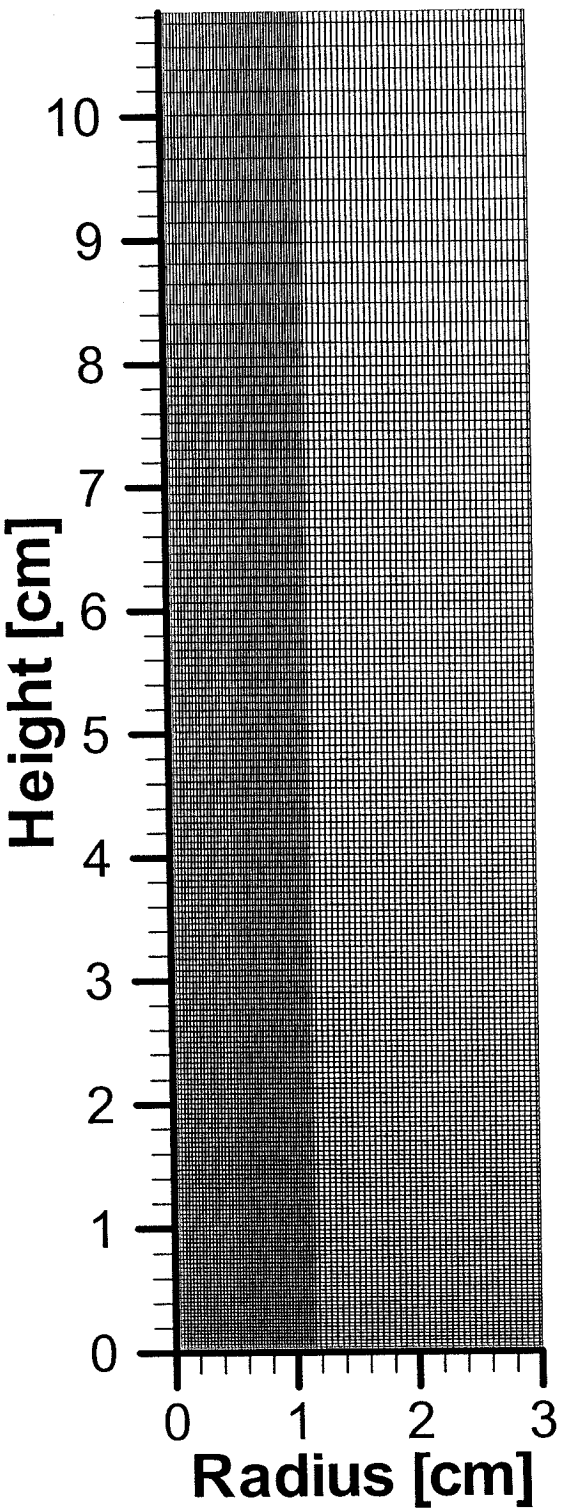

Figure 3-19 Grid for Numerical Simulation

The chemical kinetic model used had to be changed because, in this case, the model had to account for the species encountered in our simulation resulting from the propane fuel. The model presented by Qin et al. [35] was chosen since it was optimized for C_3 species combustion. Although the model was seen by the authors to agree well with experimental ignition delays and flame speed, some rates had to be modified in this case to obtain flame heights and soot concentrations consistent with our experimental results. The modified reaction rates are listed in Table 3-2 where $K=AT^n\exp(-E/RT)$. For full set of reaction rates, please see Appendix A.

Table 3-2 Modified Reaction Rates

Reactions	Reaction Rate Parameters			Relative Difference in K
	A (mol, cm3, s)	n	E (cal/mol)	
[397] $C_3H_3 + C_3H_3 \Leftrightarrow C_6H_5 + H$	3.00 E + 11			K[36]/ 6.67
(Original Reaction Rate Qin [35])	(10.20 E + 12)			
[398] $C_3H_3 + C_3H_3 \Leftrightarrow C_6H_6$	5.00 E + 10			K[36]/ 6.67
(Original Reaction Rate Qin [35])	(5.78 E + 12)			
[400] $n\text{-}C_4H_3 + C_2H_2 \Leftrightarrow C_6H_5$	3.20 E + 03	2.9	1400	K[8]x1.14
(Original Reaction Rate Qin [35])	(9.6 E + 70)	(-17.7)	(313)	
[403] $n\text{-}C_4H_5 + C_2H_2 \Leftrightarrow C_6H_6 + H$	3.20 E + 03	2.9	1400	K[8]x1.14
(Original Reaction Rate Qin [35])	(1.6 E + 16)	(-1.33)	(5400)	

The soot model was also changed. Owing to computational considerations, an extensive soot model like that developed by Wang and Frenklach [6] could not be implemented. The simpler two-equation model developed by Leung and Lindstedt [54] and Fairweather et al. [55] was therefore chosen as a viable option. This model is called a two-equation model because it uses two transport equations to solve for the soot mass fraction and soot number density. However, this implementation was somewhat different from the original model and was based on that presented by Guo et al. [56]. Contrary to the original model, in this implementation, the inception calculation is not based on the acetylene concentration but on the benzene and phenyl concentrations as proposed by Beltrame et al. [36]. This inception

model then accounts for different pathways to first ring formation, including those involving odd-carbon numbered species, not only acetylene-based paths. The phenyl concentration is present to account for the formation of complex PAHs from this species. The soot inception is therefore based on the following reaction:

$$C_6H_6 + C_6H_5 \Leftrightarrow 12C(s) + 5H_2 + H \qquad \text{(Eq. 3-9)}$$

The reaction rate found to reproduce experimental results accurately in this case was:

$$k_i = 16.0E + 17 \exp(\frac{-21000}{T}) \qquad \text{(Eq. 3-10)}$$

The soot surface growth was modeled according to the HACA (hydrogen abstraction, carbon addition) mechanism [57]. For both the surface growth and oxidation, the model used was as presented by Guo et al. [56]. However, the parameter α which represents the fraction of the reactive surface sites available for reaction was modeled by a temperature dependent expression, similar to that presented by Kazakov et al. [58]. In this case, α was calculated as:

$$\alpha = (\tanh(\frac{8168}{T} - 4.57) + 1))/1.34 \qquad \text{(Eq. 3-11)}$$

As well, in this case, the number of carbons found in an incipient soot particle (Ca) was taken as 32. This is consistent with the assumption made by Frenklach [9] who considers the four ring aromatic (pyrene) the precursor to soot nucleation.

It should be noted as well that work by Guo et al. [53] has concluded that the preheating of the fuel in the fuel nozzle should be considered in the modeling of the flame. Therefore, all initial inlet conditions were obtained from a simulation accounting for the preheating of the fuel in the fuel tube.

4 RESULTS

4.1 Experimental Results

The 2D LOSA technique yielded maps of the soot volume fraction in the flame. This preliminary experimental data was gathered to provide an initial overview of the sooting behaviour of the different mixtures. Commonalities were found among the sooting profiles of all the fuels. As explained previously, the first step in the sooting process of all flames is the pyrolysis of the fuel; this will occur in the lower part of the flame, near the burner. Following this, soot will start forming in the lower part of the flame on the outside of the flame where the combustion occurs. The soot formed will then go through the growth process described and, as it is in contact with oxygen in a high temperature region, will start oxidizing. As this occurs, soot will start forming on the centerline of the flame and will subsequently oxidize. This process is illustrated in Figure 4-1.

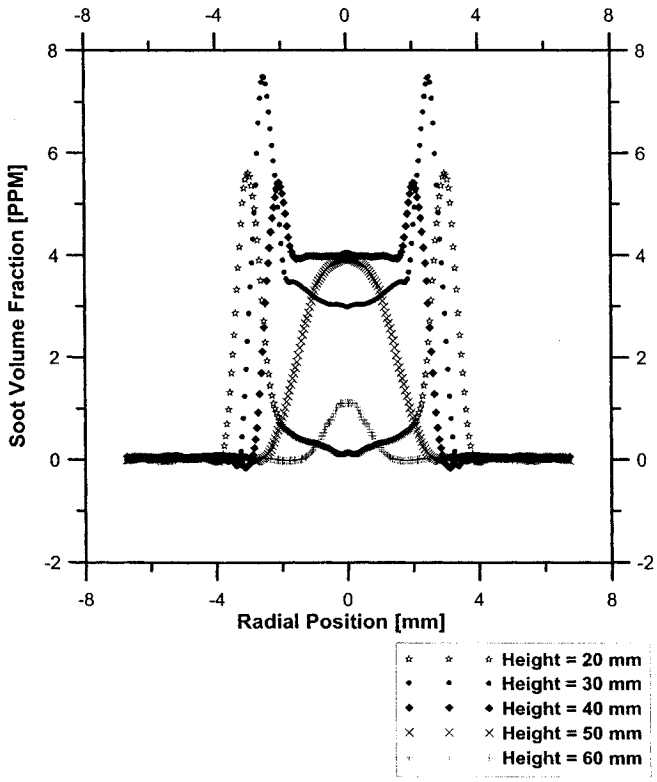

Figure 4-1 Ethylene Flame Sooting Profile over Flame Height

Although this is common to all fuels, the relative importance of the different regions varies. For the ethylene flame, the maximum soot volume fraction is on the outside of the flame and is found at a flame height of 30 mm. For the methane flame, the maximum soot volume fraction is found higher in the flame, at a height of 48 mm, on the centerline of the flame. The resulting soot profile over height for the methane flame is illustrated in Figure 4-2.

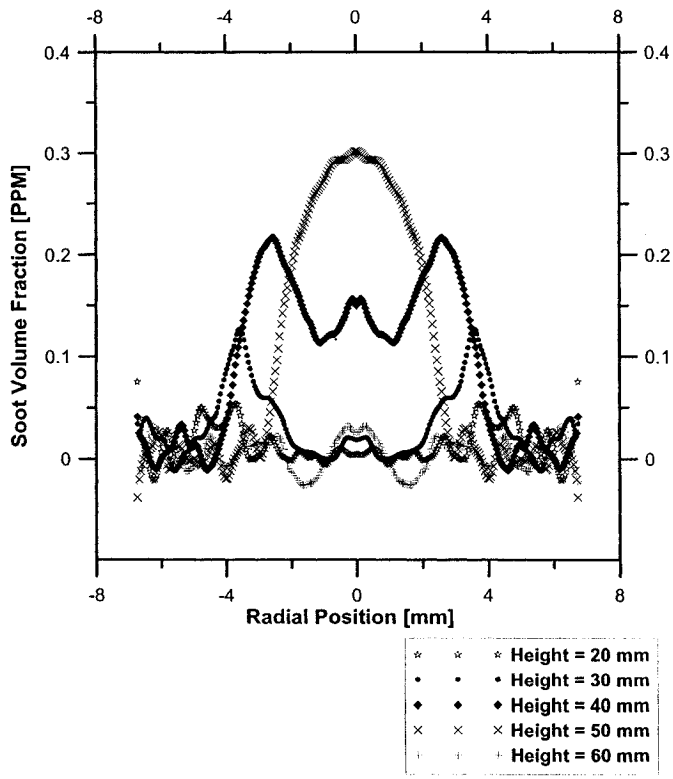

Figure 4-2 Methane Flame Sooting Profile over Flame Height

It is important to remember here that the spatial resolution of the experimental measurement is 22.4 μm, this high resolution yield further confidence in the fact that the different radial sooting profiles are accurately represented. The different behaviours of the fuels are illustrated in Figure 4-3 where the peak soot volume fraction is plotted over flame height.

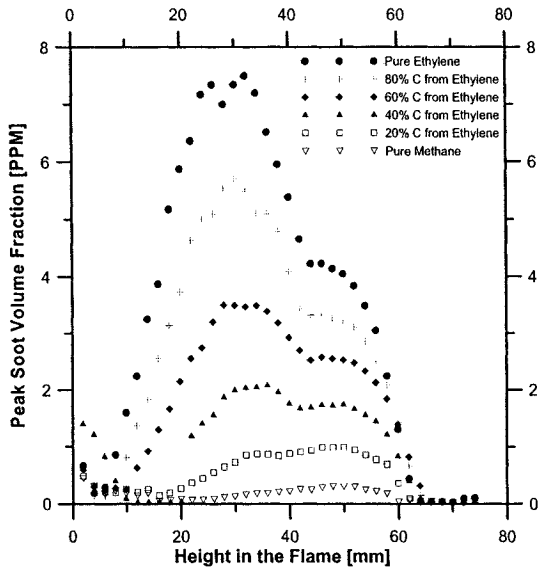

Figure 4-3 Peak Soot Volume Fraction over Height of Flame for Methane/Ethylene Mixture

Knowing that a peak soot concentration lower in the flame is on the side of the flame, and that a peak higher is on the centreline, this figure can be interpreted as indicating a shift of the peak soot volume fraction from a radial position on the side of the flame to the centre of the flame over the mixture range. Interestingly, for the propane flame, the peak soot volume fraction over height shown in Figure 4-4 indicates that the soot volume fraction on the outside of the flame and in the centerline are similar, inducing a strong bimodal behaviour.

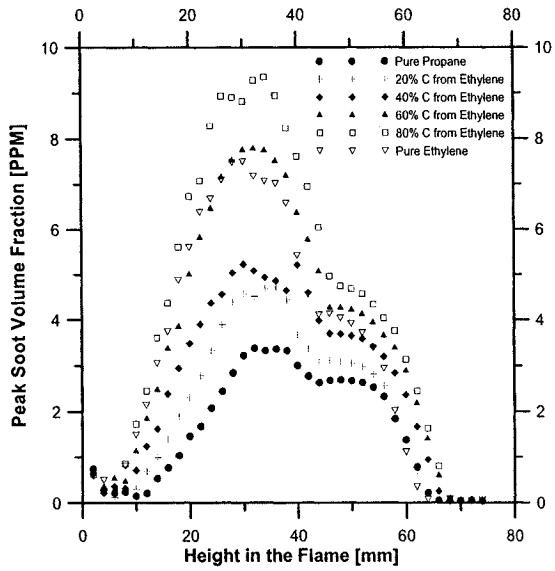

Figure 4-4 Peak Soot Volume Fraction over Height of Flame for Propane/Ethylene Mixture

This reinforces the need to obtain the soot yield. As explained previously, the soot yield at a given height is the mass flux of soot at that height divided by the carbon mass flux obtained from a radial integration of the soot volume fraction multiplied by the density of soot and the velocity at this height. The radial integration weighs the relative area of the location of peak soot concentration.

It was also noticed that the measurements in the lower part of the flames indicated the presence of significant amounts of soot. For low sooting flames like those of methane, this value was larger than the maximum soot volume fraction found in the higher part of the flame. However, during experiments, the lower portion of the methane flame was seen to be blue, indicating the absence of soot. However, soot precursors could be present at this height. As well, the noise in this region of the flame is high. This noise also resulted in the measurement of negative amounts of soot which is physically impossible.

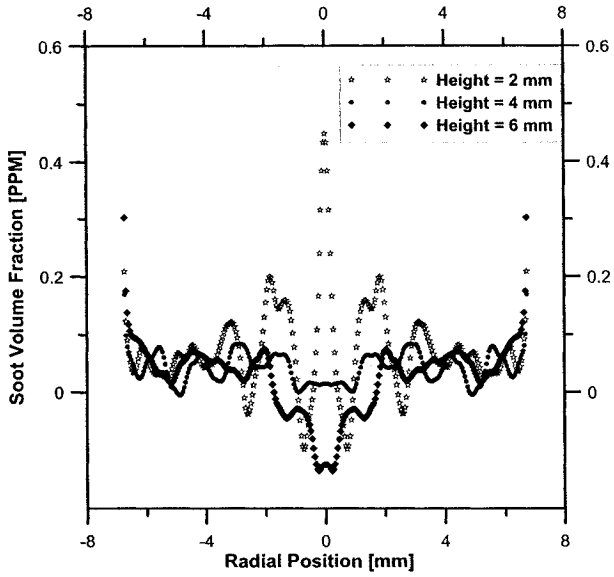

Figure 4-5 Methane Flame Sooting Profile over Flame Height 2 to 8 mm

However, even for low sooting flames, the 2D LOSA technique was found to have very good repeatability as illustrated in Figure 4-6. The standard deviation is found to be higher in the lower and top portion of the flame for the peak soot volume fraction. The soot concentration in these regions is smaller, leading to larger noise to signal ratios. However, in the main portion of the flame where the soot concentration is higher, the standard deviation is negligible for both the peak soot volume fraction and soot yield. Please refer to section 3.1.3.2 for the method used to calculate soot yield. The methane flame data shown has the smallest soot concentration; this should represent the worst case for noise to signal ratio and repeatability. It should be noted that these measurements where done over two days to ensure day to day repeatability.

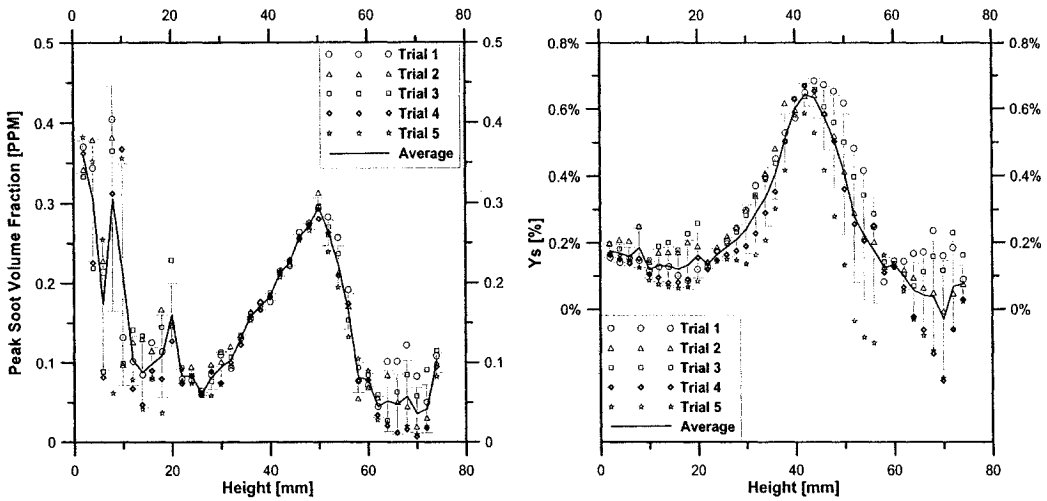

Figure 4-6 Repeatability of Measurement in Methane Flame

It should be noted that there is a number of uncertainties associated with this technique. A significant variable is the value for the refractive index function for absorption (E(m)). This value is still not fully agreed upon, however, it was determined that this value is expected to be the same for a given wavelength for all fuel type [43]. Therefore, since the relative behaviour is considered in this study, this uncertainty is thought to be negligible. Another source of uncertainty in this technique is the assumption that scattering from the soot particles would be negligible. This was found to be true for small aggregates, but subject to larger uncertainties as the aggregate size grew [41]. It is therefore estimated that for all the fuels studied, ethylene, having the largest soot concentration would also have the largest aggregate size, leading to the largest uncertainty. The scattering to absorption ratio in an ethylene flame at this wavelength was found to be 0.3 [43], leading to an maximum error of 23%. As explained previously, this is the worst case scenario for all the fuels studied. Another potential source of uncertainty would be the inversion mechanism. This is known to amplify the experimental noise. This is more dramatic in the centreline region of the flame [59], in the first 10% of the radial location. Outside of this region, the noise amplification is comparatively small. The radial integration performed in the processing of the results minimizes this random error.

The map of soot profiles illustrated in Figure 4-7 illustrates the major differences in the sooting behaviour of the different fuels.

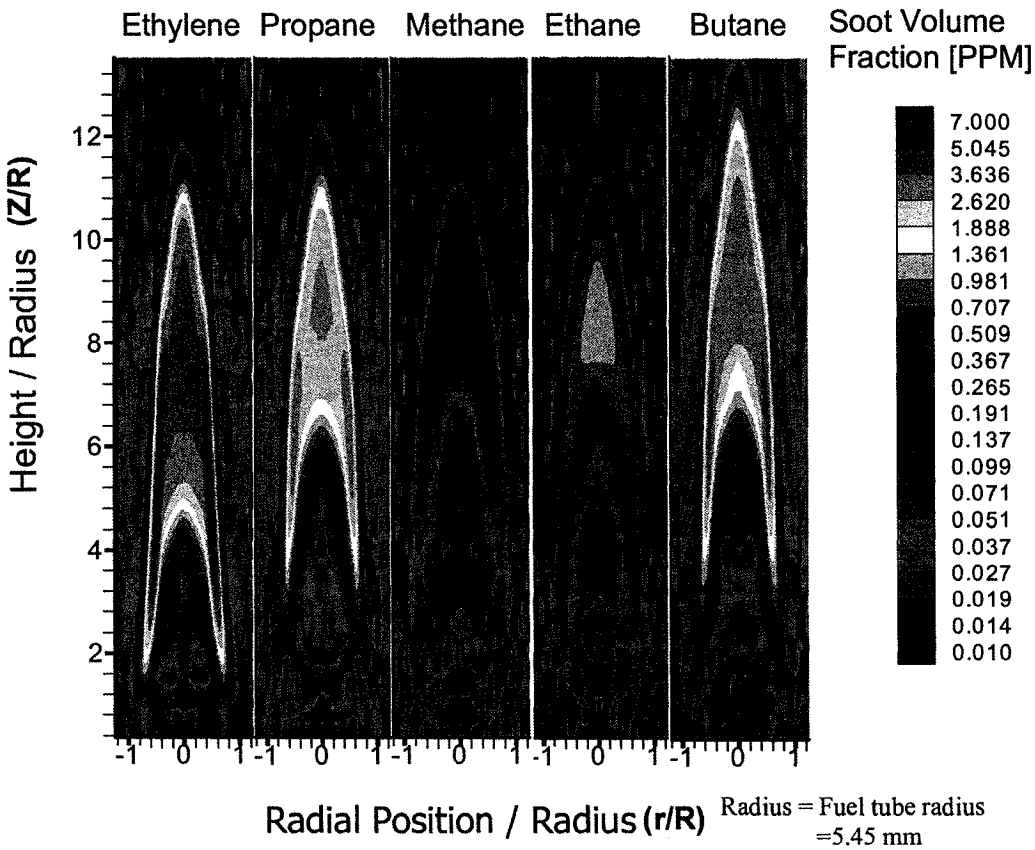

Figure 4-7 Soot Profile of Ethylene, Propane, Methane Ethane and Butane Flame

The butane flame has the highest flame height for the fuels tested. The methane flame is the shortest flame but is more bulbous at the top portion of the flame. As well, with the soot maps, the regions of maximum soot production can easily be identified. For the methane and ethane flame, this region is on the centerline in the top part of the flame. For ethylene and butane, this region is on the side of the flame. Again, for propane the soot concentrations measured in the annular region and on the centerline are similar. It is important to consider all these parameters when attempting to assess the sooting behaviour over mixture ranges of these fuels.

4.1.1 Ethylene / Propane Mixtures

The presence of a synergistic effect in the sooting propensity of a fuel mixture of ethylene (C_2H_4) and propane (C_3H_8) has been previously identified [30]. It was the purpose of this experiment to confirm and further elucidate this effect by using a different optical diagnostics method and a different type of flame. As well, these experimental results provided a basis for the validation of the numerical simulations.

The flame height was seen to vary slightly over the mixture range as shown in Figure 4-8, indicating that the residence time in the flames might be slightly different over the mixture range. Using the acceleration previously presented in section 3.1.3.2, it was estimated that the difference in residence time between a flame height of 62 mm and 68 mm is 0.003 seconds, representing a difference of 5% over the total estimated residence time. It was therefore assumed that this variation was small and no correction was done for the residence time variation.

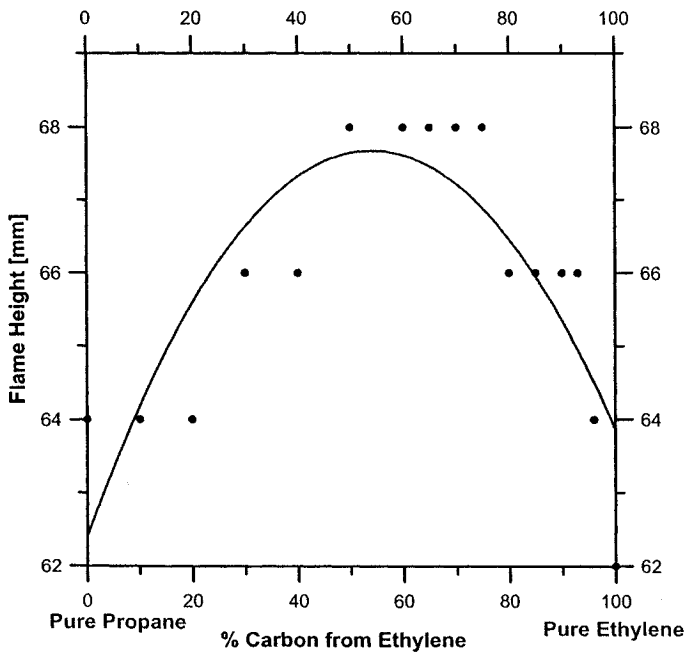

Figure 4-8 Flame Height over Mixture Range (The line represent a quadratic fit of the data)

In the case of ethylene/propane mixture, both the peak soot volume fraction and the soot yield demonstrated a very strong synergistic effect as shown in Figure 4-9 and Figure 4-10. As explained previously, it is thought that the peak soot volume fraction is not a valid comparison basis for the different mixtures, it is presented here for comparison with results obtained by previous researchers which have used this value [30]. However, due to reasons presented previously, the soot yield is considered more accurate.

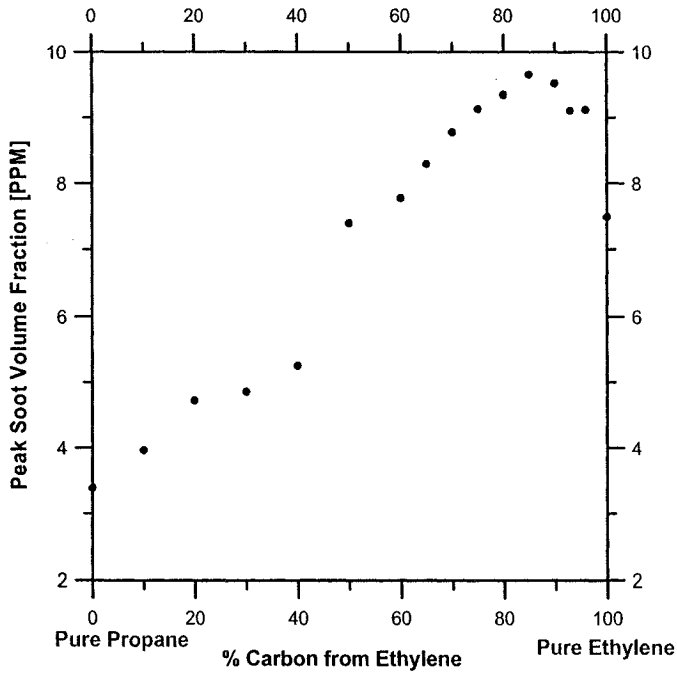

Figure 4-9 Peak Soot Volume Fraction over Ethylene/Propane Mixture Range

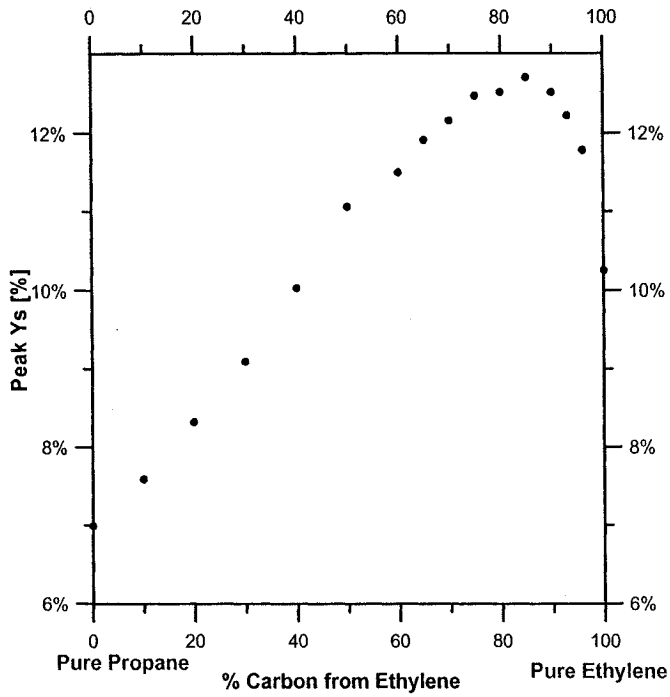

Figure 4-10 Soot Yield over Ethylene/Propane Mixture Range

The peak soot volume fraction showed a very noticeable synergistic effect when the percent carbon in the fuel obtained from ethylene was between 60% and 100%. The maximum value was found at a mixture of 85%. This agrees with the findings of Hwang et al. [30]. The peak soot volume fraction at a mixture of 85% was measured to be 9.7 PPM, a 29% increase from the peak soot volume fraction measured for a pure ethylene flame which was 7.5 PPM. This increase is similar to the increase of the peak soot volume fraction reported by other researchers in the counter flow flame which was 31% [30].

The soot yield calculated showed this same effect, and again, the peak value was obtained at a mixture where the contribution of carbon from ethylene was 85%. At this point, the soot yield was 12.0%, an increase of 16.5% over the pure ethylene soot yield of 10.3%. These increases indicate a considerable synergistic effect resulting from the addition of a small quantity of propane.

4.1.2 Methane / Ethylene Mixtures

Since the ethylene/propane (C_2H_4/C_3H_8) mixture demonstrated a very strong synergistic effect, we would expect the methane/ethylene (CH_4/C_2H_4) mixture to exhibit a similar behaviour. As mentioned previously, some researchers had attempted to measure this effect in a co-flow diffusion flame but had found that the behaviour of the peak soot volume fraction over the mixture range was linear [30]. Other researchers have successfully identified a synergistic effect of the peak soot volume fraction in this mixture by keeping the adiabatic flame temperature constant through dilution [33].

Our first attempt in analyzing this mixture was done without controlling the flame temperature. An initial look at the peak soot volume fraction indicates a non-linear behaviour over the mixture range as shown in Figure 4-11 but did not indicate a synergistic effect.

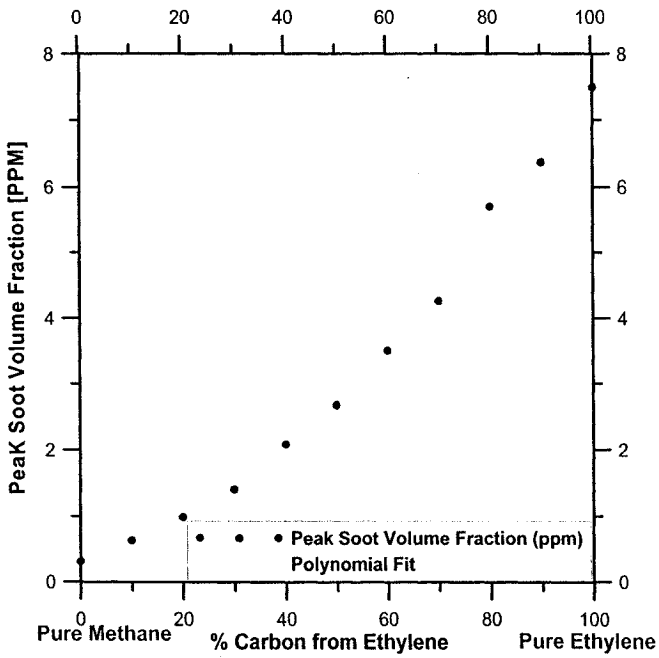

Figure 4-11 Peak Soot Volume Fraction over Methane/Ethylene Range

However, as mentioned previously, for ethylene, the peak soot volume fraction is lower in the flame, in the annular regions, whereas for methane, the peak soot volume fraction is higher in the flame, in the center region. This indicates that the peak soot volume fraction is not the optimal comparison basis for these different flames and highlights the need to account for the relative amount of soot these different behaviours represent by calculating the soot yield. It was found that, contrary to the peak soot volume fraction, the soot yield showed the possible presence of a synergistic effect when it is compared to a linear behaviour as shown in Figure 4-12. This confirms that it is essential to compare the different sooting behaviours of the fuel mixtures based on the soot yield to uncover any underlying effect that may not be visible when only the peak soot volume fraction is considered.

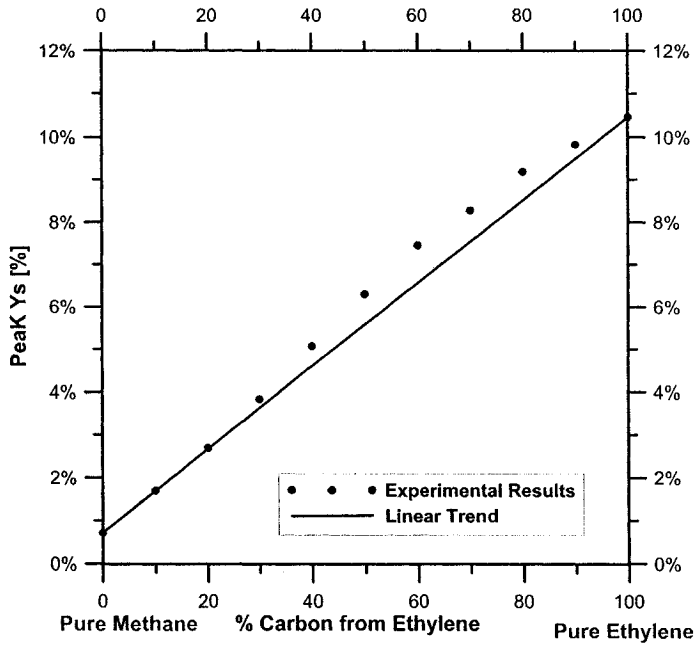

Figure 4-12 Peak Soot Yield over Methane/Ethylene Fuel Mixture

There is an obvious pattern in the deviation from the linear fit of the soot yield. The percent deviation from linear fit is plotted in Figure 4-13 to illustrate this trend clearly.

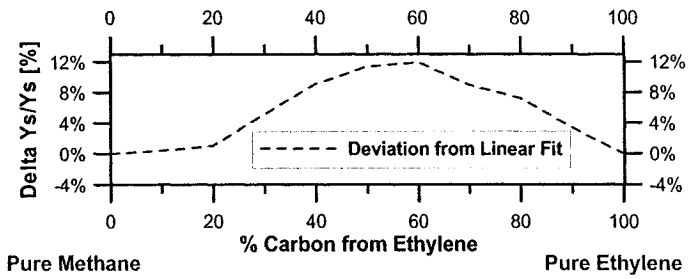

Figure 4-13 Deviation from Linear Fit of Soot Yield over Methane/ethylene Mixture Range

Although a synergistic effect could not be identified in the peak soot volume fraction over the mixture range in these experiments, it is present when considering soot yield. Other researchers have found such an effect in the peak soot volume fraction but only when the mixture was kept under constant adiabatic flame temperature [33]. It is then possible that the synergistic effect is masked and diminished by the flame temperature variation. The calculated adiabatic flame temperature is seen to vary over the mixture range by about 150 K as shown in Figure 4-14.

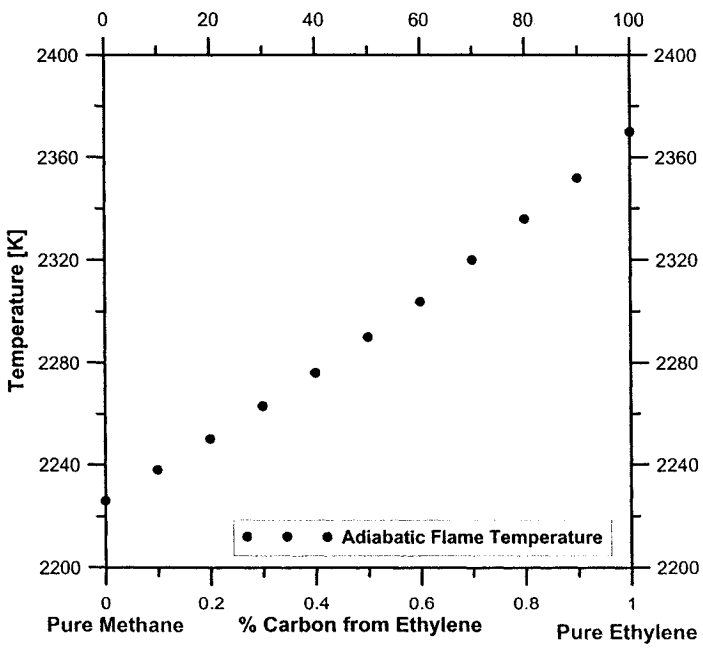

Figure 4-14 Adiabatic Flame Temperature over Methane/ethylene Mixture Range

This prompted interest in measuring and controlling this variable. The temperature variation could be, according to the adiabatic flame temperature, large enough to obscure the synergistic effect. Therefore, to confirm the presence of a synergistic effect, the removal of the flame temperature as a variable is essential.

4.1.3 Methane / Propane Mixtures

To clarify if in fact the synergistic effect was due to an interaction between even-carbon numbered species and odd-carbon numbered species, the sooting behaviour of the methane/propane (CH_4/C_3H_8) mixture, composed of two odd-carbon numbered species, was observed. Because of the nature of the fuels, it is expected that the production of even-carbon numbered species is minimal in both these fuels compared to ethylene. Therefore, if an interaction between even and odd carbon species in the pathways to soot formation induces the synergistic effect, it is expected that such an effect would not be seen over the range of methane/propane mixtures because odd-carbon numbered species are dominant. Our measurements indicated that in fact, for methane/propane mixtures, no synergistic effect was present. The peak soot volume fraction behaved linearly within noise limitations over the mixture range as shown in Figure 4-15.

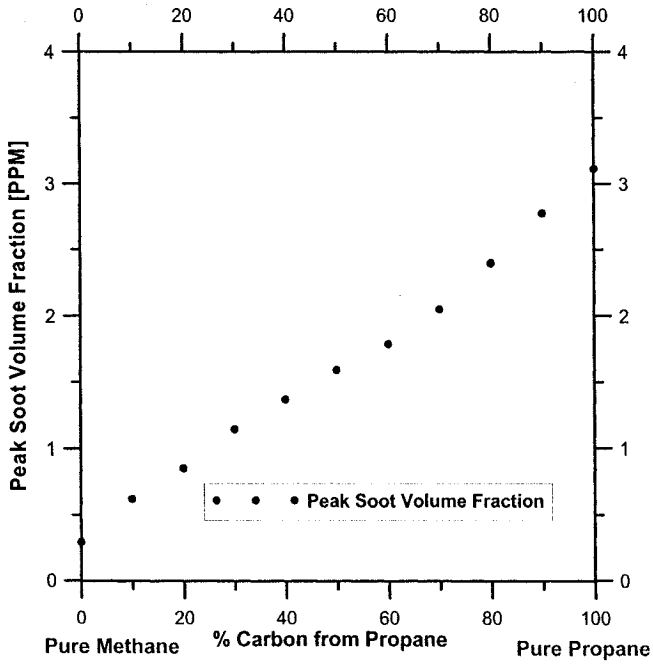

Figure 4-15 Peak Soot Volume Fraction over Methane/Propane Range

To account for the different sooting behaviours over the mixture range, the soot yield was also calculated and is illustrated in Figure 4-16. The deviation from the linear fit is not conclusive as to a synergistic trend. As well, it was found that, although the calculated percent deviation was of a similar range as to that found for the methane/ethylene mixture, considering the small signal to noise ratio for these low sooting fuels, the difference in an absolute sense could not be considered significant.

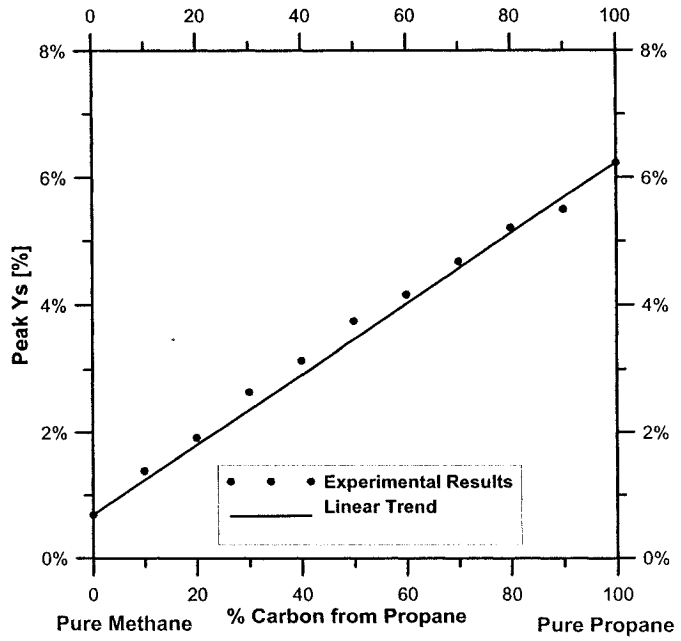

Figure 4-16 Peak Soot Yield over Methane/Propane Mixture Range

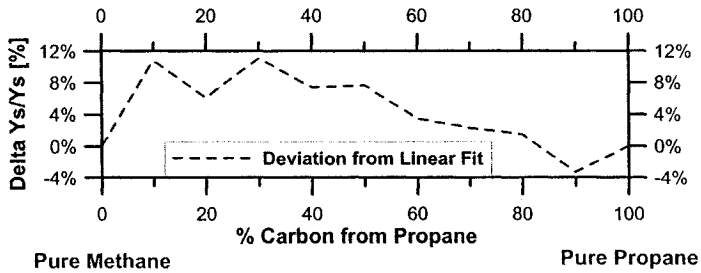

Figure 4-17 Deviation from Linear Fit of Soot Yield over Methane/Propane Mixture Range

From these measurements, no synergistic effect is apparent. The absence of such an effect is evidence that the synergistic effect measured in the propane/ethylene and methane/ethylene mixtures may in fact be due to an interaction between even and odd-carbon numbered species in the pathways to soot formation.

4.1.4 Methane / Ethane Mixtures

The sooting behaviour over the mixture range of the methane/ethane (CH_4/C_2H_6) mixtures was assessed. The soot yield indicated the presence of a strong synergistic effect as illustrated in Figure 4-18. It was expected that ethane (C_2H_6) pyrolysis would lead to high concentrations of even-carbon numbered species and that therefore the path to the first ring formation for the ethane flame would be dominated by the acetylene-based pathways.

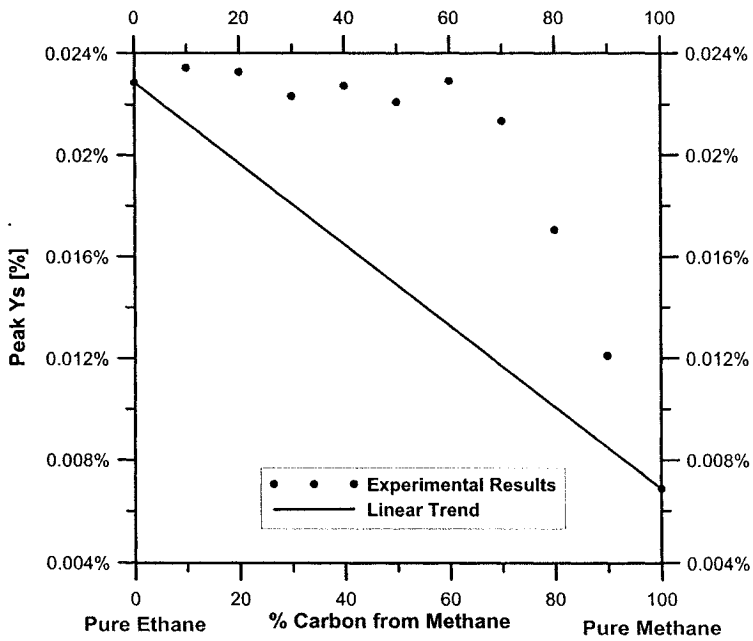

Figure 4-18 Soot Yield over Methane/Ethane Mixture Range

The presence of a synergistic effect again hints at an interaction between odd- and even-carbon numbered species in the pathways to soot formation.

4.1.5 Methane / Butane Mixtures

Studying the sooting behaviour of mixtures of butane (C_4H_{10}) and methane (CH_4) can yield more insight as to the possible interaction of even and odd-numbered carbon species based pathways since butane is an even-carbon based species and methane is an odd-carbon based species. It was expected that the butane pyrolysis would lead other even-carbon species. It was then expected that, if the interaction between even and odd-numbered carbon species is responsible for the synergistic effect, the sooting propensity over the mixture range for this mixture would in fact show a synergistic effect. By contrast, the experimentally measured soot yield did not show a synergistic behaviour over the mixture range as shown in Figure 4-19.

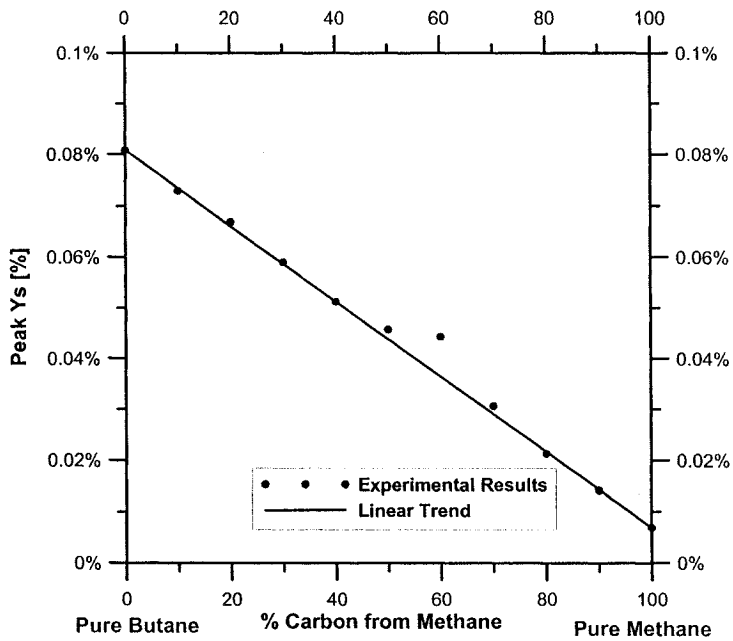

Figure 4-19 Peak Soot Yield over Methane/Butane Mixture Range

However, a potential explanation for this anomaly can be found in the actual pyrolysis behaviour of butane. It was shown that the pyrolysis of butane behaved very similarly to that of propane, readily forming odd-carbon numbered species [60] rather than even-carbon based species as might otherwise be expected. Therefore, the absence of a synergistic effect in this mixture is explained by the fact that both species behave like odd-carbon numbered species and indicates that the pathways to soot formation in propane, butane and methane are similar. Again, the absence of a synergistic effect tends to indicate that the synergistic effect measured in the propane/ethylene and methane/ethylene mixtures are in fact due to an interaction between even and odd-carbon numbered species.

4.1.6 Ethane / Propane Mixtures

From the results obtained with the methane/ethane mixture, it would be expected that the ethane/propane (C_2H_6/C_3H_8) mixture would exhibit a similar behaviour. Surprisingly however, the soot yield over the mixture range behaved essentially linearly as illustrated in Figure 4-20.

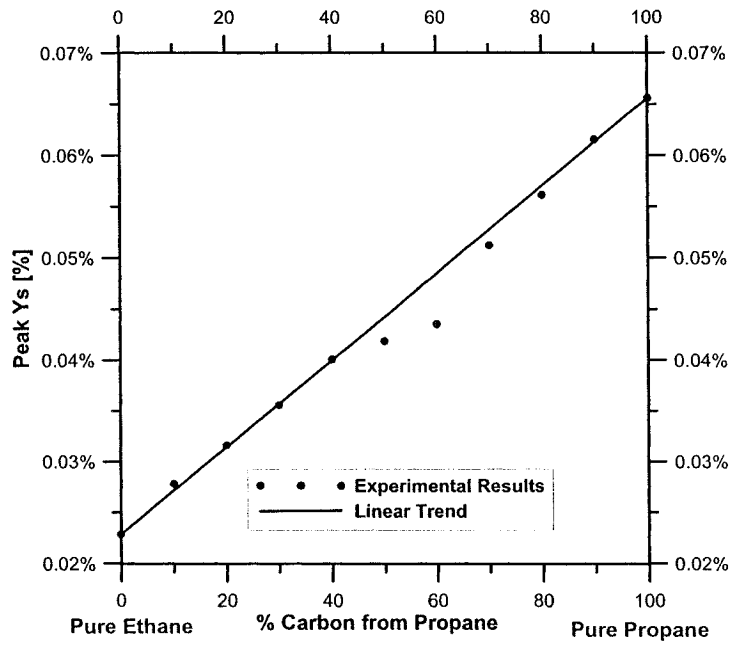

Figure 4-20 Soot Yield over Ethane/Propane Mixture Range

Although there is a slight negative deviation of the soot yield from the linear trend at a mixture of 60%, this deviation is attributed to experimental uncertainty and is not thought to indicate a real phenomena.

The absence of a synergistic effect in this mixture is surprising, considering the presence of a strong effect in the methane/ethane mixture. If the synergistic effect in the methane/ethane mixture is interpreted to be due to an interaction between even and odd-carbon numbered species in the path to soot formation, it would then be expected that such an effect would also be present in the ethane/propane mixture. To further clarify this discrepancy, the ethane/ethylene mixture was analyzed as well.

4.1.7 Ethane / Ethylene Mixtures

Since no synergistic effect was found in the ethane/propane mixtures but was identified in the methane/ethane mixtures, it was essential to further clarify the issue by analyzing the sooting propensity of ethane/ethylene (C_2H_6/C_2H_4) mixtures. It has been reported by other researchers that a synergistic effect could be found in ethane/ethylene mixtures [30]. Our experiments confirmed this. The soot yield, illustrated in Figure 4-21, demonstrates a strong synergistic effect with only small amounts of C_2H_6.

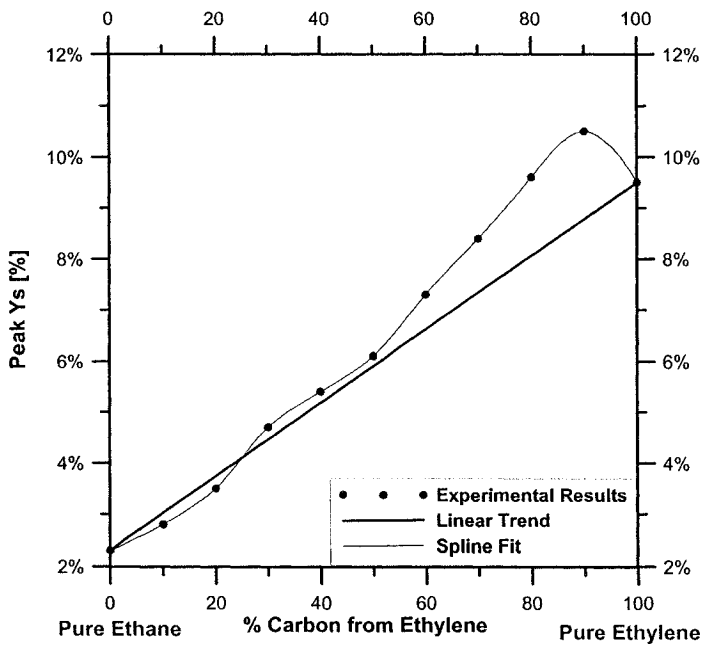

Figure 4-21 Peak Soot Yield over Ethane/Ethylene Mixtures

The deviation from the linear fit, illustrated in Figure 4-22, confirms this trend.

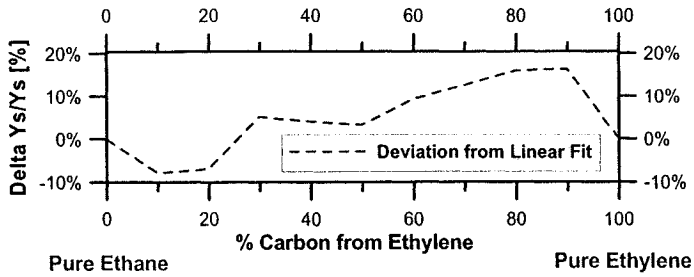

Figure 4-22 Deviation from Linear Fit of Soot Yield over Ethane/Ethylene Mixture Range

This synergistic effect was also visible in the peak soot volume fraction over the mixture range. This behaviour is similar to that described by previous researchers. This behaviour, combined with the knowledge that a synergistic effect also exists for the methane/ethane mixtures, and no effect exists for the propane/ethane mixture leads to the conclusion that, for these mixtures, the interactions between even and odd-carbon species on the path to soot formation can not fully explain the synergistic effect.

In an effort to clarify all the experimental results, Table 4-1 summarizes the findings obtained at this point.

Table 4-1 Summary of Experimental Results

Mixture	**Methane**	**Ethane**	**Propane**
Ethylene	Slight Synergistic Effect	Strong Synergistic Effect	Strong Synergistic Effect
Propane	No Synergistic Effect	No Synergistic Effect	
Ethane	Strong Synergistic Effect		
Butane	No Synergistic Effect		

As previously mentioned, it is possible that for certain mixtures, the variation of the flame temperature could be obscuring the synergistic effect, especially in the ethylene/methane mixtures. Therefore, an additional series of experiments were done where the flame temperature variation was countered by preheating the fuel and air. The removal of the flame temperature as a variable will allow to further confirm the presence of a synergistic effect.

4.1.8 Effect of Flame Temperature

The flame temperature is a key variable in the sooting propensity of any fuel. To understand and isolate any chemical phenomena leading to synergistic effects in certain fuel mixtures, experiments to control the flame temperature were performed. The initial evaluation of the flame temperature was done. The gas temperatures calculated for the ethylene flame were compared to temperatures obtained by other researchers using Coherent Antistokes Raman Spectroscopy (CARS) for a similar ethylene flame [61]. Both temperature profiles are compared in Figure 4-23. The temperatures were found to be within the combined uncertainties of the measurement. It was noticed that the spatial resolution of measurements done with thermocouples was much less than for the CARS technique. However, since the relative behaviour of the temperature is the result of interest, the accuracy of the measurement was deemed sufficient.

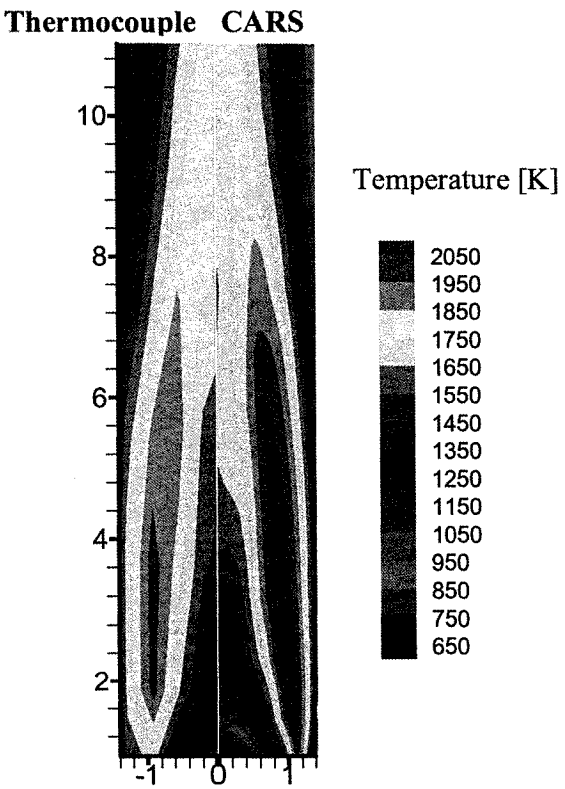

Figure 4-23 Comparison of Thermocouple and CARS Measurement for Ethylene Flame

Because the ethylene flame contains a lot of soot, the measurements are less accurate than for a low sooting flame, for example the methane flame.

The adiabatic flame temperature was chosen as an indicator for the actual flame temperature. It is known that the actual behaviour of the flame temperature is far more complex than indicated by the adiabatic flame temperature. However, it was verified, through the measurement of the flame temperature profile of the three main fuels (ethylene, methane and propane), that this variable would still be adequate in assessing the relative flame temperature behaviour of the different fuels. As mentioned previously, the adiabatic flame temperature of these fuels follows the order of ethylene > propane > methane as shown in Table 4-2 [62].

Table 4-2 Pure Fuels Adiabatic Flame Temperatures

Fuel	Ethylene	Propane	Methane
Adiabatic Flame Temperature	2370	2267	2226

As illustrated in Figure 4-24, the flame temperature in the top part of the flame does not correspond to the trend indicated by the adiabatic flame temperature.

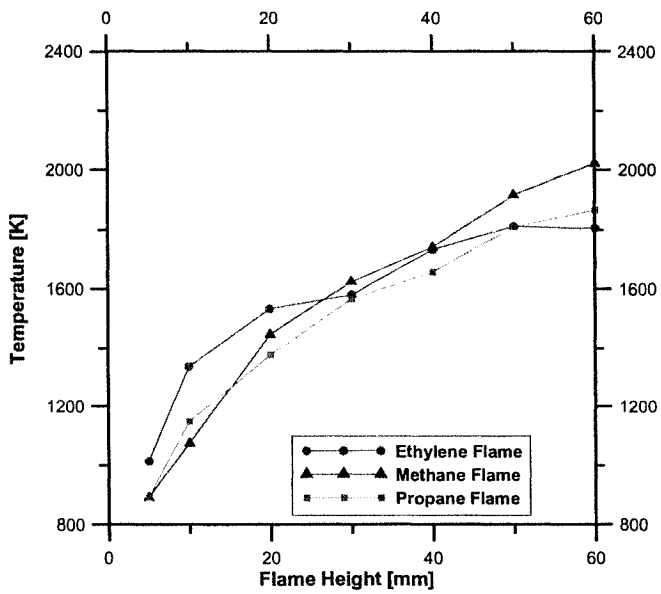

Figure 4-24 Centerline Flame Temperature for Pure Fuels

However, this order is not applicable in the top part of the flame because of the different soot concentrations in the flames. A flame with more soot will cool more rapidly; this explains the reversed order of the temperatures in the top part of the flame. However, in the lower part of the flame, the adiabatic flame temperature seems to be a relatively good indicator of the behaviour. As mentioned previously, pyrolysis, which is very temperature dependent, is the rate-controlling step of the sooting propensity of any fuel. This pyrolysis is known to take place in the lower part of the flame; therefore, it is concluded that the adiabatic flame temperature would be an adequate indication of the flame temperature which would be controlling the sooting propensity of a fuel. The preheating was therefore evaluated to keep this adiabatic flame temperature constant for all mixtures. Table 4-2 list the preheating temperatures for both the fuel and the air necessary to maintain constant adiabatic flame temperature over the mixture ranges.

Table 4-3 Preheating Temperature over Mixture Range for Constant Adiabatic Flame Temperature Condition

% Carbon from Ethylene	Preheating Temperature [K]		% Carbon from Propane	Preheating Temperature [K]
	Ethylene/ Propane	Methane/ Ethylene		Methane/ Propane
100 % (pure Ethylene)	298	298	100 % (pure Propane)	298
90 %	325	340	90 %	310
80 %	350	380	80 %	320
70 %	375	415	70 %	328
60 %	400	450	60 %	338
50 %	420	480	50 %	346
40 %	445	507	40 %	354
30 %	464	533	30 %	362
20 %	485	558	20 %	370
10 %	506	583	10 %	376
0 %	527	605	0 %	380

Both the air and fuel were preheated using an electric heater and electric heating tape respectively. Their temperatures were measured close to the air and fuel outlet using K type (Chromel/Alumel) thermocouples. These temperatures were used as feedback by the controllers, which insured that the desired temperature was achieved and maintained. This preheating had a noticeable impact on the actual flame temperature as illustrated in Figure 4-25.

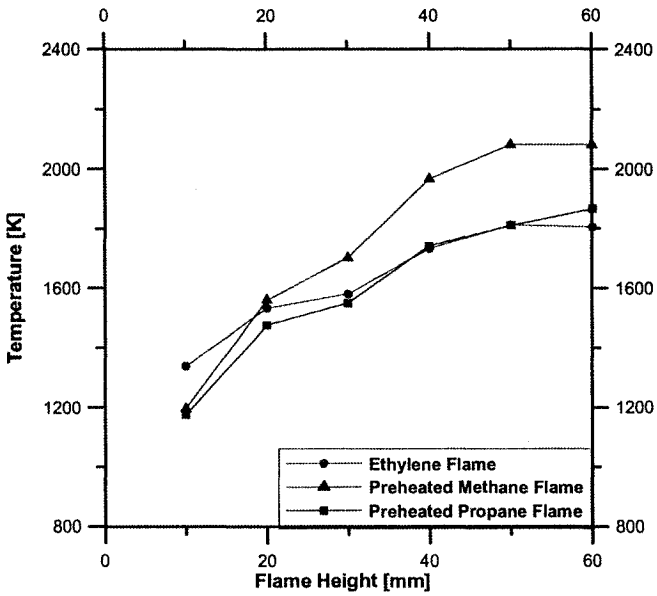

Figure 4-25 Preheated Centerline Temperature for Pure Fuels

For the ethylene/propane mixture, an evaluation of the centerline flame temperature indicated that the preheating did maintain fairly constant flame temperatures in the lower parts of the flame.

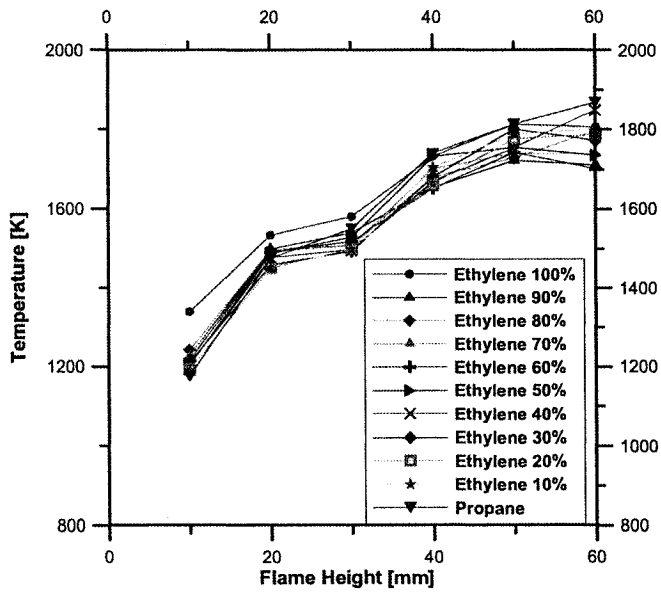

Figure 4-26 Centerline Flame Temperature of Preheated Ethylene/Propane Mixture

The sooting behaviour of the mixtures was measured under these constant temperature conditions. The preheating was seen to have a very significant effect on the sooting propensity as illustrated in Figure 4-27.

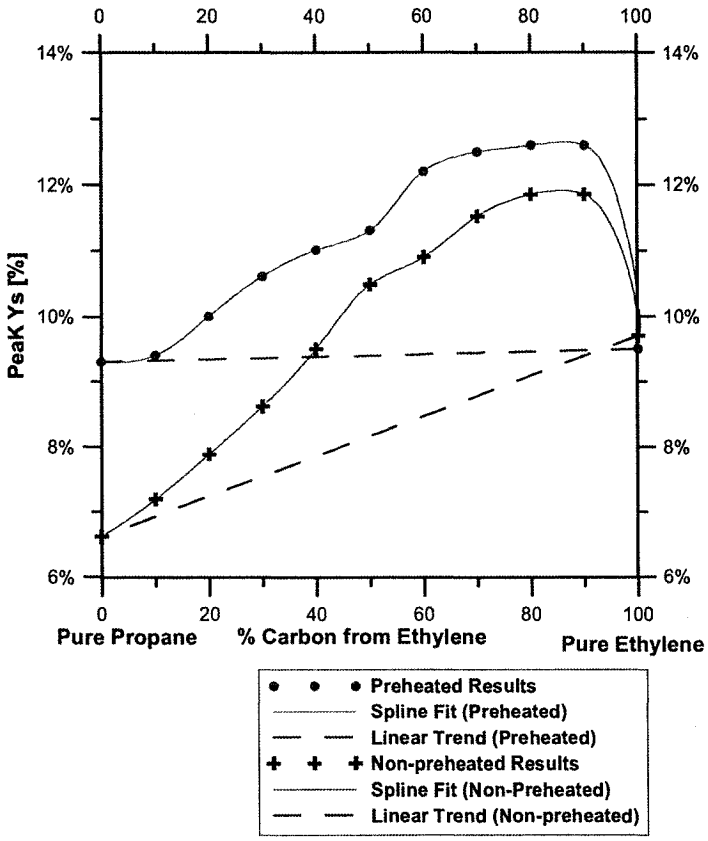

Figure 4-27 Soot Yield over Ethylene/Propane Preheated Mixture Range

It is interesting to notice that, although the sooting propensity was noticeably increased by the preheating of the fuel mixtures, the deviation from the linear fit and therefore the magnitude of the synergistic effect did not increase as seen in Figure 4-28. Therefore, the synergistic effect was not increased by the increased temperature.

It is also interesting to point out that the sooting propensity of the propane flame was equal to that of the ethylene flame under the preheated condition. This reiterates the importance of the odd-carbon based pathways to soot formation, namely propargyl combination, which are thought to be dominant in a propane flame. This reaction is temperature-dependent, which would explain the preheating effect.

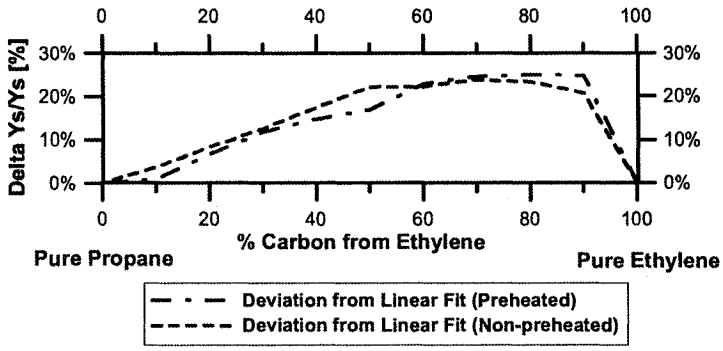

Figure 4-28 Deviation from Linear Fit of Soot Yield over Preheated Ethylene/Propane Mixture Range

It was presented previously that a small synergistic effect could be detected in the methane/ethylene mixtures and that this effect was indicative of a much stronger phenomena which would be somewhat hidden by the temperature variation. It was found by other researchers that by maintaining the adiabatic flame temperature constant through dilution, a stronger synergistic effect could be uncovered. In this case a similar method was employed, but the fuel mixtures were preheated. The preheating yielded very similar flame temperatures for all mixtures in the lower portion of the flame.

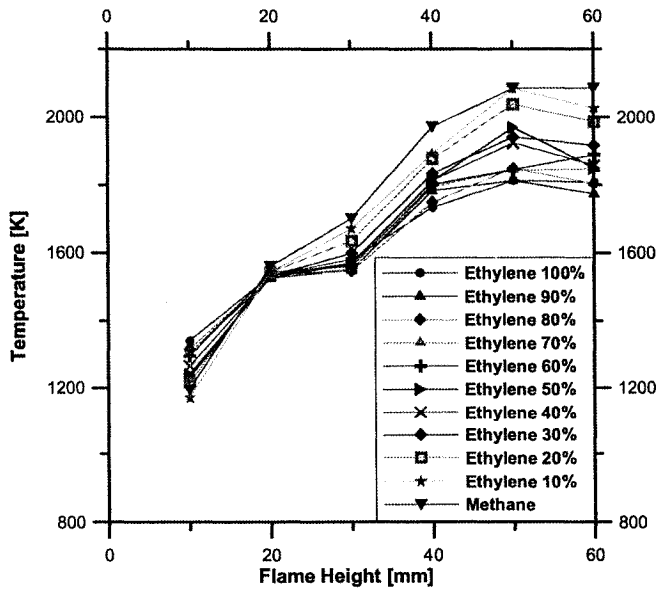

Figure 4-29 Centerline Flame Temperature of Preheated Methane/ethylene Mixture

The resulting sooting behaviour was greatly enhanced by the preheating as illustrated in Figure 4-30.

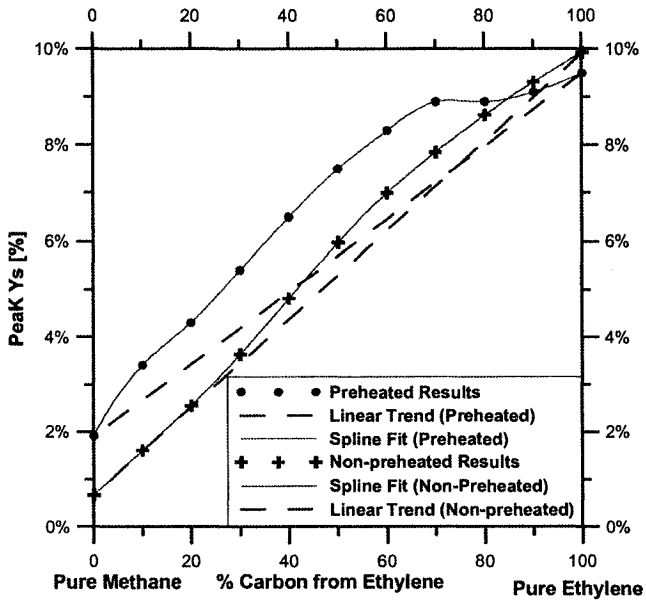

Figure 4-30 Soot Yield over Methane/ethylene Preheated Mixture Range

Unlike the ethylene/propane mixture, in this case the deviation from the linear fit was greatly enhanced by the preheating of the fuel.

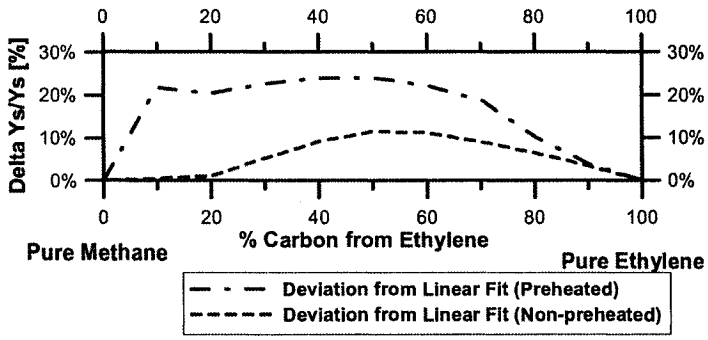

Figure 4-31 Deviation from Linear Fit of Soot Yield over Preheated Methane/ethylene Mixture Range

This indicates that the reactions responsible for the synergistic effect in this mixture are greatly influenced by the temperature variation, which was greater than for the

ethylene/propane mixture. This could indicate that the reactions responsible for the synergistic effect in the ethylene/propane and methane/ethylene mixtures are different.

As for the methane/propane mixtures, it was proposed that the actual difference in the adiabatic flame temperatures was too small to be hiding any underlying synergistic effect. The measured sooting behaviour of the preheated mixtures confirmed this as illustrated in Figure 4-32.

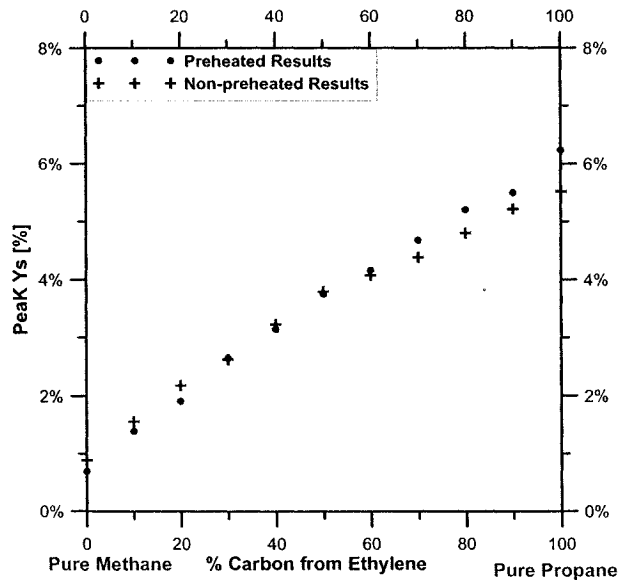

Figure 4-32 Soot Yield over Methane/propane Preheated Mixture Range

The preheating of the methane/propane mixture did not influence the soot yield, which confirms that there is no underlying synergistic effect. Therefore, it is confirmed that there is no interaction between different sooting pathways in the methane/propane mixtures. All these results are summarized in Table 4-4.

Table 4-4 Summary of Experimental Results

Mixture	Methane	Ethane	Propane
Ethylene	Slight Synergistic Effect, Highly temperature dependent	Strong Synergistic Effect	Strong Synergistic Effect, Not temperature Dependent
Propane	No Synergistic Effect	No Synergistic Effect	
Ethane	Strong Synergistic Effect		
Butane	No Synergistic Effect		

Following this analysis, useful additional information has been gained. In the ethylene/propane flame, although the sooting propensity over the mixture range was greatly enhanced by the preheating, the deviation from the linear fit, or the magnitude of the synergistic effect did not vary. For the methane/ethylene flame, the sooting propensity and the magnitude of the synergistic effect were greatly enhanced by the preheating. The preheating in the methane/ethylene flame was much greater than for the ethylene/propane flame due to the larger difference in adiabatic flame temperature. Therefore, the different degree of influence on the synergistic effect is either due to the difference in preheating, or to the fact that the synergistic effect is caused in the two mixtures by different pathways with different temperature dependences. As for the methane/propane mixture, the difference in adiabatic flame temperature was known to be minimal; consequently, preheating of the fuels did not highlight any underlying synergistic effect between these two fuels. This absence of an effect would tend to indicate that the dominating pathways to soot formation for both fuels are the same. Interpreting on this assumption, it would then be concluded that the synergistic effects found in the ethylene/propane and methane/ethylene mixtures are caused by the interaction of the same reactions, meaning that the difference seen in the influence of the preheating on the magnitude of the synergistic effect would be due to the difference in preheating.

4.2 Numerical Results

Numerical simulations were essential in understanding the root cause of the sooting behaviour of the fuel mixtures since it is impossible to experimentally monitor all the species of interest. The first soot model used was found to provide good agreement with the experimental flames for both flame heights and soot concentrations.

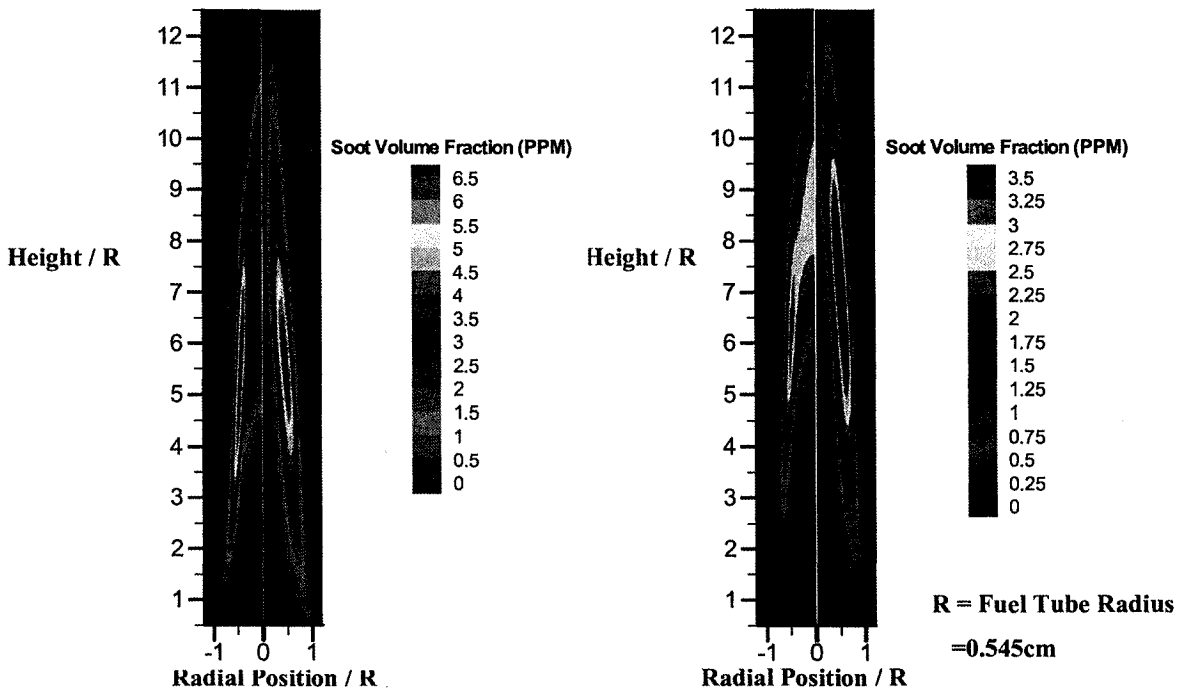

Experimental versus Numerical Experimental versus Numerical

Figure 4-33 Soot profile Ethylene and Propane Flame

The ethylene flame sooting profile illustrated in Figure 4-33 was found to have very good agreement between the experimental, shown on the left, and numerical behaviours, shown on the right. As well, the peak soot volume fraction obtained numerically was 6.9 PPM, 9% less than the experimental maximum of 7.5 PPM. As for the propane flame, the experimental profile is again shown on the left hand side while the numerical profile

is on the right hand side in Figure 4-33. The agreement between the flame heights is good; however, the model tends to overestimate the soot concentration by 33%. This is considered to be acceptable. The comparison of the numerical and experimental sooting profiles over height for both fuels shown in Figure 4-34 indicates that there is very good agreement as to the height of the peak concentration as well as the height of the flame. This confirms the change in reactions rates explained previously and shown in Table 2. It is noticed, however, that although the experimental measurement illustrate a bimodal behaviour as explained previously, this is not reproduced in the modeling. The model is presently underestimating the soot concentration on the flame centerline, leading to an obscuring of the bimodal behaviour

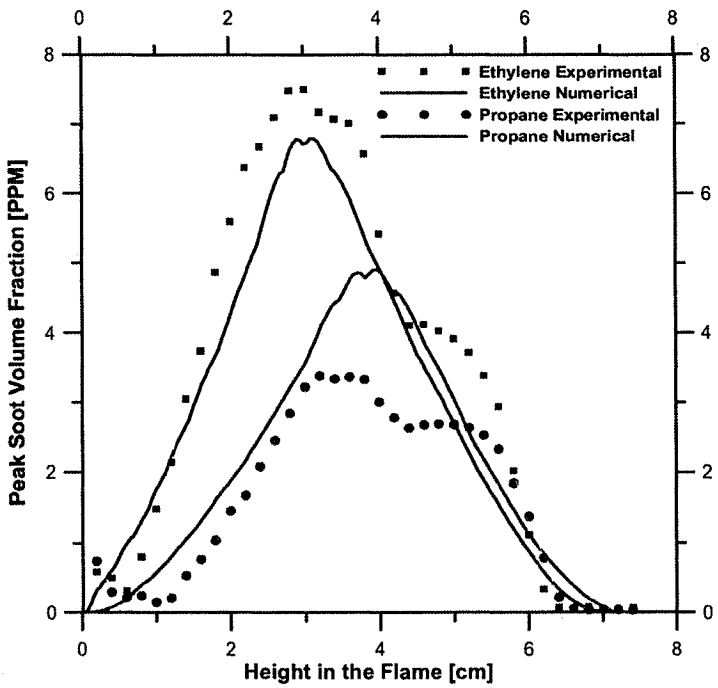

Figure 4-34 Peak Soot Concentration over Height: Numerical vs. Experimental

As well, to further validate the model, the flame temperatures for both pure fuels were compared, as shown in Figure 4-35, and it was found that there was reasonable agreement between experimental and numerical flame temperatures when the uncertainty of both values are considered. As well, it is interesting to note that the model was seen to underestimate the propane flame temperature higher in the flame. This could be due to

the over-predicted soot concentration which would lead to higher radiation heat loss and therefore lower temperatures.

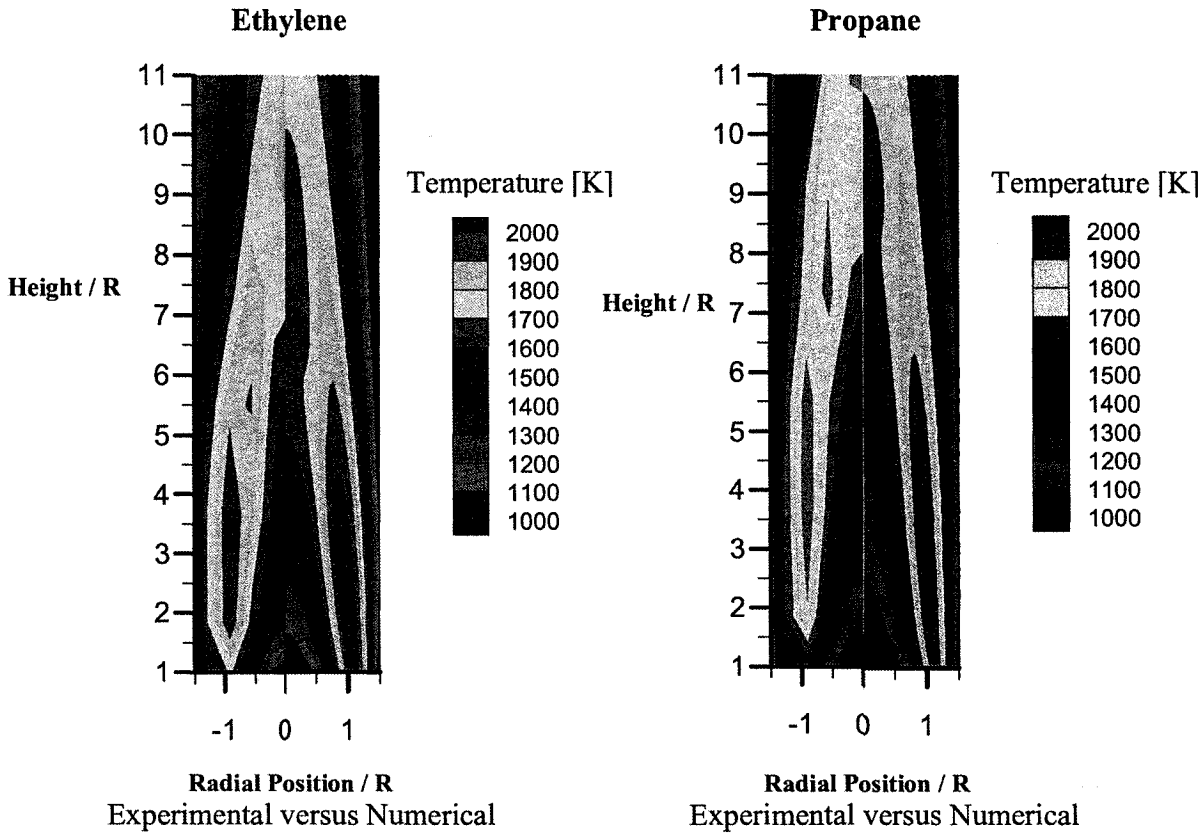

Figure 4-35 Temperature Profile Ethylene and Propane Flames

The model was also found to qualitatively reproduce the synergistic effect for both peak soot volume fraction and soot yield. However, as shown in Figure 4-36 and Figure 4-37 , the increase is not as pronounced as what was measured experimentally. At its peak, the increase over the pure ethylene flame was of only 4% for both peak soot volume fraction and peak soot yield compared to increases of 29% and 16.5% respectively obtained experimentally. As well, this maximum increase was found at a mixture where the contribution of ethylene to the carbon input was 96%. However, it was found that the benzene concentration had a very strong synergistic behaviour over the mixture range as shown in Figure 4-38.

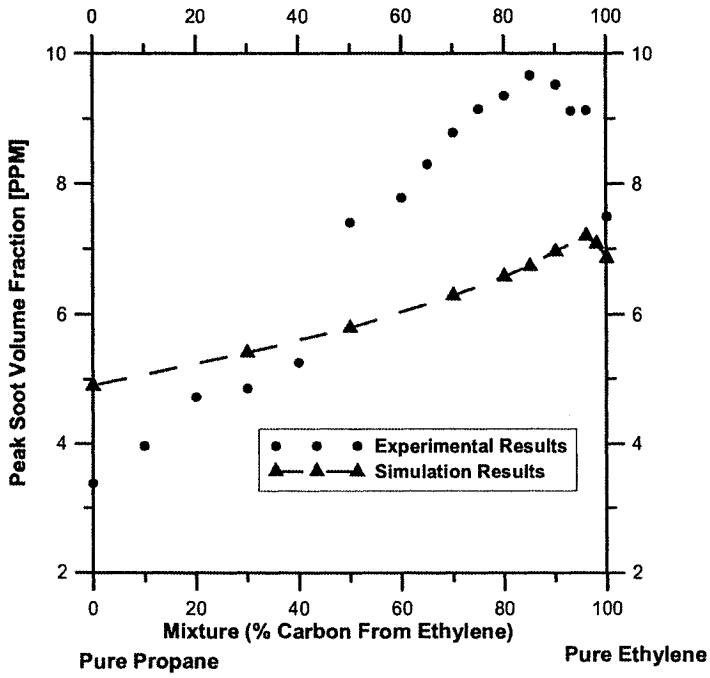

Figure 4-36 Numerical Peak Soot Volume Fraction over Propane/Ethylene Mixture Range

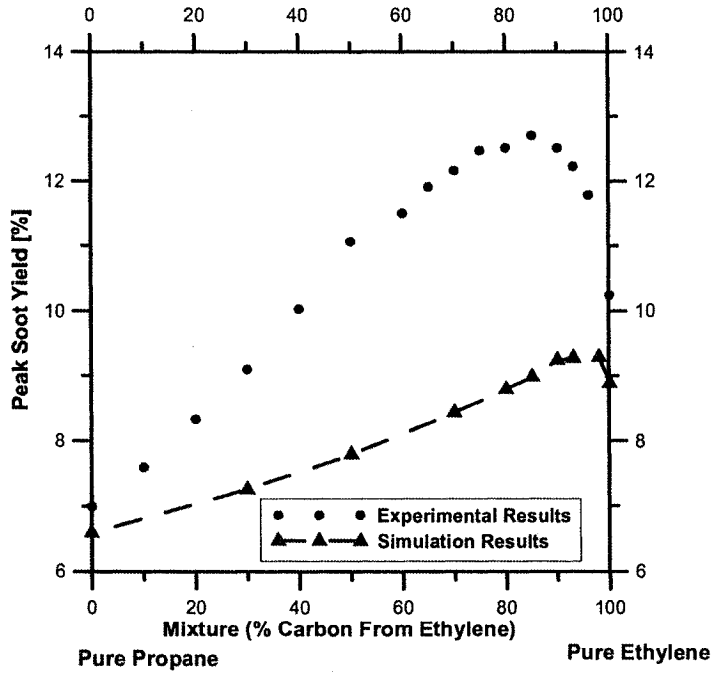

Figure 4-37 Numerical Peak Soot Yield over Propane/Ethylene Mixture Range

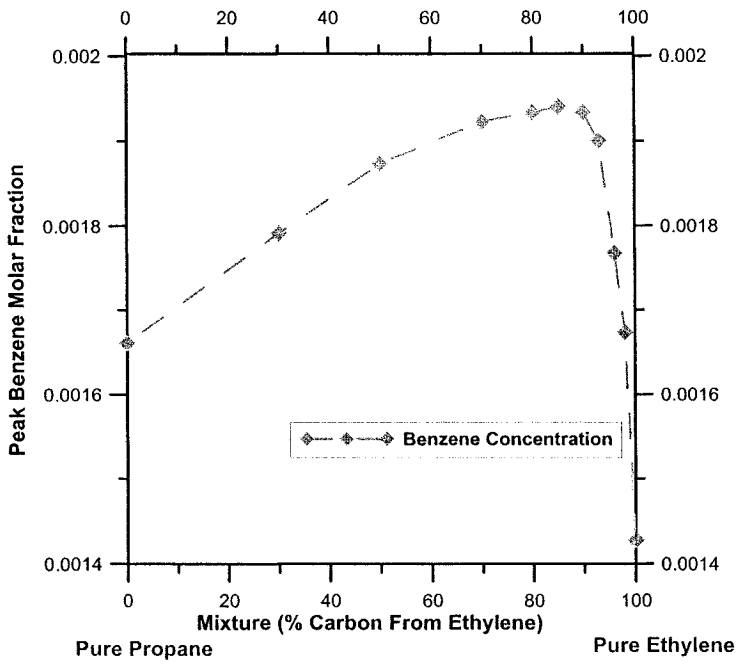

Figure 4-38 Numerical Peak Benzene Molar Fraction over Propane/Ethylene Mixture Range

This benzene behaviour is indicative of the soot behaviour because of the known benzene-dependent paths to soot formation. The benzene concentration peaks at a mixture of 85%, corresponding to the peak soot concentration measured experimentally. The increase over the molar fraction for pure ethylene is of 35%. As well, the phenyl (C_6H_5) concentration also indicated a strong synergistic effect over the mixture range as shown in Figure 4-39.

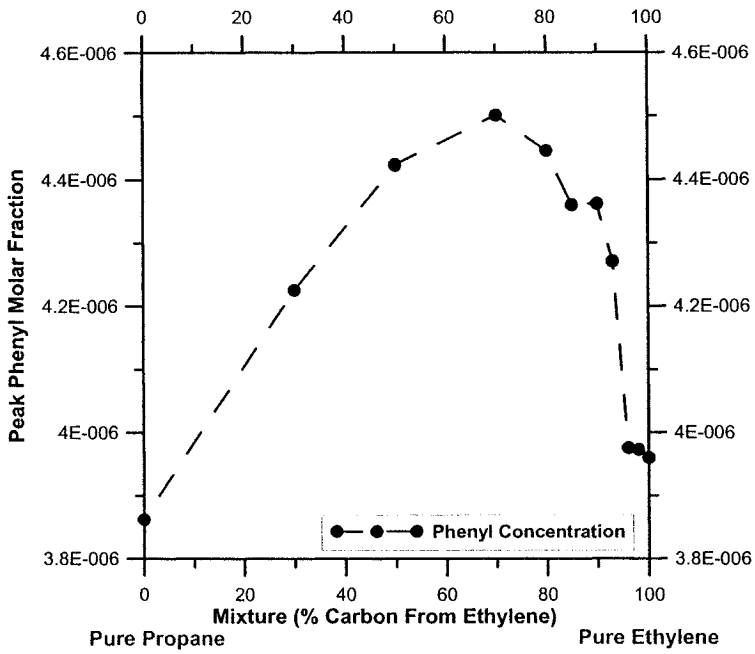

Figure 4-39 Numerical Peak Phenyl Molar Fraction over Propane/Ethylene Mixture Range

The difference of behaviour between benzene and phenyl and the sooting behaviour over the mixture range is an indication that although the chemical kinetics model could be accurate in reproducing the synergistic effect, the simplified soot model could be hiding this effect. As mentioned previously, the soot growth was based solely on the acetylene addition model, whereas recent evidence has indicated that odd-carbon species could also play an influential role. It would therefore be beneficial to undertake further modeling with a more sophisticated soot model, allowing additional computational capabilities. However, this model was successful in qualitatively reproducing the desired synergistic effect in the sooting behaviour and could therefore help understanding the actual source of the synergistic from the analysis of its species and reaction rates.

It was found that, as expected, the acetylene concentration decreased rapidly as propane was added to the mixture. The synergistic effect can therefore not be explained by this pathway alone. As suggested by other researchers, the synergistic effect seen could be due to the propargyl (C_3H_3) based pathway to first ring formation [30]. Similar to this

previous study, the present modeling results also show a small synergistic behaviour for the peak propargyl concentration in the co-flow flame at a mixture of 20% of carbon from ethylene, as illustrated in Figure 4-40. However, this synergistic effect is found at a concentration of ethylene much lower than that at which the synergistic effect for the benzene and soot concentrations are seen. This prompted further analysis of the species concentrations and reactions rates

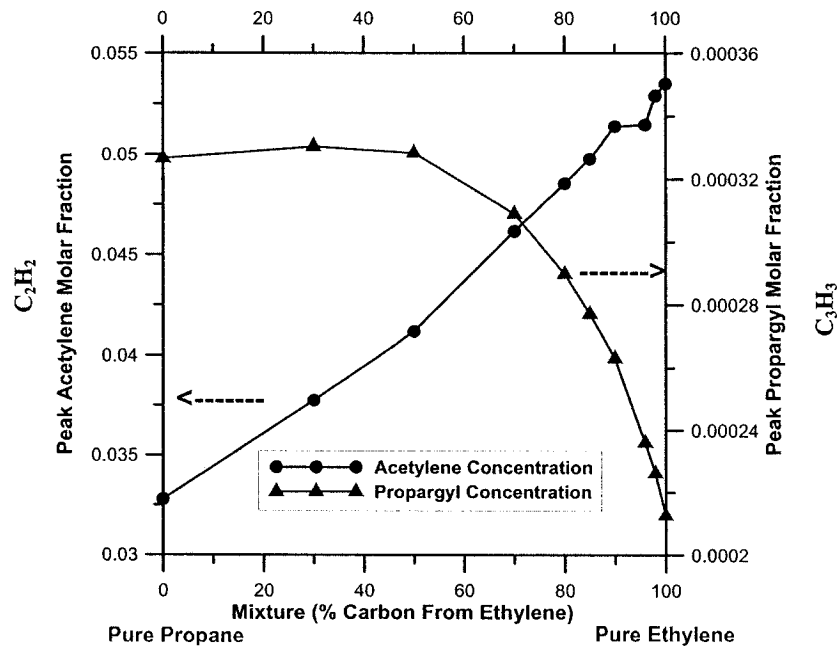

Figure 4-40 Peak Acetylene and Propargyl Molar Fraction over Mixture Range

An analysis of the reaction rates for benzene production and consumption revealed that the maximum production was found in the lower part of the flame as shown in Figure 4-41.

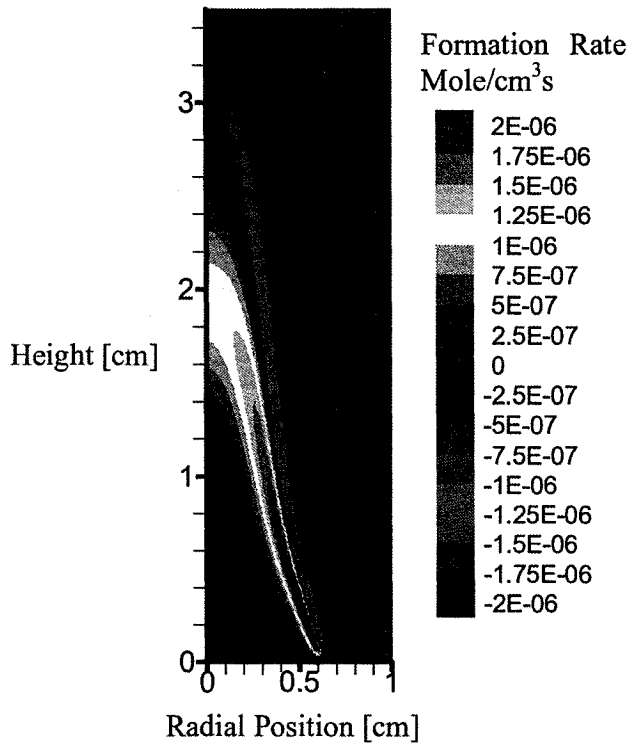

Figure 4-41 Total Benzene Formation Rate in Ethylene Flame

The analysis of the rate of benzene (C_6H_6) production at this height revealed that the dominating reaction for benzene formation for all mixtures was the following reaction as illustrated in Figure 4-42 :

$$n\text{-}C_4H_5+C_2H_2 \Leftrightarrow A_1+H \qquad \text{[Reaction 403]}$$

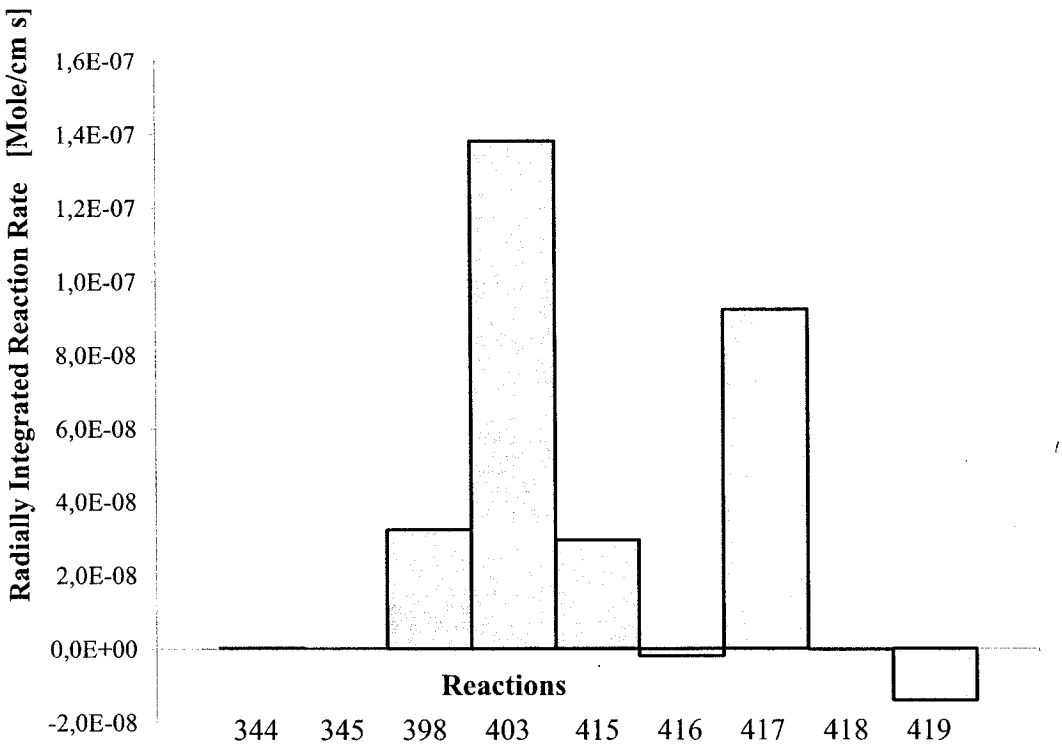

Figure 4-42 Radially Integrated Reaction Rates for Benzene Formation Height=5mm in Ethylene Flame

As for the phenyl (C_6H_5) formation, in the lower part of the flame, the dominating reaction was propargyl based [reaction 397], whereas the acetylene-based reaction [reaction 400] was second in importance as shown in Figure 4-43.

$C_3H_3+C_3H_3 \Leftrightarrow A_1\text{-}+H$ [Reaction 397]

$n\text{-}C_4H_3+C_2H_2 \Leftrightarrow A_1\text{-}$ [Reaction 400]

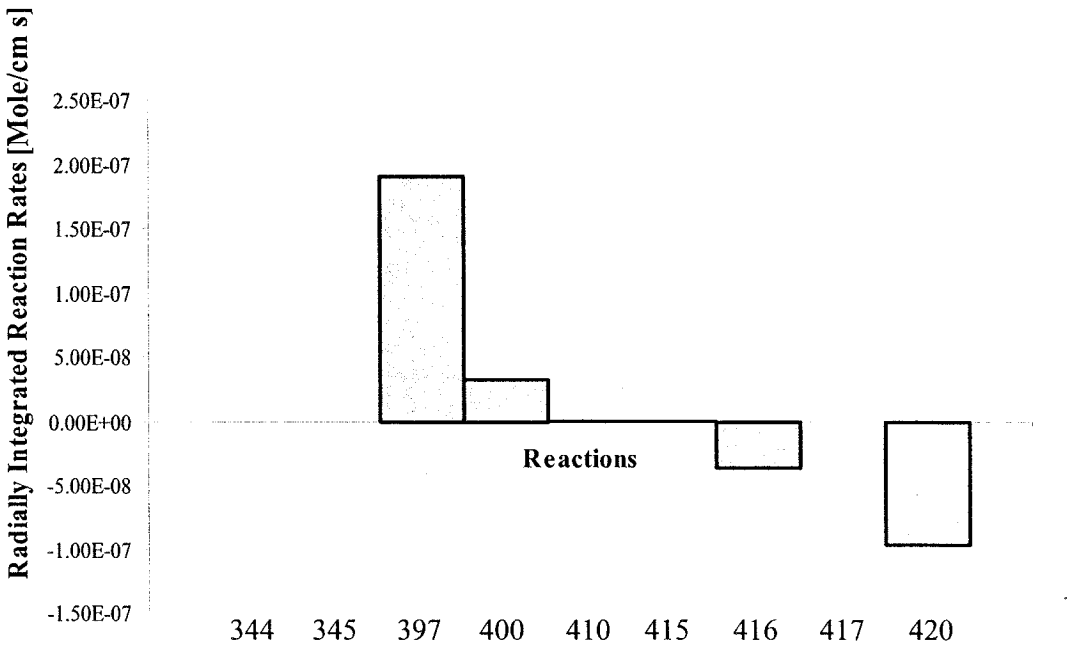

Figure 4-43 Radially Integrated Reaction Rates for Phenyl Formation Height=5mm in Ethylene Flame

The analysis of the mass flow rate of phenyl at this height indicated that it behaved with a strongly synergistic pattern as shown in Figure 4-44. This mass flow rate was found by radially integrating the species volume fraction mutiplied by the density of this species and the velocity at each grid point. The density of each species was obtained from the numerical results.

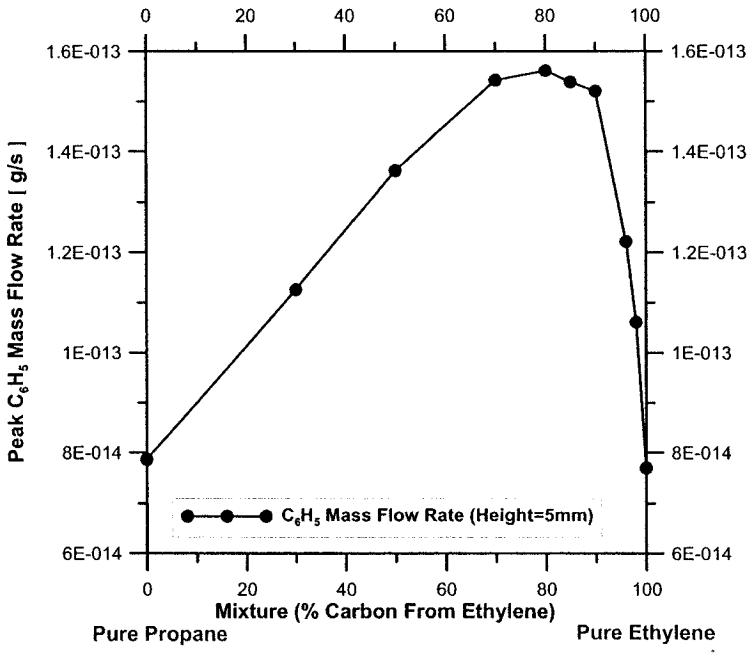

Figure 4-44 Mass Flow Rate Phenyl over Mixture Range at Height of 5 mm

To understand the origin of this behaviour, the behaviour of propargyl was analyzed and it was found that although the propargyl mass flow rate did demonstrate a slight synergistic effect, the pattern of this behaviour differs significantly from the phenyl synergistic effect as shown in Figure 4-45.

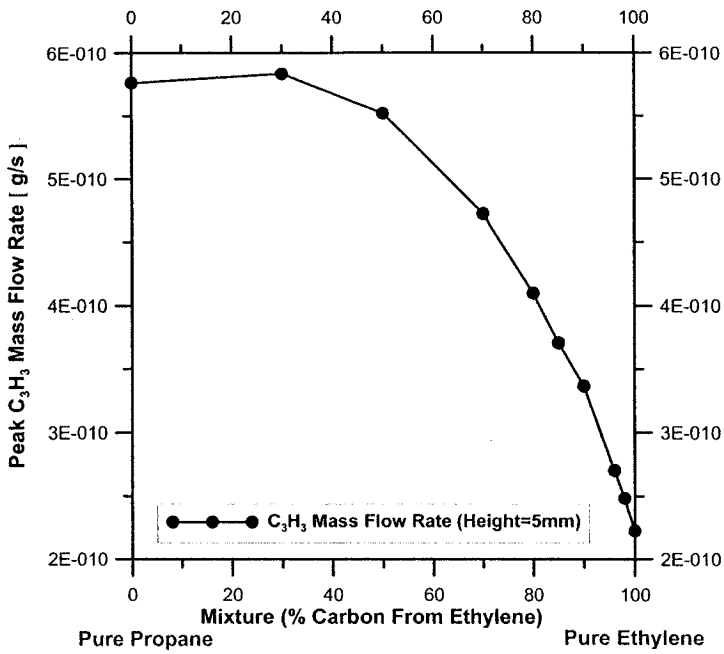

Figure 4-45 Mass Flow Rate C_3H_3 over Mixture Range at Height of 5 mm

It was found that the mass flow rate of n-C_4H_3 showed a very strong synergistic behaviour as shown in Figure 4-46. This behaviour was very similar to that of phenyl and indicates that the strong synergistic effect of phenyl would be due to the synergistic effect of n-C_4H_3 through reaction 400.

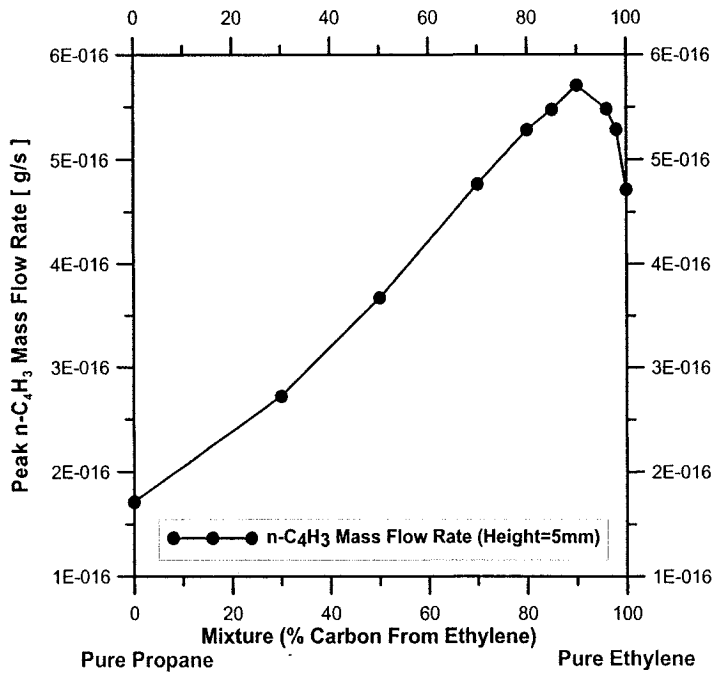

Figure 4-46 Mass Flow Rate n-C_4H_3 over Mixture Range at Height of 5 mm

As well, it was found that in the higher part of the flame, the formation of phenyl is dominated by the reactions involving benzene [reactions 416-417] as illustrated in Figure 4-47.

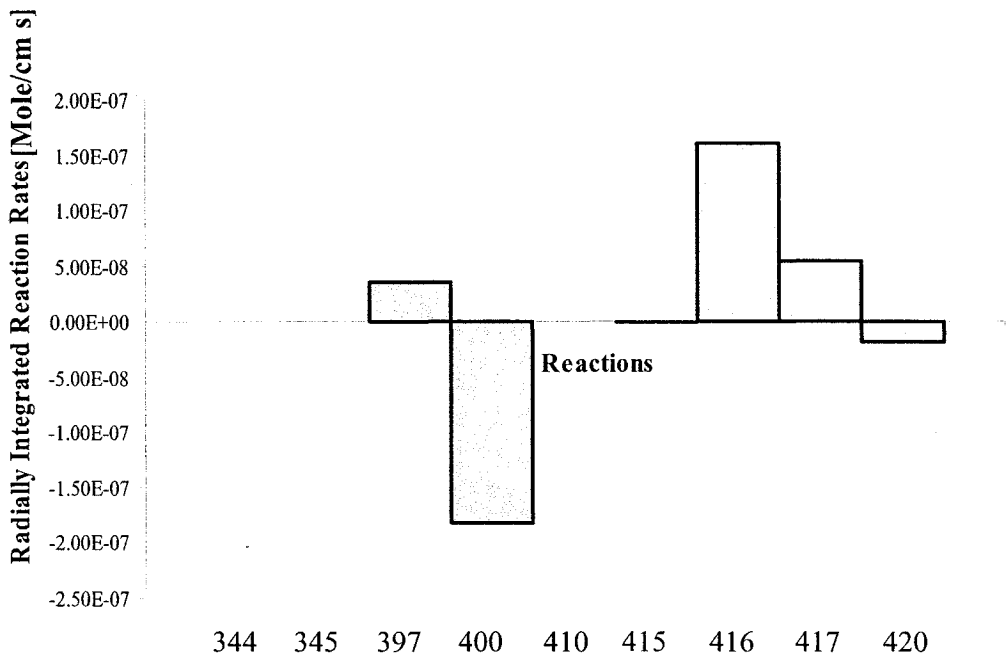

Figure 4-47 Radially Integrated Reaction Rates for Phenyl Formation Height=2.5mm in Ethylene Flame

A_1+OH ⇔ A_1- +H_2O [Reaction 416]

A_1-+H(+M) ⇔ A_1(+M) [Reaction 417]

Therefore, the phenyl formation would also be highly dependent on the benzene concentration, which in itself is highly dependent on the acetylene and n-C_4H_5 concentrations

From this analysis, it was concluded that the path leading to the synergistic effect in the soot concentration was through the reactions involving acetylene and n-C_4H_5 as well as, to a lesser extent, acetylene and n-C_4H_3. Surprisingly, these reactions are acetylene based. Although the peak concentrations for the whole flame of acetylene, n-C_4H_5 and n-C_4H_3 were found to decrease linearly as propane was added, it was found that at the flame heights where the production rate of benzene was maximal, the mass flow rate of n-C_4H_5

showed a strong synergistic behaviour as illustrated in Figure 4-48. A synergistic behaviour for n-C_4H_3 was also found as previously shown in Figure 4-44.

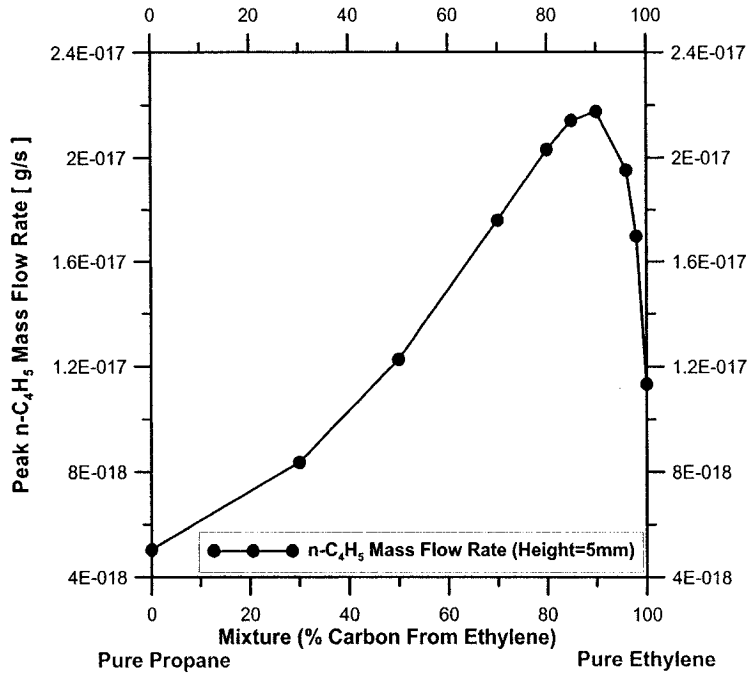

Figure 4-48 Mass Flow Rate n-C_4H_5 over Mixture Range at Height of 5 mm

To trace back the reason for this synergistic effect, the formation rates of these species were analyzed.

The formation of n-C_4H_5 was traced back to the dehydrogenation of C_4H_6 as illustrated in Figure 4-49.

$C_4H_6+H \Leftrightarrow n\text{-}C_4H_5+H_2$ [Reaction 381]

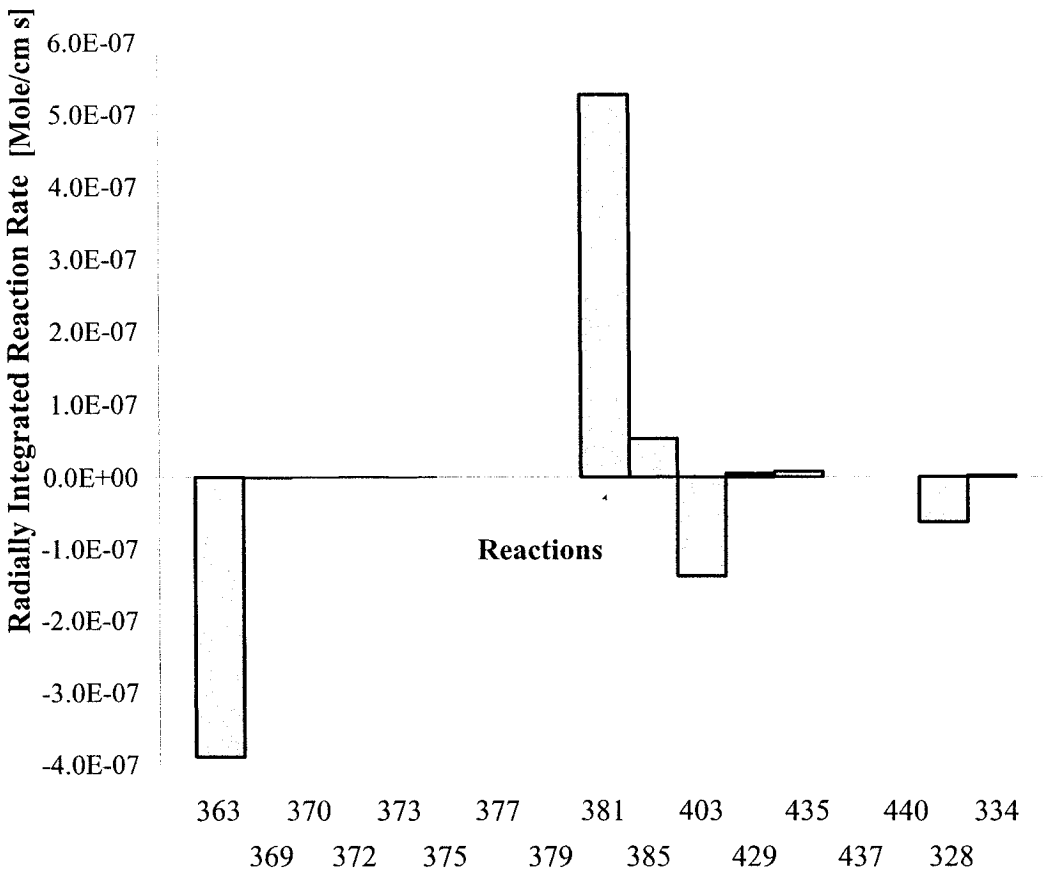

Figure 4-49 Radially Integrated Reaction Rates for n-C_4H_5 Formation Height=5mm in Ethylene Flame

This species also had synergistic behaviour over the mixture range as illustrated in Figure 4-50.

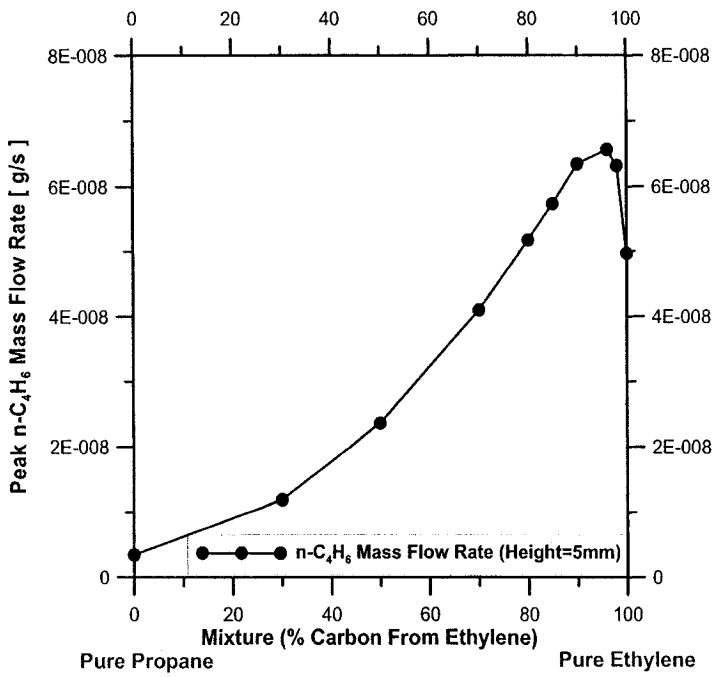

Figure 4-50 Mass Flow Rate n-C_4H_6 over Mixture Range at Height of 5 mm

This effect could similarly be traced back to the reaction of the vinyl radical (C_2H_3) with ethylene (C_2H_4) and the combination reaction of the vinyl radical (C_2H_3) species.

$C_2H_4+C_2H_3 \Leftrightarrow C_4H_6+H$ [Reaction 331]

$C_2H_3+C_2H_3 \Leftrightarrow C_4H_6$ [Reaction 332]

The vinyl radical concentration also demonstrated a synergistic effect over the mixture as shown in Figure 4-51.

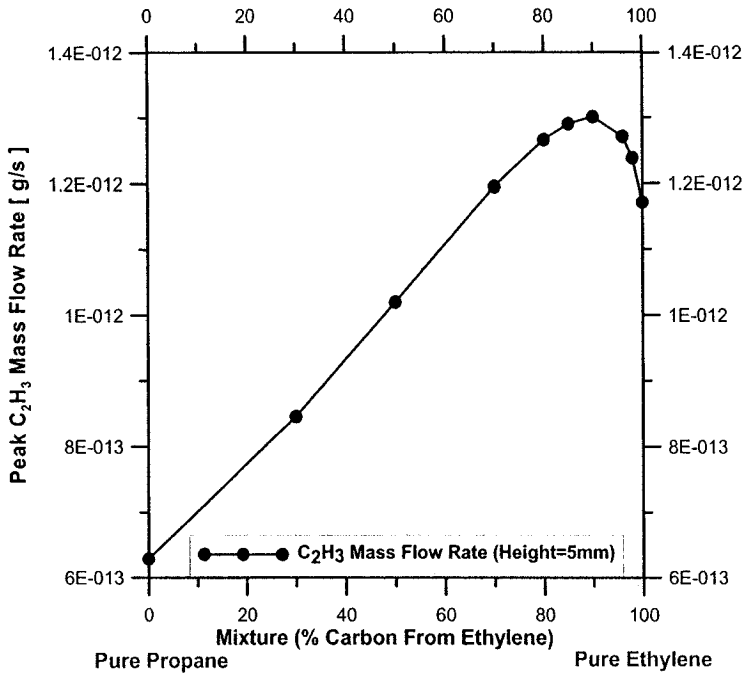

Figure 4-51 Mass Flow Rate C_2H_3 over Mixture Range at Height of 5 mm

Similarly, the synergistic effect indicated in the n-C_4H_3 concentration was traced back. It was found that this species was formed through the C_4H_4 dehydrogenation.

$C_4H_4+H \Leftrightarrow n\text{-}C_4H_3+H_2$ [Reaction 365]

The C_4H_4 species itself was formed according to the following reactions:

$C_2H_2+C_2H_3 \Leftrightarrow C_4H_4+H_2$ [Reaction 327]

$C_4H_4+H \Leftrightarrow n\text{-}C_4H_5$ [Reaction 363]

$C_4H_4+H \Leftrightarrow i\text{-}C_4H_5$ [Reaction 364]

It was found that the vinyl radical formation was dependent on three major reactions:

$H+C_2H_4 \Leftrightarrow C_2H_3+H_2$ [Reaction 75]

$OH+C_2H_4 \Leftrightarrow C_2H_3+H_2O$ [Reaction 112]

$CH_3+C_2H_4 \Leftrightarrow C_2H_3+CH_4$ [Reaction 164]

Inidividually, these reactions did not exhibit a synergisic effect over the mixture range, however, the added rates exhibited a slight synergistic effect as shown in Figure 4-52.

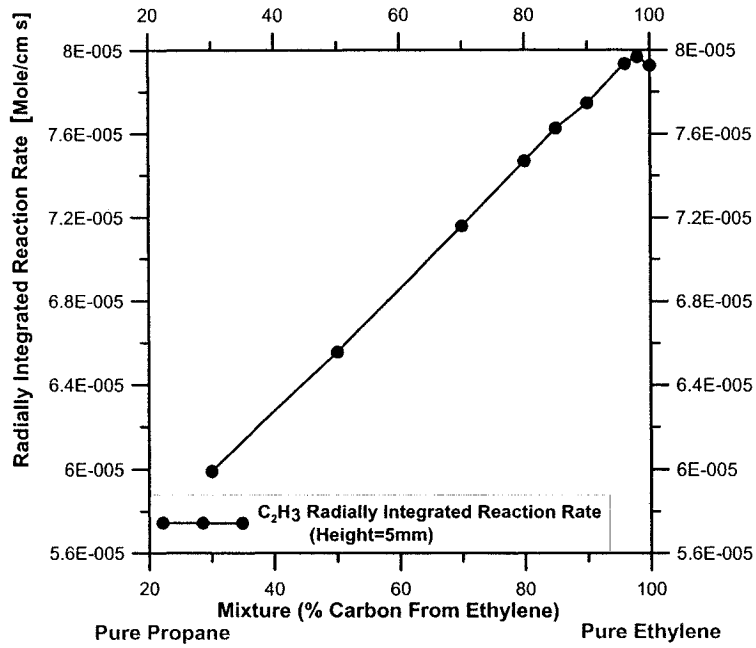

Figure 4-52 Radially Integrated Rates for Reactions 75+112+164 over Mixture Range at Height=5mm

Although this synergistic effect is slight, it could indicate that the root cause for the synergistic behaviour of the benzene and soot concentrations could be in fact due to the interaction of even- and odd-carbon numbered species, namely ethylene (C_2H_4) and the methyl radical (CH_3). Over the mixture range, the methyl concentration increases as propane is added and the ethylene concentration decreases as illustrated in Figure 4-53.

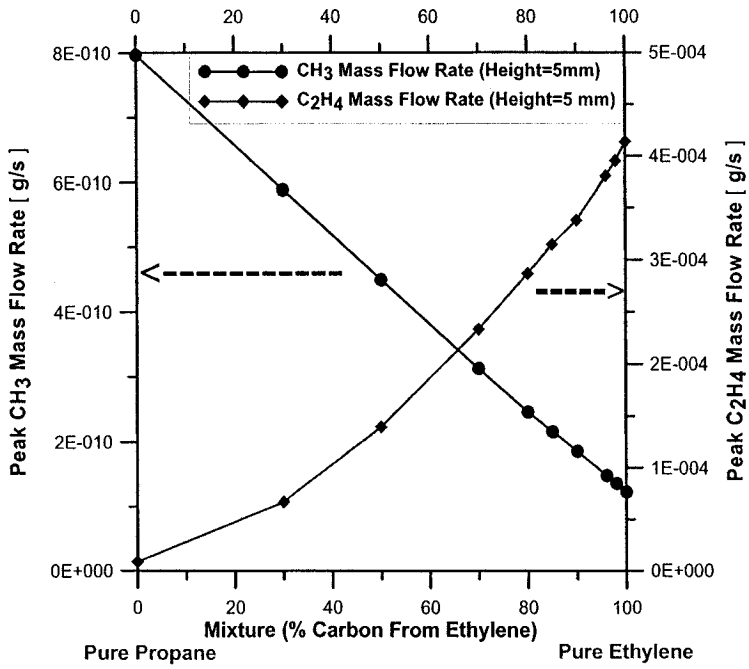

Figure 4-53 Mass Flow Rate CH_3 and C_2H_4, over Mixture Range at Height of 5 mm

This would corroborate the work presented by McNesby al [63], where it was evaluated that adding ethanol to the fuel side of an opposed flow flame would lead to a significant increase in the methyl radical concentration which would then lead to a significant increase in the C_2H_3 concentration through reaction 164. The researchers have identified that this would then contribute to an increase of the n-C_4H_5 concentration and consequently an increased benzene and soot formation through this path. It is therefore established that an increase in methyl radical has a significant impact on the sooting propensity through this path. This increase combined with the C_2H_4 species concentration reduction could then lead to the synergistic effect of the combined reaction rates shown in Figure 4-52. This would highlight a different interaction between even and odd-carbon numbered species in the sooting propensity of fuel mixtures than what has been previously identified.

It should be noted that our modification of the reaction rates for benzene formation have led to an increased importance of the acetylene-based pathways. It has been argued by Miller and Melius [8] that these could not be the dominant pathways due to the higher stability of the isomers i-C_4H_5 and i-C_4H_3, which would lead to lower concentrations of n-C_4H_5 and n-C_4H_3, reducing the importance of the paths dependent on these species. However, the relative stability of these species and their isomers is still debated [9,10] and the acetylene-based pathways are still considered important. It is possible, however, that in this case, its importance was overestimated.

Summarizing the numerical results, the synergistic effect in the ethylene/propane mixtures was found to be due to an interaction between the even and odd-carbon numbered species, namely ethylene (C_2H_4) and methyl radical (CH_3), in the vinyl species (C_2H_3) formation, leading to a synergistic effect in the acetylene based pathways to soot formation from the two following reactions:

$n\text{-}C_4H_3+C_2H_2 \Leftrightarrow A_1\text{-}$ [Reaction 400]

$n\text{-}C_4H_5+C_2H_2 \Leftrightarrow A_1+H$ [Reaction 403]

Previous researchers had presented that the synergistic effect would be effectively acting through the propargyl combination pathways [31]. However, according to the results presented here, this path is unlikely for the concentration profile of propargyl over the mixture range considered.

4.2.1 Comparison of Numerical and Experimental Results

To further validate this possible pathway to the synergistic effect in the soot formation, it is essential to correlate experimental results with these numerical findings. The following results were experimentally obtained for the sooting propensities of the mixtures over the mixture ranges.

Table 4-5 Summary of Experimental Results

Mixture	**Methane**	**Ethane**	**Propane**
Ethylene	Slight Synergistic Effect, Highly temperature dependent	Strong Synergistic Effect	Strong Synergistic Effect, Not temperature Dependent
Propane	No Synergistic Effect	No Synergistic Effect	
Ethane	Strong Synergistic Effect		
Butane	No Synergistic Effect		

The numerical findings correlated the synergistic effect identified in the ethylene/propane mixtures. It can be proposed that the synergistic effect measured in the methane/ethylene mixture could follow the same pathway. This seems warranted if we consider that, being a component of both mixtures; the ethylene (C_2H_4) concentration in both mixtures should have similar behaviour over the mixture range. As well, it is expected that the methane (CH_4) pyrolysis would readily form methyl radical (CH_3) species following the dehydrogenation reaction. It therefore seems likely that an interaction between these two species could occur in a similar fashion as in the ethylene/propane mixture. However, it was found that, contrary to the ethylene/propane mixture, the preheating of the fuel had a

very strong influence on the extent of the synergistic effect in the methane/ethylene mixtures. As mentioned previously, it is expected that for both mixtures, the ethylene concentration would behave in a similar fashion. Therefore, the distinguishing factor in the sooting synergistic behaviour for these two mixtures would be due to the methyl radical formation since this species was found to be responsible for the synergistic effect through its interaction with ethylene.

A previous study done in a counter-flow diffusion flame has highlighted the main difference found from the addition of propane and the addition of methane in an ethylene flame [32]. It was found that the addition of propane to an ethylene flame increased the methyl radical production in the low temperature regions of the flame, i.e. the lower portion of the flame [32]. The fact that the addition of this fuel was found to have an effect in the lower temperature region is key when contrasted against the effect of methane addition to an ethylene flame. The methane addition did not have a strong influence in the low temperature region of the flame but increased the production rate of methyl radical significantly in the high temperature region of the flame [32]. This would be due to the fact that the bond energy for the C-H bond in methane is stronger than the C-C bond in propane, requiring a larger activation energy to break [32]. This difference in behaviour is key in understanding the strong influence of temperature on the synergistic effect on the methane/ethylene mixtures. The preheating of the fuel allowed the easier formation of the methyl radical in a lower part of the flame by increasing the temperature in the low temperature region of the flame, where the benzene formation was found to be dominant. The methyl radical formation would be influenced by temperature in a lesser degree in the ethylene/propane mixtures, explaining the smaller effect of the preheating on the magnitude of the synergistic effect. Therefore, it is warranted to propose that for both the ethylene/propane and methane/ethylene mixtures, the interactions identified numerically would lead to the synergistic effect measured experimentally.

It is important to note here that, although the preheating was found to enhance the synergistic effect significantly in the methane/ethylene mixture, previous researchers have also identified a strong synergistic effect by maintaining the flame temperature constant through dilution [33]. These researchers have therefore cooled the flames as to maintain a pure methane flame temperature. The fact that this rendered the synergistic effect visible enforces that preheating is not solely responsible for the synergistic effect, but that the effect is also obscured by the temperature variation over the mixture range.

Other mixtures were found to demonstrate a synergistic effect, namely the methane/ethane and ethane/ethylene mixtures. Interestingly, no synergistic effect was measured in the ethane/propane mixtures. The synergistic effect in the ethane/ethylene mixture had been previously identified in a counter-flow diffusion flame where it has been demonstrated that the addition of ethane to an ethylene flame resulted in an increase of the methyl radical concentration in the low temperature portion of the flame [32]. This increase was lower than for the propane/ethylene flame, which would explain the smaller synergistic effect. Therefore, for the ethane/ethylene mixtures, the synergistic effect can again be attributed to the same phenomena as identified for the ethylene/propane and methane/ethylene mixtures.

Ethane (C_2H_6) is known to produce large amounts of ethylene (C_2H_4) during its pyrolysis through its dehydrogenation [60]. Therefore, the interaction between ethylene and methyl radical species could again explain the synergistic effect in the mixture of methane/ethane. It is important to note that, in this case, the adiabatic flame temperature of ethane is 2260 K [62], which is about 100 K lower than for ethylene. Therefore, the temperature variation over the mixture range is much smaller than for the methane/ethylene mixture, meaning that the synergistic effect is not obscured by this temperature variation.

However, if such an effect existed in the methane/ethane mixture, it would be expected that the synergy should be present in the ethane/propane mixture as well. Therefore, at this point, it is proposed that the synergistic effect in the ethane/propane and methane/ethane mixtures could be due to different causes. To clarify this issue, further numerical simulations would be essential.

The absence of a synergistic effect in the methane/propane and methane/butane mixtures was expected considering the path previously presented to explain the synergistic effect. This synergistic effect was found to be due to an interaction between the methyl radical and the ethylene concentrations for the vinyl radical formation. For methane, propane and butane, it was found that small amounts of ethylene were produced during their pyrolysis [60], rendering any interaction insignificant. The ratio of odd-carbon to even-carbon species produced for these fuels is comparable, yielding a similar sooting behaviour over the mixture range [60]. At first glance, this is surprising for the butane fuel since it is an even-carbon numbered species; however, in-depth analysis of its pyrolysis behaviour has shown that it is similar to the pyrolysis of propane [60]. Therefore, the absence of synergistic effect in these mixtures further validates that the synergistic effect measured in other mixtures is due to the interaction between even and odd-carbon numbered species.

5 CONCLUSION

The sooting propensity of an array of fuel mixtures was measured experimentally. It was found that for the mixtures of ethylene/propane, methane/ethylene, methane/ethane and ethane/ethylene there was a synergistic effect in the sooting propensity over the mixture range. Such an effect was not found in mixtures of ethane/propane, methane/propane and methane/butane.

To further clarify the reason for this effect, experiments were done in which the fuel and air were preheated to maintain a constant adiabatic flame temperature over the mixture range. With preheating, the sooting propensity of the ethylene/propane mixture was enhanced and the soot yield from pure propane was found to be similar to the soot yield of an ethylene flame. However, from the analysis of the deviation from linear fit, it was found that the magnitude of the synergistic effect was not influenced by the preheating. The preheating of the methane/ethylene mixture was found to enhance the sooting propensity over the mixture range as well as significantly increase the magnitude of the synergistic effect. The preheating of the methane/propane mixture did not reveal any underlying synergistic effect.

Numerical simulations of the ethylene/propane mixtures were successful in reproducing the synergistic effect qualitatively. Through an analysis of these results, it was found that the synergistic effect was not due to the propargyl combination reactions as presented by other researchers, but traced back to an interaction between the methyl radical (CH_3) and ethylene (C_2H_4) in the formation of the vinyl radical (C_2H_3), leading to a synergistic behaviour over the mixture range of the even-carbon based reactions for first ring formation.

This interaction successfully explained the synergistic effect in the ethylene/propane, methane/ethylene and ethane/ethylene mixtures. As well, the dependence of this synergistic effect on the methyl radical concentration explained the relative effect of the

preheating on the sooting propensity of the ethylene/propane and methane/ethylene mixtures through the different activation energies of the reactions forming this species in methane and propane. As well, the absence of a synergistic effect in the methane/propane and methane/butane mixtures further validates this interaction of even and odd-numbered carbon species as responsible for the sooting behaviour.

However, at this point, the presence of a synergistic effect in the methane/ethane mixtures and the absence of such an effect in the ethane/propane mixtures could not be explained. It is thought that other reactions could be involved in this effect and that further numerical simulations targeting these fuels would be essential in understanding this phenomenon.

6 REFERENCES

[1] U.S. EPA (2004) "Air Quality Criteria for Particulate Matter", United States Environmental Protection Agency (U.S. EPA), Vol. I and II, 2048 pages, October 2004.

[2] Glassman, I., "Soot formation in combustion processes", Proceedings of the Combustion Institute, Vol 22 (1988), 295-311.

[3] Schug, K. P., Manheimer-Timnat, Y., Yaccarino P., and Glassman I, "Sooting behaviour of gaseous hydrocarbon diffusion flames and the influence of additives", Combustion Science and Technology, Vol 22 (1980), 235-250.

[4] Kent, J.H., and Wagner, H G., "Temperature and fuel effects in sooting diffusion flames", Proceedings of the Combustion Institute, Vol 20 (1984), 1007-1015.

[5] Westmoreland, P. R., Dean, A. M., Horward J. B., and Longwell, J. P., "Forming benzene in flames by chemically activated isomerization", Journal of physical Chemistry, Vol 93 (1989), 8171-8180.

[6] Wang, H., Frenklach, M., "A detailed kinetic modeling study of aromatics formation in laminar premixed acetylene and ethylene flames", Combustion and Flame, Vol 110 (1997), 173-221.

[7] Cole, J. A., Bittner, J. D., Longwell, J. P., and Howard, J. B., "Formation mechanisms of aromatic compounds in aliphatic flames", Combustion and Flame, Vol 56 (1984), 51-70.

[8] Miller, J. A., and Melius, C. F., "Kinetics and thermodynamic issues in the formation of aromatic compounds in flames of aliphatic fuels", Combustion and Flame, Vol 91 (1992), 21-39.

[9] Frenklach, M., "Reaction mechanism of soot formation in flames", Phys. Chem. Chem. Phys., Vol 4 (2002), 2028-2037.

[10] Wheeler, S. E., Allen, W. D., and Schaefer III, H. F., "Thermochemistry of disputed soot formation intermediates C4H3 and C4H5", Journ. Chemical Physics, Vol 121 (2004), 8800-8813.

[11] Stein, S. E., Walker, J. A., Suryan, M. M., and Fahr, A., "A new path to benzene in flames", Proceedings of the Combustion Institute, Vol 23 (1990), 85-90.

[12] Senkan, S., and Castaldi, M.. "Formation of polycyclic aromatic hydrocarbons (PAH) in methane combustion: Comparative new results from premixed flames", Combustion and Flame, Vol 107 (1996), 141-150.

[13] Wu, C. H., and Kern, R. D., "Schock-tube study of allene pyrolysis", Journ. Physical Chemistry, Vol 91 (1987), 6291-6296.

[14] D'Anna, A., and Violi, A., "Kinetic model for the formation of aromatic hydrocarbons in premixed laminar flames", Proceedings of the Combustion Institute, Vol 27 (1998) 425-433.

[15] Marinov, N. M., Castaldi, M. J., Melius, C. F., and Tsang, W., "Aromatic and polycyclic aromatic hydrocarbon formation in a premixed propane flame", Combustion Science and Technology, Vol 128 (1997), 295-342.

[16] Marinov, N. M., Pitz, W. J., Westbrook, C. K., Castaldi, M. J., and Senkan, S. M., "Modeling of aromatic and polycyclic hydrocarbon formation in premixed and ethane flames", Combustion Science and Technology, Vol 116-117 (1997), 211-287.

[17] Marinov, N. M. , Pitz, W. J., Westbrook, C. K., Lutz, A.E., Vincitore, A.M., and Senkan, S. M., "Chemical kinetic modeling of a methane opposed-flow diffusion flame and comparison to experiments", Proceedings of the Combustion Institute, Vol 27 (1998), 605-613.

[18] Marinov, N. M., Pitz, W. J., Westbrook, C. K., Vincitore, A. M., Castaldi, M. J., Senkan S. M., and Melius C. F., "Aromatic and polycyclic aromatic hydrocarbons formation in a laminar premixed n-butane flame", Combustion and Flame, Vol 114 (1998), 192-213.

[19] Skjøth-Rasmussen, M. S. et al., "Formation of polycyclic aromatic hydrocarbons and soot in fuel-rich oxidation of methane in a laminar flow reactor", Combustion and Flame, Vol 136 (2004), 91-128.

[20] Frenklach, M., and Warnatz, J., "Detailed Modeling of PAH Profiles in a Sooting Low-Pressure Acetylene Flame", Combustion Science and Technology, Vol 51 (1987), 265-283.

[21] McEnally, C. S., and Pfefferle, L. D., "The effect of slight premixing on fuel decomposition and hydrocarbon growth in benzene-doped methane nonpremixed flames", Combustion and Flame, Vol 129 (2002), 305-323.

[22] Melius, C. F. , Colvin, M., Marinov, N. M., Pitz, W. J., and Senkan, S. M., "Reaction mechanisms in aromatic hydrocarbon formation involving the C_5H_5 cyclopentadienyl moity", Proceedings of the Combustion Institute, Vol 26 (1996), 685-692.

[23] Smedley, J.M., Williams, A., Bartle, K.D., "A mechanism for the formation of soot particles and soot deposits", Combustion and Flame, Vol 91 (1992), 71-82.

[24] McKinnon, J. T., and Horward, J. B., "The roles of PAH and acetylene in soot nucleation and growth", Proceedings of the Combustion Institute, Vol 24 (1992), 963-972.

[25] Neoh, K. G., Howard, J.B., and Sarofim, A. F., "Particulate carbon, formation during combustion", Plenum press. (1981), 261-282.

[26] Roesler, J.F., Auphan de Tessan M., and Montagne, X., "Evidence for the contribution of methane in the formation of aromatics and soot in fuel-rich pre-mixed combustion", Chemosphere, Vol 42 (2001), 823-826.

[27] Roesler, J. F., and Auphan de Tessan, M., "Aromatics and soot growth enhancement by methane addition to fuel-rich n-heptane combustion in a flow reactor", Combustion Science and Technology, Vol 161 (2000), 254-268.

[28] Miller, J. A., Volponi, J. V., and Pauwels, J.-F., "The effect of allene addition on the structure of a rich C_2H_2/O_2 Ar flame", Combustion and Flame, Vol 105 (1996), 451-461.

[29] Frenklach, M., Yuan, T., and Ramachandra, M.K., "Soot formation in binary hydrocarbon mixtures", Energy and Fuels, Vol 2 (1988), 462-480.

[30] Hwang, J. Y., Lee, W, Kang, H. G., and Chung, S.H., "Synergistic effect of ethylene-propane mixture on soot formation in laminar diffusion flames", Combustion and Flame, Vol 114 (1998), 370-380.

[31] Hwang, J.Y., Chung, S.H., and Lee, W., "Effects of oxygen and propane addition on soot formation in counterflow ethylene flames and the role of C_3 chemistry", Proceedings of the Combustion Institute, Vol 27 (1998), 1531-1538.

[32] Yoon, S.S., Lee, S.M., and Chung, S.H., "Effect of mixing methane, ethane, propane and propene on the synergistic effect of PAH and soot formation in ethylene-base counterflow diffusion flames", Proceedings of the Combustion Institute, Vol 30 (2005), 1417-1424.

[33] Roesler, J. F., Martinot, S., McEnally, C.S., Pfefferle, L.D,. Delfau, J.-L., and Voyelle, C., "Investigating the role of methane on the growth of aromatic hydrocarbons and soot in fundamental combustion processes", Combustion and Flame, Vol 134 (2003), 249-260.

[34] Lee, S.M., Yoon, S.S., and Chung, S.H., "Synergistic effect on soot formation in counterflow diffusion flames of ethylene-propane mixtures with benzene addition", Combustion and Flame, Vol 136 (2004), 493-500.

[35] Qin, Z., Lissianski, V. V., Yang, H., Gardiner, W.C., and Davis, S. G., "Combustion chemistry of propane: A case study of detailed reaction mechanism optimization", Proceedings of the Combustion Institute, Vol 28 (2000), 1663-1669.

[36] Beltrame, A., Porshnov, P., Merchan-Merchan, W., Saveliev, A., Fridman, A., Kennedy, L. A., Petrova, O., Zhdanok, S., Amouri F., and Charon, O., "Soot and NO formation in methane–oxygen enriched diffusion flames", Combustion and Flame, Vol 124 (2001), 295-310.

[37] Gülder, Ö., "Effect of oxygen on soot formation in methane, propane and n-butane diffusion flames", Combustion and Flame, Vol 101 (1995), 302-310.

[38] Gülder, Ö., Snelling, D. R., "Influence of nitrogen dilution and flame temperature on soot formation in diffusion flames", Combustion and Flame, Vol 92 (1993), 115-124.

[39] Snelling, D. R., Thomson, K. A., Smallwood, G. J., and Gülder, Ö., "Two-dimensional imaging of soot volume fraction in laminar diffusion flames", Applied Optics, Vol 38 (1999), 2478-2485.

[40] Greenberg, P. S., and Ku, J. C., "Soot volume fraction imaging", Applied Optics, Vol 36 (1997), 5514-5522.

[41] Faeth, G. M. and Köylü, Ü. Ö, "Soot morphology and optical properties in nonpremixed turbulent flame environments", Combustion Science and Technology, Vol 108 (1995), 207-229.

[42] Mountain, R. D., and Mulholland, G. W., "Light scattering from simulated smoke aggregate", Langmuir, 4 (1988), 1321-1326.

[43] Krishnan, S. S., Lin, K. C., and Faeth, G. M., "Extinction and scattering properties of soot emitted from buoyant turbulent diffusion flames", Journal of Heat Transfer, Vol 123 (2001), 331-339

[44] Dasch, C. J., "One-dimensional tomography: A comparison of Abel, onion-peeling, and filtered back projection methods", Applied Optics, Vol 31 (1992), 1146-1152.

[45] Nishida, O., and Mukõhara, S.,"Optical measurement of soot particles in a laminar diffusion flame", Combustion Science and Technology, 35 (1983), 157-173.

[46] Santoro, R.J., Yeh, T. T., Hovarth, J. J., and Semerjian, H. G., "The transport and growth of soot particles in laminar diffusion flames", Combustion Science and.Technology, Vol 53 (1987), 89-115.

[47] Roper, F. G., Smith, C., and Cunnignham, A.C., "The prediction of laminar jet diffusion flame sizes: Part II. Experimental verification", Combustion and Flame, Vol 29 (1977), 227-234.

[48] Roper, F. G., "Soot escape from diffusion flames: A comparison of recent work in this field", Combustion Science and Technology, Vol 40 (1984), 323-329.

[49] McEnally, C. S., Köylü, Ü. Ö., Pfefferle, L. D., and Rosner, D. F., "Soot volume fraction and temperature measurements in laminar nonpremixed flames using thermocouples", Combustion and Flame, Vol 109 (1997), 701-720.

[50] Cundy, V. A., Morse, J. S., and Senser, D. W., "Constant-tension thermocouple rake suitable for use in flame mode combustion studies", Review Scientific Instruments, Vol 57 (1986), 1209-1210.

[51] Acrivos, A., and Taylor, T. D., "Heat and Mass Transfer from Single Spheres in Stokes Flow", Phys. Fluids, Vol 5 (1962), 387-394.

[52] Bradley, D, and Entwistle, A. G., "Determination of the emissivity, for total radiation, of small diameter platinum-10% rhodium wires in the temperature range 600-1450°C", British Journal of Applied Physics, Vol 12 (1961), 708-711.

[53] Guo, H., Liu, F., Smallwood G. J., and Gülder, Ö. L., "The flame preheating effect on numerical modelling of soot formation in a two-dimensional laminar ethylene–air diffusion flame", Combustion Theory and Modelling, Vol 6 (2002), 173-187.

[54] Leung, K. M., and Lindstedt, R. P., "A simplified reaction mechanism for soot formation in nonpremixed flame", Combustion and Flame, Vol 87 (1991), 289-305.

[55] Fairweather, M., Jones, W. P., Lindstedt, R. P., "Predictions of radiative transfer from a turbulent reacting jet in a cross-wind", Combustion and Flame, Vol 89 (1992), 45-63.

[56] Guo, H., Liu, F., and Smallwood, G. J., "A numerical study of the influence of hydrogen addition on soot formation in a laminar counterflow ethylene/oxygen/nitrogen diffusion flame", Proceedings of IMECE2004-59407.

[57] Appel, J.,. Bockhorn, H., and Frenklach, M., "Kinetic modeling of soot formation with detailed chemistry and physics: Laminar premixed flames of C_2 hydrocarbons", Combustion and Flame, Vol 121 (2000), 122-136.

[58] Kazakov, A., Wang, H., and Frenklach, M., "Detailed Modeling of Soot Formation in Laminar Premixed Ethylene Flames at a Pressure of 10 Bar", Combustion and Flame, Vol 100 (1995), 111-120.

[59] Daun, K. J, Thomson, K. A., Liu, F., and Smallwood, G. J., "Solutions of Abel's equation using Tikhonov regularization", IMECE2005-81435.

[60] McEnally, C. S., and Pfefferle, L. D., "Comparison of non-fuel hydrocarbon concentrations measured in coflowing nonpremixed flames fuelled with small hydrocarbons", Combustion and Flame, Vol 117 (1999), 362-372.

[61] Gülder, Ö., Snelling, D. R., and Sawchuck, R. A., "Influence of hydrogen addition to fuel on temperature field and soot formation in diffusion flames", Proceedings of the Combustion Institute, Vol 26 (1996), 2351-2358.

[62] Reynolds, W.C., STANJAN: Version 3.8C, May 1988, Stanford Univ.

[63] K. McNesby et al., "Experimental and computational studies of oxidizer and fuel side addition of ethanol to opposed flow air/ethylene flames", Combustion and Flame, Vol 142 (2005), 413-427.

APPENDIX A CHEMICAL KINETICS

The chemical kinetic model used is presented here. This model is based on that presented by Qin [35]. The rates of reactions 397, 398, 400, 403 have been modified.

The units are as follows:
A [mole-cm-s-K]
E [Cal/mole]

	REACTIONS CONSIDERED	(k = A T**b exp(-E/RT)) A	b	E
1.	2O+M<=>O2+M	1.20E+17	-1.0	0.0
2.	O+H+M<=>OH+M	5.00E+17	-1.0	0.0
3.	O+H2<=>H+OH	3.87E+04	2.7	6260.0
4.	O+HO2<=>OH+O2	2.00E+13	0.0	0.0
5.	O+H2O2<=>OH+HO2	9.63E+06	2.0	4000.0
6.	O+CH<=>H+CO	5.70E+13	0.0	0.0
7.	O+CH2<=>H+HCO	8.00E+13	0.0	0.0
8.	O+CH2*<=>H2+CO	1.50E+13	0.0	0.0
9.	O+CH2*<=>H+HCO	1.50E+13	0.0	0.0
10.	O+CH3<=>H+CH2O	5.06E+13	0.0	0.0
11.	O+CH4<=>OH+CH3	1.02E+09	1.5	8600.0
12.	O+CO(+M)<=>CO2(+M)	1.80E+10	0.0	2385.0
13.	O+HCO<=>OH+CO	3.00E+13	0.0	0.0
14.	O+HCO<=>H+CO2	3.00E+13	0.0	0.0
15.	O+CH2O<=>OH+HCO	3.90E+13	0.0	3540.0
16.	O+CH2OH<=>OH+CH2O	1.00E+13	0.0	0.0
17.	O+CH3O<=>OH+CH2O	1.00E+13	0.0	0.0
18.	O+CH3OH<=>OH+CH2OH	3.88E+05	2.5	3100.0
19.	O+CH3OH<=>OH+CH3O	1.30E+05	2.5	5000.0
20.	O+C2H<=>CH+CO	5.00E+13	0.0	0.0
21.	O+C2H2<=>H+HCCO	1.35E+07	2.0	1900.0
22.	O+C2H2<=>OH+C2H	4.60E+19	-1.4	28950.0
23.	O+C2H2<=>CO+CH2	6.94E+06	2.0	1900.0
24.	O+C2H3<=>H+CH2CO	3.00E+13	0.0	0.0
25.	O+C2H4<=>CH3+HCO	2.50E+07	1.8	220.0
26.	O+C2H5<=>CH3+CH2O	2.24E+13	0.0	0.0
27.	O+C2H6<=>OH+C2H5	8.98E+07	1.9	5690.0
28.	O+HCCO<=>H+2CO	1.00E+14	0.0	0.0
29.	O+CH2CO<=>OH+HCCO	1.00E+13	0.0	8000.0
30.	O+CH2CO<=>CH2+CO2	1.75E+12	0.0	1350.0
31.	O2+CO<=>O+CO2	2.50E+12	0.0	47800.0
32.	O2+CH2O<=>HO2+HCO	1.00E+14	0.0	40000.0
33.	H+O2+M<=>HO2+M	2.80E+18	-0.9	0.0
34.	H+2O2<=>HO2+O2	2.08E+19	-1.2	0.0
35.	H+O2+H2O<=>HO2+H2O	1.13E+19	-0.8	0.0
36.	H+O2+N2<=>HO2+N2	2.60E+19	-1.2	0.0
37.	H+O2+AR<=>HO2+AR	7.00E+17	-0.8	0.0
38.	H+O2<=>O+OH	2.65E+16	-0.7	17041.0
39.	2H+M<=>H2+M	1.00E+18	-1.0	0.0
40.	2H+H2<=>2H2	9.00E+16	-0.6	0.0
41.	2H+H2O<=>H2+H2O	6.00E+19	-1.3	0.0
42.	2H+CO2<=>H2+CO2	5.50E+20	-2.0	0.0
43.	H+OH+M<=>H2O+M	2.20E+22	-2.0	0.0
44.	H+HO2<=>O+H2O	3.97E+12	0.0	671.0
45.	H+HO2<=>O2+H2	7.75E+13	0.0	1068.0
46.	H+HO2<=>2OH	4.20E+13	0.0	635.0
47.	H+H2O2<=>HO2+H2	1.21E+07	2.0	5200.0
48.	H+H2O2<=>OH+H2O	1.00E+13	0.0	3600.0
49.	H+CH<=>C+H2	1.65E+14	0.0	0.0

50.	H+CH2(+M)<=>CH3(+M)	6.00E+14	0.0	0.0
51.	H+CH2*<=>CH+H2	3.00E+13	0.0	0.0
52.	H+CH3(+M)<=>CH4(+M)	1.39E+16	-0.5	536.0
53.	H+CH4<=>CH3+H2	6.60E+08	1.6	10840.0
54.	H+HCO(+M)<=>CH2O(+M)	1.09E+12	0.5	-260.0
55.	H+HCO<=>H2+CO	7.34E+13	0.0	0.0
56.	H+CH2O(+M)<=>CH2OH(+M)	5.40E+11	0.5	3600.0
57.	H+CH2O(+M)<=>CH3O(+M)	5.40E+11	0.5	2600.0
58.	H+CH2O<=>HCO+H2	5.74E+07	1.9	2742.0
59.	H+CH2OH(+M)<=>CH3OH(+M)	1.06E+12	0.5	86.0
60.	H+CH2OH<=>H2+CH2O	2.00E+13	0.0	0.0
61.	H+CH2OH<=>OH+CH3	1.65E+11	0.7	-284.0
62.	H+CH2OH<=>CH2*+H2O	3.28E+13	-0.1	610.0
63.	H+CH3O(+M)<=>CH3OH(+M)	2.43E+12	0.5	50.0
64.	H+CH3O<=>H+CH2OH	4.15E+07	1.6	1924.0
65.	H+CH3O<=>H2+CH2O	2.00E+13	0.0	0.0
66.	H+CH3O<=>OH+CH3	1.50E+12	0.5	-110.0
67.	H+CH3O<=>CH2*+H2O	2.62E+14	-0.2	1070.0
68.	H+CH3OH<=>CH2OH+H2	1.70E+07	2.1	4870.0
69.	H+CH3OH<=>CH3O+H2	4.20E+06	2.1	4870.0
70.	H+C2H(+M)<=>C2H2(+M)	1.00E+17	-1.0	0.0
71.	H+C2H2(+M)<=>C2H3(+M)	5.60E+12	0.0	2400.0
72.	H+C2H3(+M)<=>C2H4(+M)	6.08E+12	0.3	280.0
73.	H+C2H3<=>H2+C2H2	3.03E+13	0.0	0.0
74.	H+C2H4(+M)<=>C2H5(+M)	7.83E+11	0.5	1820.0
75.	H+C2H4<=>C2H3+H2	1.33E+06	2.5	12240.0
76.	H+C2H5(+M)<=>C2H6(+M)	5.21E+17	-1.0	1580.0
77.	H+C2H5<=>H2+C2H4	2.00E+12	0.0	0.0
78.	H+C2H6<=>C2H5+H2	1.15E+08	1.9	7530.0
79.	H+HCCO<=>CH2*+CO	1.00E+14	0.0	0.0
80.	H+CH2CO<=>HCCO+H2	5.00E+13	0.0	8000.0
81.	H+CH2CO<=>CH3+CO	1.13E+13	0.0	3428.0
82.	H+HCCOH<=>H+CH2CO	1.00E+13	0.0	0.0
83.	H2+CO(+M)<=>CH2O(+M)	4.30E+07	1.5	79600.0
84.	OH+H2<=>H+H2O	2.16E+08	1.5	3430.0
85.	2OH(+M)<=>H2O2(+M)	7.40E+13	-0.4	0.0
86.	2OH<=>O+H2O	3.57E+04	2.4	-2110.0
87.	OH+HO2<=>O2+H2O	1.45E+13	0.0	-500.0
88.	OH+H2O2<=>HO2+H2O	2.00E+12	0.0	427.0
89.	OH+H2O2<=>HO2+H2O	1.70E+18	0.0	29410.0
90.	OH+C<=>H+CO	5.00E+13	0.0	0.0
91.	OH+CH<=>H+HCO	3.00E+13	0.0	0.0
92.	OH+CH2<=>H+CH2O	2.00E+13	0.0	0.0
93.	OH+CH2<=>CH+H2O	1.13E+07	2.0	3000.0
94.	OH+CH2*<=>H+CH2O	3.00E+13	0.0	0.0
95.	OH+CH3(+M)<=>CH3OH(+M)	2.79E+18	-1.4	1330.0
96.	OH+CH3<=>CH2+H2O	5.60E+07	1.6	5420.0
97.	OH+CH3<=>CH2*+H2O	6.44E+17	-1.3	1417.0
98.	OH+CH4<=>CH3+H2O	1.00E+08	1.6	3120.0
99.	OH+CO<=>H+CO2	4.76E+07	1.2	70.0
100.	OH+HCO<=>H2O+CO	5.00E+13	0.0	0.0
101.	OH+CH2O<=>HCO+H2O	3.43E+09	1.2	-447.0
102.	OH+CH2OH<=>H2O+CH2O	5.00E+12	0.0	0.0
103.	OH+CH3O<=>H2O+CH2O	5.00E+12	0.0	0.0
104.	OH+CH3OH<=>CH2OH+H2O	1.44E+06	2.0	-840.0
105.	OH+CH3OH<=>CH3O+H2O	6.30E+06	2.0	1500.0
106.	OH+C2H<=>H+HCCO	2.00E+13	0.0	0.0
107.	OH+C2H2<=>H+CH2CO	2.18E-04	4.5	-1000.0
108.	OH+C2H2<=>H+HCCOH	5.04E+05	2.3	13500.0
109.	OH+C2H2<=>C2H+H2O	3.37E+07	2.0	14000.0
110.	OH+C2H2<=>CH3+CO	4.83E-04	4.0	-2000.0
111.	OH+C2H3<=>H2O+C2H2	5.00E+12	0.0	0.0
112.	OH+C2H4<=>C2H3+H2O	1.80E+06	2.0	2500.0
113.	OH+C2H6<=>C2H5+H2O	3.54E+06	2.1	870.0
114.	OH+CH2CO<=>HCCO+H2O	7.50E+12	0.0	2000.0
115.	2HO2<=>O2+H2O2	1.30E+11	0.0	-1630.0
116.	2HO2<=>O2+H2O2	4.20E+14	0.0	12000.0
117.	HO2+CH2<=>OH+CH2O	2.00E+13	0.0	0.0
118.	HO2+CH3<=>O2+CH4	1.00E+12	0.0	0.0

119.	HO2+CH3<=>OH+CH3O	2.87E+13	0.0	0.0
120.	HO2+CO<=>OH+CO2	1.50E+14	0.0	23600.0
121.	HO2+CH2O<=>HCO+H2O2	5.60E+06	2.0	12000.0
122.	C+O2<=>O+CO	5.80E+13	0.0	576.0
123.	C+CH2<=>H+C2H	5.00E+13	0.0	0.0
124.	C+CH3<=>H+C2H2	5.00E+13	0.0	0.0
125.	CH+O2<=>O+HCO	6.71E+13	0.0	0.0
126.	CH+H2<=>H+CH2	1.08E+14	0.0	3110.0
127.	CH+H2O<=>H+CH2O	5.71E+12	0.0	-755.0
128.	CH+CH2<=>H+C2H2	4.00E+13	0.0	0.0
129.	CH+CH3<=>H+C2H3	3.00E+13	0.0	0.0
130.	CH+CH4<=>H+C2H4	6.00E+13	0.0	0.0
131.	CH+CO(+M)<=>HCCO(+M)	5.00E+13	0.0	0.0
132.	CH+CO2<=>HCO+CO	1.90E+14	0.0	15792.0
133.	CH+CH2O<=>H+CH2CO	9.46E+13	0.0	-515.0
134.	CH+HCCO<=>CO+C2H2	5.00E+13	0.0	0.0
135.	CH2+O2=>OH+H+CO	5.00E+12	0.0	1500.0
136.	CH2+H2<=>H+CH3	5.00E+05	2.0	7230.0
137.	2CH2<=>H2+C2H2	1.60E+15	0.0	11944.0
138.	CH2+CH3<=>H+C2H4	4.00E+13	0.0	0.0
139.	CH2+CH4<=>2CH3	2.46E+06	2.0	8270.0
140.	CH2+CO(+M)<=>CH2CO(+M)	8.10E+11	0.5	4510.0
141.	CH2+HCCO<=>C2H3+CO	3.00E+13	0.0	0.0
142.	CH2*+N2<=>CH2+N2	1.50E+13	0.0	600.0
143.	CH2*+AR<=>CH2+AR	9.00E+12	0.0	600.0
144.	CH2*+O2<=>H+OH+CO	2.80E+13	0.0	0.0
145.	CH2*+O2<=>CO+H2O	1.20E+13	0.0	0.0
146.	CH2*+H2<=>CH3+H	7.00E+13	0.0	0.0
147.	CH2*+H2O(+M)<=>CH3OH(+M)	4.82E+17	-1.2	1145.0
148.	CH2*+H2O<=>CH2+H2O	3.00E+13	0.0	0.0
149.	CH2*+CH3<=>H+C2H4	1.20E+13	0.0	-570.0
150.	CH2*+CH4<=>2CH3	1.60E+13	0.0	-570.0
151.	CH2*+CO<=>CH2+CO	9.00E+12	0.0	0.0
152.	CH2*+CO2<=>CH2+CO2	7.00E+12	0.0	0.0
153.	CH2*+CO2<=>CO+CH2O	1.40E+13	0.0	0.0
154.	CH2*+C2H6<=>CH3+C2H5	4.00E+13	0.0	-550.0
155.	CH3+O2<=>O+CH3O	3.56E+13	0.0	30480.0
156.	CH3+O2<=>OH+CH2O	2.31E+12	0.0	20315.0
157.	CH3+H2O2<=>HO2+CH4	2.45E+04	2.5	5180.0
158.	2CH3(+M)<=>C2H6(+M)	6.77E+16	-1.2	654.0
159.	2CH3<=>H+C2H5	6.84E+12	0.1	10600.0
160.	CH3+HCO<=>CH4+CO	2.65E+13	0.0	0.0
161.	CH3+CH2O<=>HCO+CH4	3.32E+03	2.8	5860.0
162.	CH3+CH3OH<=>CH2OH+CH4	3.00E+07	1.5	9940.0
163.	CH3+CH3OH<=>CH3O+CH4	1.00E+07	1.5	9940.0
164.	CH3+C2H4<=>C2H3+CH4	2.27E+05	2.0	9200.0
165.	CH3+C2H6<=>C2H5+CH4	6.14E+06	1.7	10450.0
166.	HCO+H2O<=>H+CO+H2O	1.50E+18	-1.0	17000.0
167.	HCO+M<=>H+CO+M	1.87E+17	-1.0	17000.0
168.	HCO+O2<=>HO2+CO	1.35E+13	0.0	400.0
169.	CH2OH+O2<=>HO2+CH2O	1.80E+13	0.0	900.0
170.	CH3O+O2<=>HO2+CH2O	4.28E-13	7.6	-3530.0
171.	C2H+O2<=>HCO+CO	1.00E+13	0.0	-755.0
172.	C2H+H2<=>H+C2H2	5.68E+10	0.9	1993.0
173.	C2H3+O2<=>HCO+CH2O	4.58E+16	-1.4	1015.0
174.	C2H4(+M)<=>H2+C2H2(+M)	8.00E+12	0.4	86770.0
175.	C2H5+O2<=>HO2+C2H4	8.40E+11	0.0	3875.0
176.	HCCO+O2<=>OH+2CO	3.20E+12	0.0	854.0
177.	2HCCO<=>2CO+C2H2	1.00E+13	0.0	0.0
178.	O+CH3=>H+H2+CO	3.37E+13	0.0	0.0
179.	O+C2H4<=>H+CH2CHO	3.35E+06	1.8	220.0
180.	O+C2H5<=>H+CH3CHO	1.10E+14	0.0	0.0
181.	OH+HO2<=>O2+H2O	5.00E+15	0.0	17330.0
182.	OH+CH3=>H2+CH2O	8.00E+09	0.5	-1755.0
183.	CH+H2(+M)<=>CH3(+M)	1.97E+12	0.4	-370.0
184.	CH2+O2=>2H+CO2	5.80E+12	0.0	1500.0
185.	CH2+O2<=>O+CH2O	2.40E+12	0.0	1500.0
186.	CH2+CH2=>2H+C2H2	2.00E+14	0.0	10989.0
187.	CH2*+H2O=>H2+CH2O	6.82E+10	0.3	-935.0

188. C2H3+O2<=>O+CH2CHO	1.21E+11	0.3	11.0
189. C2H3+O2<=>HO2+C2H2	1.34E+06	1.6	-384.0
190. O+CH3CHO<=>OH+CH2CHO	2.92E+12	0.0	1808.0
191. O+CH3CHO=>OH+CH3+CO	2.92E+12	0.0	1808.0
192. O2+CH3CHO=>HO2+CH3+CO	3.01E+13	0.0	39150.0
193. H+CH3CHO<=>CH2CHO+H2	2.05E+09	1.2	2405.0
194. H+CH3CHO=>CH3+H2+CO	2.05E+09	1.2	2405.0
195. OH+CH3CHO=>CH3+H2O+CO	2.34E+10	0.7	-1113.0
196. HO2+CH3CHO=>CH3+H2O2+CO	3.01E+12	0.0	11923.0
197. CH3+CH3CHO=>CH3+CH4+CO	2.72E+06	1.8	5920.0
198. H+CH2CO(+M)<=>CH2CHO(+M)	4.87E+11	0.4	-1755.0
199. O+CH2CHO=>H+CH2+CO2	1.50E+14	0.0	0.0
200. O2+CH2CHO=>OH+CO+CH2O	1.81E+10	0.0	0.0
201. O2+CH2CHO=>OH+2HCO	2.35E+10	0.0	0.0
202. H+CH2CHO<=>CH3+HCO	2.20E+13	0.0	0.0
203. H+CH2CHO<=>CH2CO+H2	1.10E+13	0.0	0.0
204. OH+CH2CHO<=>H2O+CH2CO	1.20E+13	0.0	0.0
205. OH+CH2CHO<=>HCO+CH2OH	3.01E+13	0.0	0.0
206. CH3+C2H<=>C3H3+H	2.41E+13	0.0	0.0
207. C2H2+CH<=>C3H2+H	3.00E+13	0.0	0.0
208. C2H2+CH2<=>C3H3+H	1.20E+13	0.0	6620.0
209. C2H2+CH2*<=>C3H3+H	2.00E+13	0.0	0.0
210. C2H2+HCCO<=>C3H3+CO	1.00E+11	0.0	3000.0
211. C3H2+O<=>C2H2+CO	6.80E+13	0.0	0.0
212. C3H2+OH<=>HCO+C2H2	6.80E+13	0.0	0.0
213. C3H2+O2<=>HCCO+H+CO	2.00E+12	0.0	1000.0
214. C3H2+H<=>C3H3	1.00E+13	0.0	0.0
215. C3H3+H<=>pC3H4	8.55E+12	0.0	0.0
216. C3H3+H<=>aC3H4	8.25E+11	0.0	0.0
217. C3H3+H<=>C3H2+H2	5.00E+13	0.0	1000.0
218. C3H3+O<=>CH2O+C2H	2.00E+13	0.0	0.0
219. C3H3+OH<=>C3H2+H2O	1.42E+13	0.0	0.0
220. C3H3+O2<=>CH2CO+HCO	4.17E+10	0.0	2868.0
221. C3H3+HO2<=>OH+CO+C2H3	8.00E+11	0.0	0.0
222. C3H3+HO2<=>aC3H4+O2	9.00E+11	0.0	0.0
223. C3H3+HO2<=>pC3H4+O2	1.10E+12	0.0	0.0
224. C3H3+HCO<=>aC3H4+CO	2.50E+13	0.0	0.0
225. C3H3+HCO<=>pC3H4+CO	2.50E+13	0.0	0.0
226. aC3H4+H<=>C3H3+H2	1.30E+06	2.0	5500.0
227. aC3H4+H<=>CH3CCH2	9.46E+42	-9.4	11190.0
228. aC3H4+H<=>aC3H5	1.52E+59	-13.5	26949.0
229. aC3H4+O<=>C2H4+CO	2.00E+07	1.8	1000.0
230. aC3H4+OH<=>C3H3+H2O	5.30E+06	2.0	2000.0
231. aC3H4+CH3<=>C3H3+CH4	1.30E+12	0.0	7700.0
232. aC3H4+C2H<=>C2H2+C3H3	1.00E+13	0.0	0.0
233. pC3H4<=>cC3H4	1.20E+44	-9.9	69250.0
234. pC3H4<=>aC3H4	1.03E+61	-13.9	91117.0
235. cC3H4<=>aC3H4	4.89E+41	-9.2	49594.0
236. pC3H4+H<=>aC3H4+H	6.27E+17	-0.9	10079.0
237. pC3H4+H<=>CH3CCH2	1.66E+47	-10.6	13690.0
238. pC3H4+H<=>aC3H5	4.91E+60	-14.4	31644.0
239. pC3H4+H<=>C3H3+H2	1.30E+06	2.0	5500.0
240. pC3H4+O<=>HCCO+CH3	2.04E+13	0.0	2250.0
241. pC3H4+O<=>C2H4+CO	5.80E+12	0.0	2250.0
242. pC3H4+OH<=>C3H3+H2O	1.00E+06	2.0	100.0
243. pC3H4+C2H<=>C2H2+C3H3	1.00E+13	0.0	0.0
244. pC3H4+CH3<=>C3H3+CH4	1.80E+12	0.0	7700.0
245. C3H8+H<=>H2+nC3H7	1.30E+06	2.5	6756.0
246. C3H8+H<=>H2+iC3H7	2.60E+06	2.4	4471.0
247. C3H8+O<=>nC3H7+OH	1.90E+05	2.7	3716.0
248. C3H8+O<=>iC3H7+OH	4.76E+04	2.7	2106.0
249. C3H8+OH<=>nC3H7+H2O	1.40E+03	2.7	527.0
250. C3H8+OH<=>iC3H7+H2O	2.70E+04	2.4	393.0
251. C3H8+O2<=>nC3H7+HO2	4.00E+13	0.0	50930.0
252. C3H8+O2<=>iC3H7+HO2	4.00E+13	0.0	47590.0
253. C3H8+HO2<=>nC3H7+H2O2	4.76E+04	2.5	16490.0
254. C3H8+HO2<=>iC3H7+H2O2	9.64E+03	2.6	13910.0
255. C3H8+CH3<=>CH4+nC3H7	9.03E-01	3.6	7153.0
256. C3H8+CH3<=>CH4+iC3H7	1.51E+00	3.5	5480.0

257.	nC3H7+H(+M)<=>C3H8(+M)	3.60E+13	0.0	0.0
258.	nC3H7+H<=>C2H5+CH3	3.70E+24	-2.9	12505.0
259.	nC3H7+H<=>C3H6+H2	1.80E+12	0.0	0.0
260.	nC3H7+O<=>C2H5+CH2O	9.60E+13	0.0	0.0
261.	nC3H7+OH<=>C3H6+H2O	2.40E+13	0.0	0.0
262.	nC3H7+O2<=>C3H6+HO2	9.00E+10	0.0	0.0
263.	nC3H7+HO2<=>C2H5+OH+CH2O	2.40E+13	0.0	0.0
264.	nC3H7+HCO<=>C3H8+CO	6.00E+13	0.0	0.0
265.	nC3H7+CH3<=>CH4+C3H6	1.10E+13	0.0	0.0
266.	iC3H7+H(+M)<=>C3H8(+M)	2.40E+13	0.0	0.0
267.	iC3H7+H<=>CH3+C2H5	1.40E+28	-3.9	15916.0
268.	iC3H7+H<=>C3H6+H2	3.20E+12	0.0	0.0
269.	iC3H7+O<=>CH3CHO+CH3	9.60E+13	0.0	0.0
270.	iC3H7+OH<=>C3H6+H2O	2.40E+13	0.0	0.0
271.	iC3H7+O2<=>C3H6+HO2	1.30E+11	0.0	0.0
272.	iC3H7+HO2<=>CH3CHO+CH3+OH	2.40E+13	0.0	0.0
273.	iC3H7+HCO<=>C3H8+CO	1.20E+14	0.0	0.0
274.	iC3H7+CH3<=>CH4+C3H6	2.20E+14	-0.7	0.0
275.	C3H6+H(+M)<=>nC3H7(+M)	1.33E+13	0.0	3260.7
276.	C3H6+H(+M)<=>iC3H7(+M)	1.33E+13	0.0	1559.8
277.	C3H6+H<=>C2H4+CH3	2.58E+22	-2.4	11180.0
278.	C3H6+H<=>aC3H5+H2	8.50E+04	2.5	2490.0
279.	C3H6+H<=>CH3CCH2+H2	4.00E+05	2.5	9790.0
280.	C3H6+O<=>CH2CO+CH3+H	1.20E+08	1.6	327.0
281.	C3H6+O<=>C2H5+HCO	3.50E+07	1.6	-972.0
282.	C3H6+O<=>aC3H5+OH	1.80E+11	0.7	5880.0
283.	C3H6+O<=>CH3CCH2+OH	6.00E+10	0.7	7630.0
284.	C3H6+OH<=>aC3H5+H2O	3.97E+06	2.0	-298.0
285.	C3H6+OH<=>CH3CCH2+H2O	1.10E+06	2.0	1450.0
286.	C3H6+HO2<=>aC3H5+H2O2	9.60E+03	2.6	13910.0
287.	C3H6+CH3<=>aC3H5+CH4	2.20E+00	3.5	5675.0
288.	C3H6+CH3<=>CH3CCH2+CH4	8.40E-01	3.5	11660.0
289.	aC3H5+H(+M)<=>C3H6(+M)	3.70E+14	0.0	0.0
290.	aC3H5+H<=>aC3H4+H2	1.80E+13	0.0	0.0
291.	aC3H5+O<=>C2H3CHO+H	6.00E+13	0.0	0.0
292.	aC3H5+OH<=>C2H3CHO+H+H	4.20E+32	-5.2	30126.0
293.	C2H3+HCO<=>C2H3CHO	1.80E+13	0.0	0.0
294.	C2H3CHO+H<=>C2H4+HCO	1.08E+12	0.5	1820.0
295.	C2H3CHO+O<=>C2H3+OH+CO	3.00E+13	0.0	3540.0
296.	C2H3CHO+O<=>CH2O+CH2CO	1.90E+07	1.8	220.0
297.	C2H3CHO+OH<=>C2H3+H2O+CO	3.43E+09	1.2	-447.0
298.	aC3H5+OH<=>aC3H4+H2O	6.00E+12	0.0	0.0
299.	aC3H5+O2<=>aC3H4+HO2	4.99E+15	-1.4	22428.0
300.	aC3H5+O2<=>CH3+CO+CH2O	1.19E+15	-1.0	20128.0
301.	aC3H5+O2<=>C2H3CHO+OH	1.82E+13	-0.4	22859.0
302.	aC3H5+HO2<=>C3H6+O2	2.66E+12	0.0	0.0
303.	aC3H5+HO2<=>OH+C2H3+CH2O	6.60E+12	0.0	0.0
304.	aC3H5+HCO<=>C3H6+CO	6.00E+13	0.0	0.0
305.	aC3H5+CH3<=>aC3H4+CH4	3.00E+12	-0.3	-131.0
306.	aC3H5+aC3H5<=>C3H6+aC3H4	1.00E+13	0.0	0.0
307.	aC3H5<=>CH3CCH2	7.06E+56	-14.1	75868.0
308.	CH3CCH2+H<=>pC3H4+H2	3.34E+12	0.0	0.0
309.	CH3CCH2+O<=>CH3+CH2CO	6.00E+13	0.0	0.0
310.	CH3CCH2+OH<=>CH3+CH2CO+H	5.00E+12	0.0	0.0
311.	CH3CCH2+O2<=>CH3+CO+CH2O	1.00E+11	0.0	0.0
312.	CH3CCH2+HO2<=>CH3+CH2CO+OH	2.00E+13	0.0	0.0
313.	CH3CCH2+HCO<=>C3H6+CO	9.00E+13	0.0	0.0
314.	CH3CCH2+CH3<=>pC3H4+CH4	1.00E+11	0.0	0.0
315.	CH3+C2H2<=>pC3H4+H	1.28E+09	1.1	13644.0
316.	CH3+C2H2<=>aC3H4+H	5.14E+09	0.9	22153.0
317.	CH3+C2H2<=>CH3CCH2	4.99E+22	-4.4	18850.0
318.	CH3+C2H2<=>aC3H5	2.68E+53	-12.8	35730.0
319.	CH3+C2H3(+M)<=>C3H6(+M)	2.50E+13	0.0	0.0
320.	CH3+C2H3<=>aC3H5+H	1.50E+24	-2.8	18618.0
321.	CH3+C2H4<=>nC3H7	3.30E+11	0.0	7700.0
322.	CH3+C2H5(+M)<=>C3H8(+M)	9.60E+14	-0.5	0.0
323.	C2H3+C2H5<=>aC3H5+CH3	3.90E+32	-5.2	19747.0
324.	C2H2+C2H<=>C4H2+H	9.60E+13	0.0	0.0
325.	C2H2+C2H<=>n-C4H3	4.50E+37	-7.7	7100.0

326. C2H2+C2H<=>i-C4H3	2.60E+44	-9.5	14650.0
327. C2H2+C2H3<=>C4H4+H	2.00E+18	-1.7	10600.0
328. C2H2+C2H3<=>n-C4H5	9.30E+38	-8.8	12000.0
329. C2H2+C2H3<=>i-C4H5	1.60E+46	-11.0	18600.0
330. C2H4+C2H<=>C4H4+H	1.20E+13	0.0	0.0
331. C2H4+C2H3<=>C4H6+H	2.80E+21	-2.4	14720.0
332. C2H3+C2H3<=>C4H6	1.50E+42	-8.8	12483.0
333. C2H3+C2H3<=>i-C4H5+H	1.20E+22	-2.4	13654.0
334. C2H3+C2H3<=>n-C4H5+H	2.40E+20	-2.0	15361.0
335. C3H2+CH<=>C4H2+H	5.00E+13	0.0	0.0
336. C3H2+CH2<=>n-C4H3+H	5.00E+13	0.0	0.0
337. C3H2+CH3<=>C4H4+H	5.00E+12	0.0	0.0
338. C3H2+HCCO<=>n-C4H3+CO	1.00E+13	0.0	0.0
339. C3H3+HCCO<=>C4H4+CO	2.50E+13	0.0	0.0
340. C3H3+CH<=>i-C4H3+H	5.00E+13	0.0	0.0
341. C3H3+CH2<=>C4H4+H	5.00E+13	0.0	0.0
342. i-C4H5+H<=>C3H3+CH3	2.00E+13	0.0	2000.0
343. C3H3+CH3(+M)<=>C4H612(+M)	1.50E+12	0.0	0.0
344. A1-+pC3H4<=>A1+C3H3	2.00E+12	0.0	15000.0
345. A1-+aC3H4<=>A1+C3H3	2.00E+12	0.0	15000.0
346. C4H2+H<=>n-C4H3	1.10E+42	-8.7	15300.0
347. C4H2+H<=>i-C4H3	1.10E+30	-4.9	10800.0
348. C4H2+O<=>C3H2+CO	2.70E+13	0.0	1720.0
349. C4H2+OH<=>H2C4O+H	6.60E+12	0.0	-410.0
350. H2C4O+H<=>C2H2+HCCO	5.00E+13	0.0	3000.0
351. H2C4O+OH<=>CH2CO+HCCO	1.00E+07	2.0	2000.0
352. n-C4H3<=>i-C4H3	4.10E+43	-9.5	53000.0
353. n-C4H3+H<=>i-C4H3+H	2.50E+20	-1.7	10800.0
354. n-C4H3+H<=>C2H2+C2H2	6.30E+25	-3.3	10014.0
355. i-C4H3+H<=>C2H2+C2H2	2.80E+23	-2.5	10780.0
356. n-C4H3+H<=>C4H4	2.00E+47	-10.3	13070.0
357. i-C4H3+H<=>C4H4	3.40E+43	-9.0	12120.0
358. n-C4H3+H<=>C4H2+H2	3.00E+13	0.0	0.0
359. i-C4H3+H<=>C4H2+H2	6.00E+13	0.0	0.0
360. n-C4H3+OH<=>C4H2+H2O	2.00E+12	0.0	0.0
361. i-C4H3+OH<=>C4H2+H2O	4.00E+12	0.0	0.0
362. i-C4H3+O2<=>HCCO+CH2CO	7.86E+16	-1.8	0.0
363. C4H4+H<=>n-C4H5	1.30E+51	-11.9	16500.0
364. C4H4+H<=>i-C4H5	4.90E+51	-11.9	17700.0
365. C4H4+H<=>n-C4H3+H2	6.65E+05	2.5	12240.0
366. C4H4+H<=>i-C4H3+H2	3.33E+05	2.5	9240.0
367. C4H4+OH<=>n-C4H3+H2O	3.10E+07	2.0	3430.0
368. C4H4+OH<=>i-C4H3+H2O	1.55E+07	2.0	430.0
369. n-C4H5<=>i-C4H5	1.50E+67	-16.9	59100.0
370. n-C4H5+H<=>i-C4H5+H	3.10E+26	-3.4	17423.0
371. C4H6<=>i-C4H5+H	5.70E+36	-6.3	112353.0
372. C4H6<=>n-C4H5+H	5.30E+44	-8.6	123608.0
373. n-C4H5+H<=>C4H4+H2	1.50E+13	0.0	0.0
374. i-C4H5+H<=>C4H4+H2	3.00E+13	0.0	0.0
375. n-C4H5+OH<=>C4H4+H2O	2.00E+12	0.0	0.0
376. i-C4H5+OH<=>C4H4+H2O	4.00E+12	0.0	0.0
377. n-C4H5+O2<=>C2H4+CO+HCO	4.16E+10	0.0	2500.0
378. i-C4H5+O2<=>CH2CO+CH2CHO	7.86E+16	-1.8	0.0
379. n-C4H5+HCO<=>C4H6+CO	9.00E+13	0.0	0.0
380. i-C4H5+HCO<=>C4H6+CO	9.00E+13	0.0	0.0
381. C4H6+H<=>n-C4H5+H2	1.33E+06	2.5	12240.0
382. C4H6+H<=>i-C4H5+H2	6.65E+05	2.5	9240.0
383. C4H6+H<=>pC3H4+CH3	7.00E+12	0.0	2000.0
384. C4H6+O<=>HCO+aC3H5	6.00E+08	1.4	-860.0
385. C4H6+OH<=>n-C4H5+H2O	6.20E+06	2.0	3430.0
386. C4H6+OH<=>i-C4H5+H2O	3.10E+06	2.0	430.0
387. C4H612+H<=>C4H6+H	2.00E+13	0.0	4000.0
388. C4H612+H<=>i-C4H5+H2	1.70E+05	2.5	2490.0
389. C4H612+H<=>aC3H4+CH3	2.00E+13	0.0	2000.0
390. C4H612+H<=>pC3H4+CH3	2.00E+13	0.0	2000.0
391. C4H612+O<=>CH2CO+C2H4	1.20E+08	1.6	327.0
392. C4H612+O<=>i-C4H5+OH	1.80E+11	0.7	5880.0
393. C4H612+OH<=>i-C4H5+H2O	3.10E+06	2.0	-298.0
394. C4H612<=>C4H6	1.00E+13	0.0	65000.0

395.	C4H2+C2H<=>C6H2+H	9.60E+13	0.0	0.0	
396.	C4H2+C2H<=>C6H3	4.50E+37	-7.7	7100.0	
397.	**C3H3+C3H3<=>A1-+H**	**3.00E+11**	**0.0**	**0.0**	*
398.	**C3H3+C3H3<=>A1**	**5.00E+10**	**0.0**	**0.0**	*
399.	n-C4H3+C2H2<=>1-C6H4+H	2.50E+14	-0.6	10600.0	
400.	**n-C4H3+C2H2<=>A1-**	**3.20E+03**	**2.9**	**1400.0**	*
401.	n-C4H3+C2H2<=>c-C6H4+H	6.90E+46	-10.0	30100.0	
402.	C4H4+C2H<=>1-C6H4+H	1.20E+13	0.0	0.0	
403.	**n-C4H5+C2H2<=>A1+H**	**3.20E+03**	**2.9**	**1400.0**	*
404.	C6H2+H<=>C6H3	1.10E+30	-4.9	10800.0	
405.	C6H3+H<=>C4H2+C2H2	2.80E+23	-2.5	10780.0	
406.	C6H3+H<=>1-C6H4	3.40E+43	-9.0	12120.0	
407.	C6H3+H<=>C6H2+H2	3.00E+13	0.0	0.0	
408.	C6H3+OH<=>C6H2+H2O	4.00E+12	0.0	0.0	
409.	C6H3+O2<=>CO+C3H2+HCCO	5.00E+11	0.0	0.0	
410.	1-C6H4+H<=>A1-	1.70E+78	-19.7	31400.0	
411.	1-C6H4+H<=>c-C6H4+H	1.40E+54	-11.7	34500.0	
412.	1-C6H4+H<=>C6H3+H2	1.33E+06	2.5	9240.0	
413.	1-C6H4+OH<=>C6H3+H2O	3.10E+06	2.0	430.0	
414.	c-C6H4+H<=>A1-	2.40E+60	-13.7	29500.0	
415.	A1+H<=>A1-+H2	2.50E+14	0.0	16000.0	
416.	A1+OH<=>A1-+H2O	1.60E+08	1.4	1450.0	
417.	A1-+H(+M)<=>A1(+M)	1.00E+14	0.0	0.0	
418.	A1+O<=>C6H5O+H	2.20E+13	0.0	4530.0	
419.	A1+OH<=>C6H5OH+H	1.30E+13	0.0	10600.0	
420.	A1-+O2<=>C6H5O+O	2.60E+13	0.0	6120.0	
421.	C6H5O<=>CO+C5H5	7.41E+11	0.0	43900.0	
422.	C6H5O+H<=>CO+C5H6	3.00E+13	0.0	0.0	
423.	C6H5O+O<=>HCO+2C2H2+CO	3.00E+13	0.0	0.0	
424.	C6H5O+H(+M)<=>C6H5OH(+M)	2.50E+14	0.0	0.0	
425.	C6H5OH+H<=>C6H5O+H2	1.15E+14	0.0	12400.0	
426.	C6H5OH+O<=>C6H5O+OH	2.80E+13	0.0	7352.0	
427.	C6H5OH+OH<=>C6H5O+H2O	6.00E+12	0.0	0.0	
428.	C5H5+H(+M)<=>C5H6(+M)	1.00E+14	0.0	0.0	
429.	C5H5+O<=>n-C4H5+CO	1.00E+14	0.0	0.0	
430.	C5H5+OH<=>C5H4OH+H	5.00E+12	0.0	0.0	
431.	C5H5+HO2<=>C5H5O+OH	3.00E+13	0.0	0.0	
432.	C5H6+H<=>C5H5+H2	2.20E+08	1.8	3000.0	
433.	C5H6+O<=>C5H5+OH	1.80E+13	0.0	3080.0	
434.	C5H6+OH<=>C5H5+H2O	3.43E+09	1.2	-447.0	
435.	C5H5O<=>n-C4H5+CO	2.50E+11	0.0	43900.0	
436.	C5H5O+H<=>CH2O+2C2H2	3.00E+13	0.0	0.0	
437.	C5H5O+O<=>CO2+n-C4H5	3.00E+13	0.0	0.0	
438.	C5H4OH<=>C5H4O+H	2.10E+13	0.0	48000.0	
439.	C5H4OH+H<=>CH2O+2C2H2	3.00E+13	0.0	0.0	
440.	C5H4OH+O<=>CO2+n-C4H5	3.00E+13	0.0	0.0	
441.	C5H4O<=>CO+C2H2+C2H2	1.00E+15	0.0	78000.0	
442.	C5H4O+O<=>CO2+2C2H2	3.00E+13	0.0	0.0	
443.	aC3H5+CH3(+M)<=>C4H81(+M)	1.00E+14	-0.3	-262.3	
444.	C4H81+H<=>C2H4+C2H5	1.60E+22	-2.4	11180.0	
445.	C4H81+H<=>C3H6+CH3	3.20E+22	-2.4	11180.0	
446.	C4H81+H<=>C4H7+H2	6.50E+05	2.5	6756.0	
447.	C4H81+O<=>nC3H7+HCO	3.30E+08	1.4	-402.0	
448.	C4H81+O<=>C4H7+OH	1.50E+13	0.0	5760.0	
449.	C4H81+O<=>C4H7+OH	2.60E+13	0.0	4470.0	
450.	C4H81+OH<=>C4H7+H2O	7.00E+02	2.7	527.0	
451.	C4H81+O2<=>C4H7+HO2	2.00E+13	0.0	50930.0	
452.	C4H81+HO2<=>C4H7+H2O2	1.50E+11	0.0	14900.0	
453.	C4H81+CH3<=>C4H7+CH4	4.50E-01	3.6	7153.0	
454.	C4H7<=>C4H6+H	2.28E+52	-12.0	51230.0	
455.	C4H7+H(+M)<=>C4H81(+M)	3.60E+13	0.0	0.0	
456.	C4H7+H<=>CH3+aC3H5	2.00E+21	-2.0	11000.0	
457.	C4H7+H<=>C4H6+H2	1.80E+12	0.0	0.0	
458.	C4H7+O2<=>C4H6+HO2	1.00E+11	0.0	0.0	
459.	C4H7+HO2<=>CH2O+OH+aC3H5	2.40E+13	0.0	0.0	
460.	C4H7+HCO<=>C4H81+CO	6.00E+13	0.0	0.0	
461.	C4H7+CH3<=>C4H6+CH4	1.10E+13	0.0	0.0	
462.	C2H3+C2H4<=>C4H7	7.93E+38	-8.5	14220.0	
463.	C2H3+C2H5(+M)<=>C4H81(+M)	1.50E+13	0.0		